LBL-30292

Lawrence Berkeley Laboratory

UNIVERSITY OF CALIFORNIA

Physics Division

Hydrogenated Amorphous Silicon Radiation Detectors: Material Parameters; Radiation Hardness; Charge Collection

S. Qureshi
(Ph.D. Thesis)

January 1991

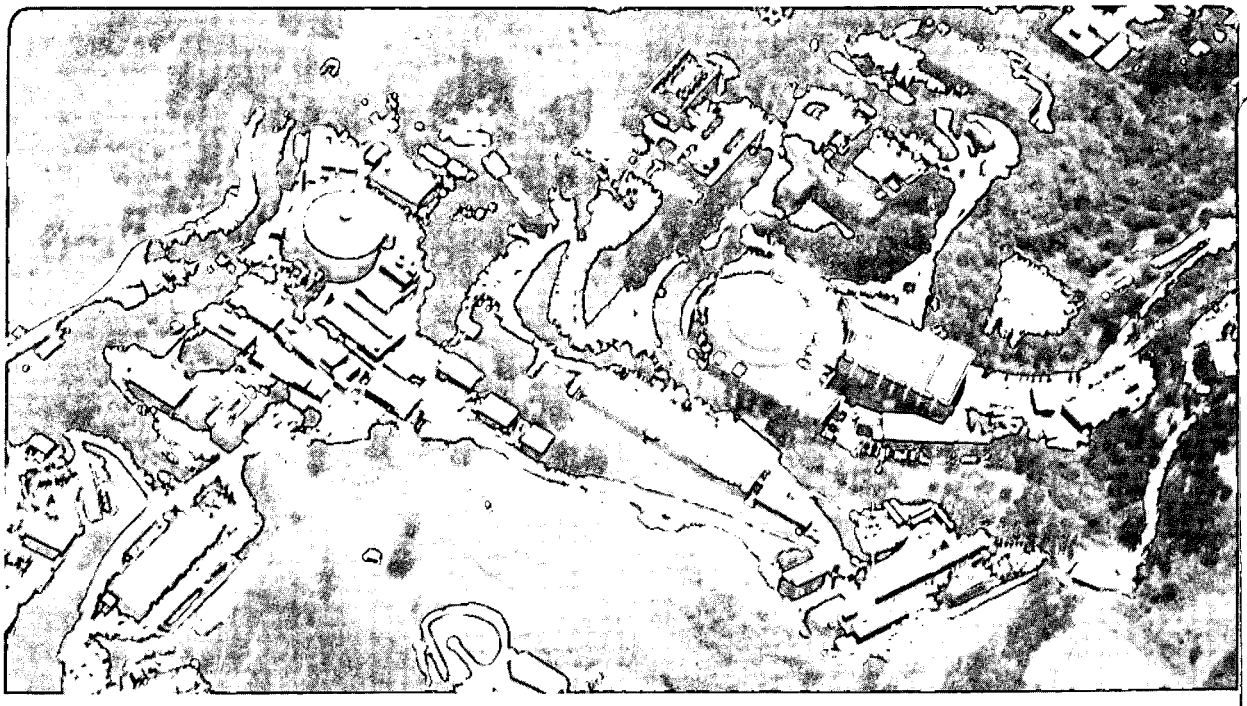

LBL-30292
Copy 1
Bldg. 50 Library.

Prepared for the U.S. Department of Energy under Contract Number DE-AC03-76SF00098.

DISCLAIMER

This document was prepared as an account of work sponsored by the United States Government. While this document is believed to contain correct information, neither the United States Government nor any agency thereof, nor the Regents of the University of California, nor any of their employees, makes any warranty, express or implied, or assumes any legal responsibility for the accuracy, completeness, or usefulness of any information, apparatus, product, or process disclosed, or represents that its use would not infringe privately owned rights. Reference herein to any specific commercial product, process, or service by its trade name, trademark, manufacturer, or otherwise, does not necessarily constitute or imply its endorsement, recommendation, or favoring by the United States Government or any agency thereof, or the Regents of the University of California. The views and opinions of authors expressed herein do not necessarily state or reflect those of the United States Government or any agency thereof or the Regents of the University of California.

LBL-30292

HYDROGENATED AMORPHOUS SILICON RADIATION DETECTORS: MATERIAL PARAMETERS; RADIATION HARDNESS; CHARGE COLLECTION

SHAFI QURESHI

PHYSICS DIVISION
Lawrence Berkeley Laboratory
University of California
Berkeley, CA 94720

JANUARY 1991

This work was supported by the U. S. Department of Energy under Contract No. DE-AC03-76SF00098.

Acknowledgements

I would like to express my immense appreciation of Professors Selig N. Kaplan and Victor Perez-Mendez for their great ideas and advising during the conduct of this research. I also express my appreciation of Professors Stanley G. Prussin and Eike Weber for their valuable suggestions and guidance in the completion of this thesis. My appreciation is extended to Dr. Robert A. Street of Xerox Palo Alto Research Center for providing valuable suggestions and expertise. I express my thanks to Dr. John S. Drewery and my fellow graduate students at LBL, Gyuseong Cho, Ichiro Fujieda, John Chun and Daniel Wildermuth for stimulating discussions we had during the course of my studies. I would like to express my thanks to Kai Lee of Lawrence Berkeley Laboratory for providing his assistance in experiment development and to Drs. P. Bhat of Glasstech Solar Inc. and C. C. Tsai of Xerox PARC for making hydrogenated amorphous silicon samples used for this research work.

This research was supported by the Director, Office of Energy Research, Office of High Energy and Nuclear Physics, Division of High Energy Physics of the U. S. Department of Energy under contract # DE-AC03-76SF00098.

Contents

Chapter 1 Introduction 1

1.1 Active detector thickness 1
1.2 Device speed 3
1.3 Device leakage current and noise 4
1.4 Device degradation 4

Chapter 2 Material properties 6

2.1 Structure of amorphous silicon 6
2.2 Effect of disorder 7
2.2.1 Mobility edge 8
2.3 Density of states 10
2.3.1 Growth conditions and density of states 15
2.4 Electrical transport 19
2.4.1 Conductivity in extended states 19
2.4.2 Conductivity in tail states 24
2.4.3 Variable range hopping conductivity 26
2.4.4 Electrical transport in a-Si:H 27
2.5 Material parameters of a-Si:H for device applications 30
2.5.1 Drift mobility by transient photoconductivity method 30
2.5.2 Gaussian transport 33
2.5.3 Dispersive (non-Gaussian) transport 35
2.5.4 Mobility-lifetime product 37
2.5.5 DC bias transient 37
2.6 Measurement of material parameters 40
2.6.1 Drift mobility measurement 42
2.6.2 Measurement of mobility-lifetime product 44
2.6.3 Defect density measurement 45

Chapter 3 Leakage current and noise of a-Si:H diode 50

Chapter 4 Radiation hardness of a-Si:H 59

4.1 Radiation damage by electrons and alpha particles 59
4.2 Radiation damage by gamma rays 60
4.3 Radiation damage by neutrons 63
4.4 Radiation damage by protons 73
4.4.1 Effect of proton irradiation on carrier mobility and lifetime 79

Chapter 5 Charge collection 83

5.1 Experimental studies on charge collection in a-Si:H diodes 85
5.2 Minimum ionizing particle detection 88
5.2.1 Minimum ionizing particle 89
5.2.2 Charge creation by interacting particle in a-Si:H 91
5.2.3 Minimum ionizing particle measurement 94
5.2.4 Beta signals at short shaping times ranging from 20-500 ns 98
5.2.5 Recent experiment with beta particles 101
5.3 High energy alpha experiment 105

Conclusion 109

Appendix 1 113

Appendix 2 116

Appendix 3 119

Table 1 dE/dx of heavy particles in silicon 121

Table 2 Range of heavy particles in silicon 125

Table 3 dE/dx and range of electrons in silicon 129

References 132

cker diodes are required for sufficient energy deposition in the material and better signal to noise ratio. One main obstacle in achieving this objective has been the production of thick a-Si:H diodes with low defect density that can be fully depleted at reasonable bias voltages. It should be emphasized that the presence of a sizeable electric field is essential for charge collection in a-Si:H devices as carrier diffusion plays little role in charge collection. One fundamental difficulty encountered in obtaining fully depleted thick diodes lies in the nature of amorphous silicon. Hydrogenated amorphous silicon has a high density of states in its band gap. These states are differentiated as being either shallow or deep states. These states control the electrical properties of the material. The shallow states have dominant influence on carrier mobility as carriers are trapped and detrapped in the shallow states during their transit [Tiedje et al., 1980]. The deep states are crucial in determining the carrier lifetime. These states are also responsible for creating space charge in the material which then shapes the electric field. The thickness to which the electric field penetrates in a thick a-Si:H p-i-n diode is crucial to its usefulness as a radiation detector. The fact that a large density of charged centers exist in the i layer when the diode is under DC bias, the electric field would no longer be uniform, unlike a crystalline p-i-n diode where the electric field in the intrinsic layer is uniform [Knoll, 1979]. This problem is further discussed at the beginning of Chapter 5. Presently made a-Si:H diodes with i layer thickness between 30 to 40 microns deplete at reasonable bias voltages

without breakdown or excess noise. Evidently the density of defect states or the dangling bond density is an important parameter for reasons stated above. Presently material with defect density ~ 1-2 $\times 10^{15}$ cm^{-3} is produced without great difficulty and enormous research is being done by various research groups to improve the quality of the material further. Chapter 2 discusses some of the material aspects relevant to my research work. In writing this chapter I have drawn heavily on the published works of various authors who specialize in this field and these works are referenced.

1.2 Device speed

The carrier mobility in hydrogenated amorphous silicon is small compared to crystalline silicon. The electron mobility is ~ 1 cm^2/V-s, a factor of ~1000 smaller compared to crystalline silicon and the hole mobility is even smaller ($\leq$ 0.01 cm^2/V-s). Consequently, one expects an amorphous silicon device to be slow. In a 30 μm thick detector at 300 V bias the transit time t_T ($t_T = d^2/\mu V$) for electrons is > 30 ns and for holes is > 3 μs limiting the device speed to several microseconds for full charge collection.

However, if one were to rely on the signal from electrons alone the device speed could be much higher. This has been demonstrated in section 5.2.4 where significant beta signal is collected at shaping times as low as 20 ns. Measurements with 860 Mev alpha particles at short shaping times also illustrate this. As thicker and improved a-Si:H diodes are realised, more energy is deposited by a

particle going through the diode. The electron collection alone would produce large enough signal making a faster a-Si:H device more realistic.

1.3 Device leakage current and noise

The leakage current of an a-Si:H p-i-n diode under reverse bias is important from noise and power dissipation considerations. In chapter 3 leakage current and noise behaviour of a well behaved a-Si:H p-i-n diode has been studied. It is found that leakage current at operating bias shows "Poole-Frenkel effect" [Hill, 1971] type of dependence on voltage and leakage current makes dominant contribution to noise in the form of "shot noise" for CR-$(RC)^4$ (pseudo-Gaussian) shaping at 3 μs shaping time.

1.4 Device degradation

Hydrogenated amorphous silicon is known to degrade on prolonged exposure to light due to Staebler-Wronski effect (i.e. the defect density of the material increases on exposure to light) [Staebler et al., 1977]. As a radiation detector little degradation has been observed in a-Si:H diodes on exposure to high radiation fluences. As discussed in Chapter 4, 1 Mev neutron fluences exceeding 10^{14} cm^{-2} produced little degradation in leakage current and noise, and the effects were annealable. 1.4 Mev proton irradiation showed more damage in terms of degradation in leakage curr-

ent and noise and it became significant at 10^{13} cm^{-2} fluence. This proton fluence corresponds to ~ 22 Mrad ionizing dose. The effects were partially annealable.

2 Material properties

2.1 Structure of amorphous silicon

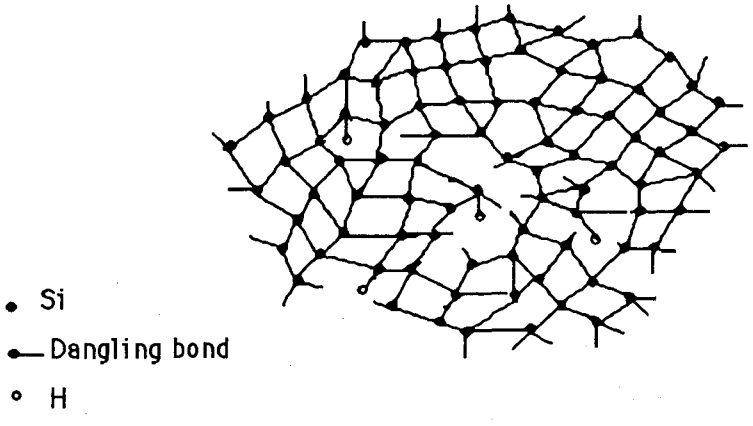

Fig. 2.1. Two-dimensional sketch of a random network of amorphous silicon incorporating several dangling bonds. Also shown are hydrogen atoms passivating some of the dangling bonds when amorphous silicon is hydrogenated.

X-ray and electron diffraction experiments show that the nearest neighbor environment in a-Si is approximately the same as that found in its crystalline counterpart. Although the long-range periodicity is absent in a-Si based materials, a high degree of short-range order is retained because of the chemical bonding resulting in nearly equal bond lengths and bond angles as in crystalline Si.

Generally, a continuous random network (CRN) in which all bonds are satisfied but in which there is no long-range order is used as a model for a-Si. It is widely believed that in the bulk of a-Si a Si atom on the average is surrounded by four other atoms at the same distance as in crystalline Si, forming a regular tetrahedron. Further, each of these atoms in turn has three more neighbors forming a well-defined second shell of 12 atoms none of which is a neighbor to any other. The resemblance of a-Si to crystalline Si ceases beyond the second shell [Madan , 1988]. In a CRN although the number of atoms associated with the nearest neighbors is the same, there is a variation in the interbond angles that rapidly leads to loss of order.

Polk [1971] first demonstrated the possibility of building a CRN for tetrahedrally bonded a-Si with coordination number of 4 by allowing $\pm 10^{o}$ spread in the tetrahedral bond angle of 109.5^{o}.

Fig. 2.1 shows two-dimensional sketch of a random network for amorphous silicon. Also shown are several dangling bonds. In amorphous silicon the density of these dangling bonds is $\sim 10^{19}$ cm^{-3}. Hydrogen incorporation lowers these dangling bonds to $\sim 10^{15}$ cm^{-3}.

2.2 Effect of disorder

Because of the absence of long-range order the conduction and valence bands in a-Si differ from those in crystalline Si in having a tail of states localized in the sense of Anderson [1958]. According to

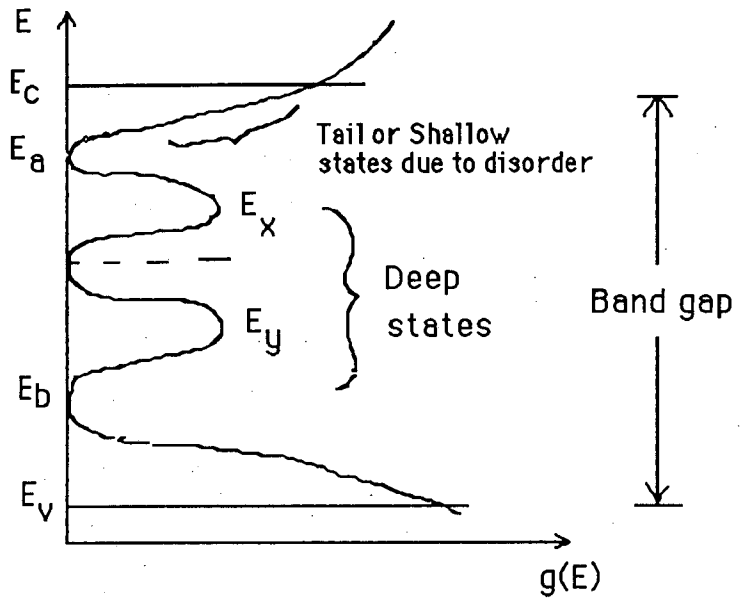

Fig. 2.2. Schematic showing states in the band gap of amorphous silicon. The shallow states are due to long-range disorder and the deep states are due to structural defects such as dangling bonds.

Anderson a state is localized if, for an electron placed in the state at t=0, there exists a finite probability of finding the electron in the state at $t=\infty$ or more simply the electron has not diffused. The localized band tail states in Fig. 2.2, that is the states between E_c and E_a, and E_v and E_b are supposed to be due to lack of long-range order and the deeper lying gap states denoted by E_x and E_y are ascribed to structural defects such as dangling bonds.

2.2.1 The mobility edge

Anderson [1958] predicted that for a carrier moving in a potential well of Fig. 2.3 all states would be localized if V_0/B exceeded a critical value. Here V_0 is the extent of the random potential as shown in Fig. 2.3(b) and B is the bandwidth when V_0 vanishes. Mott [1967] showed that if V_0/B was less than the critical value the states in the gap would be localized, a sharp energy, E_c, called the mobility edge, as illustrated in Fig. 2.4, would separate the localized from the extended states. The position of the mobility edge is an intrinsic property of the CRN and not a consequence of defects. In a-Si:H the position of the mobility edge is independent of

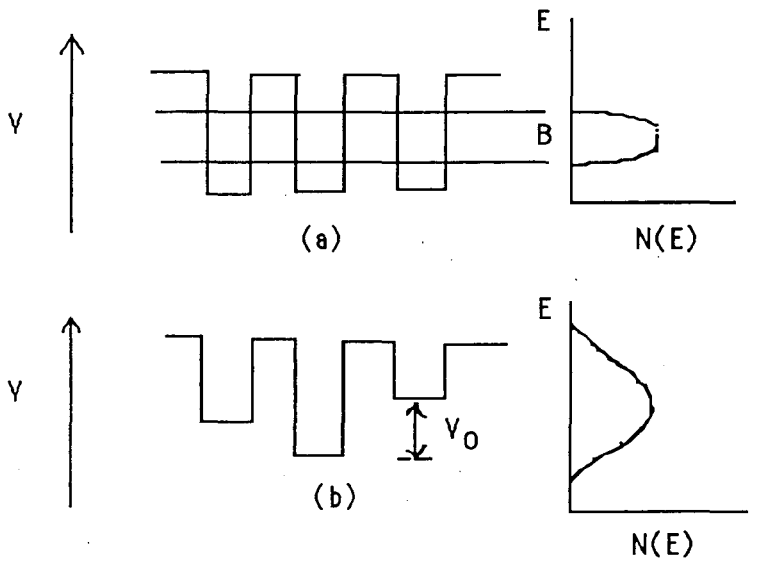

Fig. 2.3. The potential energy of an electron in the Anderson model. (a) Without random potential. (b) With random potential. B is the bandwidth when V_0 vanishes.The density of states is also shown.

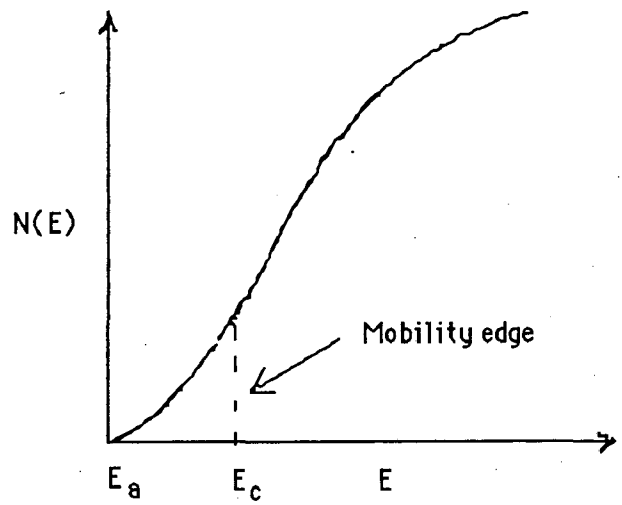

Fig. 2.4. Density of states near mobility edge, E_c. The states below the edge are localized and above it are extended and thus have distinctly higher mobility.

hydrogen content [Jones et al., 1980]. The fact that hydrogen (10% or so) widens the band gap is believed to be due to a shift of the valence band downwards. One strong evidence of the existence of mobility edge is the change in the behaviour of conductivity from extended state conductivity in the conduction band to hopping conductivity in the shallow states as temperature is lowered. This is discussed in section 2.4.4.

2.3 Density of states

The states in the gap of an amorphous semiconductor not only

control the position of the Fermi energy, E_f, but also the transport properties of the material. In addition, they act as traps and recombination centers that determine the kinetics for the restoration of equilibrium after any perturbation away from thermal equilibrium. Further, in intrinsic a-Si:H the defect centers release charge which is swept out by the electric field thus producing space charge in the material which then shapes the electric field inside the sample.

The energy associated with repulsion between two electrons with opposite spins that are present in the same spatial state is called the correlation energy , U. When an electron of either spin is present on the defect center the energy of the corresponding state for the electron with opposite spin is increased by U and this configuration forms a D^- defect center as shown in Fig. 2.5(d). For localized states U is of the order of a few tenths of an eV.

The key to understanding the electronic structure of a-Si and its related alloys, for example a-Si:H, is the fact that it forms an overconstrained network in which the average coordination is 4 in comparison to ≤ 2.4 dictated by optimal bond lengths and bond angles for covalent bonding [Adler et al., 1985] leading to local strains. For an overconstrained material one expects that most of the strain is relieved by non-optimal bond angles. This is the reason why a-Si exhibits a $\pm 10^o$ spread from the optimal tetrahedral bond angle of 109.5^o. However, during the preparation of a-Si some concentration of stretched bonds and uncoordinated atoms are likely to be introduced because of the extent of the overconstrained nature of

the network. Alloying with any element from other columns in the periodic table, e.g. hydrogen, lowers the average coordination z and this tends to reduce the overall strain. The simplest defect that uncoordination produces is a three-fold coordinated Si atom usually called a dangling bond. The conventional notation used to denote coordination and charge state of a defect is D_z^q where z is the coordination number and q is the charge state of the defect. Thus a neutral dangling bond would be denoted by D_3^0. Tight-binding calculations of Adler [1978] indicate that D_3^0 defects yield two states in the gap, a lower filled state D^0 and an upper empty state D^- separated by U. An electron removed from a D^0 center converts it to D^+ center. The D^+ and D^- centers are spin paired and exhibit no ESR signal unlike the D^0 center which is paramagnetic and can be observed by its characteristic ESR signal (g=2.0055). The ground state and several of the defect centers in a-Si are shown in Fig. 2.5.

Hydrogenated amorphous silicon, a-Si_{1-x}:H_x, has an average coordination number z = 4-3x, so that a typical concentration of 20% hydrogen decreases z from 4 to 3.4 thus inducing a considerable reduction in overall strain [Adler et al., 1985]. This reduction manifests itself by sharp decrease in local bond distortion and defects. In addition, the Si-H bond strength is approximately 3.4 eV which is about 40% greater than Si-Si bond strength of 2.4 eV. Since H is more elctronegative than Si, Si-H bonding states are deep in the a-Si:H valence band while Si-H antibonding orbitals are not too far from the conduction band mobility edge.

If unoccupied defect center D^+ is taken at zero energy and the

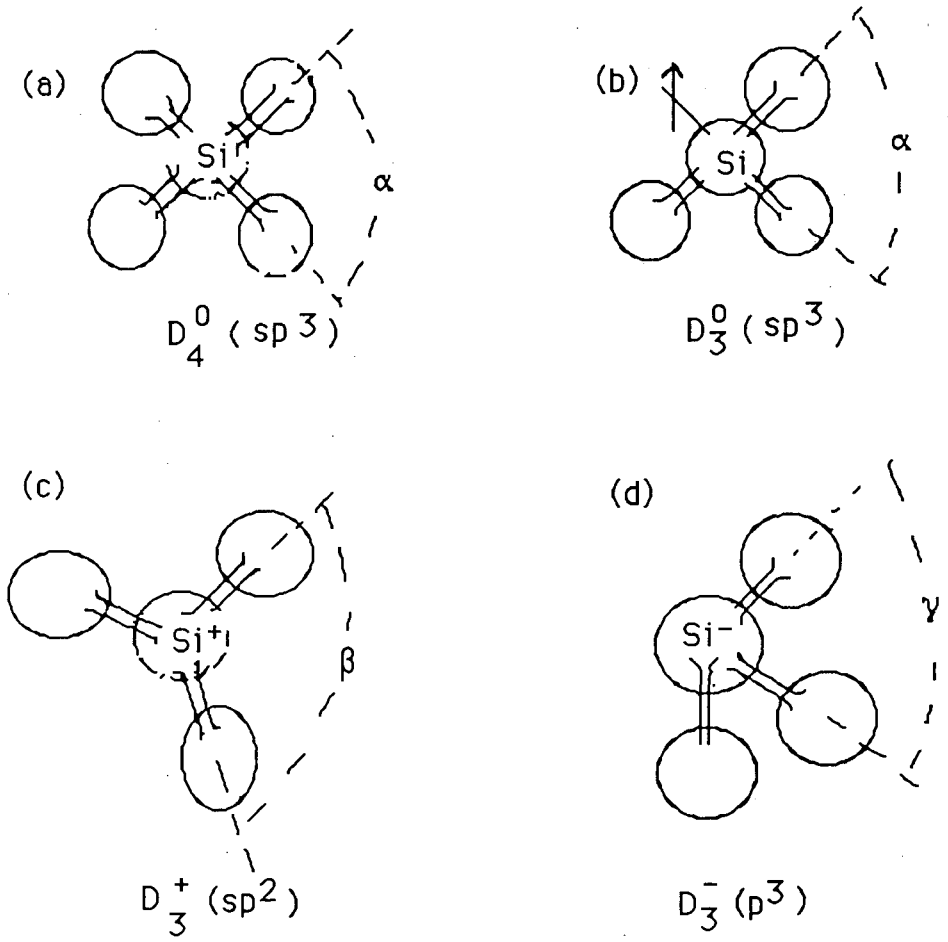

Fig. 2.5. Schematic of local bonding configurations of ground state and several defect centers in a-Si (a) ground state, D_4^0 (b) neutral dangling bond D_3^0 (c) positively charged defect center, D_3^+ (d) negatively charged defect ceter, D_3^-. The bond angles shown are $\alpha = 109.5°$, $\beta = 120°$, $\gamma = 95°$; sp and p are the spectral notations of orbitals [Adler, 1984].

energy of neutral defect center is denoted by E_d it will take energy E_c-E_d to excite an electron from a neutral defect center to the con-

duction band. A negative defect center D^- has both electrons present and the two electrons repel each other, the second electron is at energy E_d+U. Only an energy of E_c-E_d-U is needed to excite it to the conduction band. The three states D^+, D^0 and D^- all possess a minimum energy configuration which is necessarily distinct.

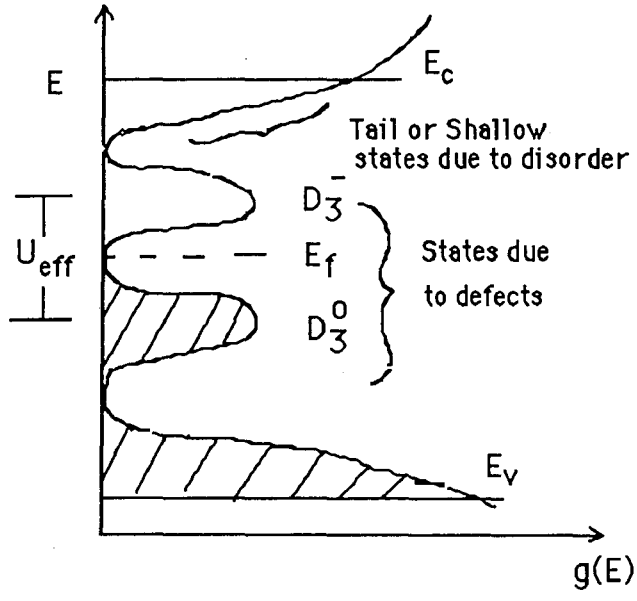

Fig. 2.6. Schematic of the density of states of intrinsic a-Si for $U_{eff} > 0$.

The correlation energy, U, can be defined as the energy required for the reaction

$$2\ D^0 \rightarrow D^+ + D^-$$

without any local atomic relaxation. However, in reality the local environment around D^+ and D^- states will relax, lowering the energy of both states and therefore the value of U. The minimum energy needed to create an oppositely charged D^+-D^- defect pair from two D^0 centers is the effective correlation energy, U_{eff}. The evidence that U_{eff} is positive in a-Si:H is provided by the ESR data [Dersch et al., 1981]. However, the possibility of negative U_{eff} in a-Si:H has been argued by some authors [Adler, 1983]. The density of states (DOS) diagram for amorphous silicon with $U_{eff} > 0$ is shown in Fig. 2.6.

2.3.1 Growth conditions and density of states

Good quality hydrogenated amorphous silicon is deposited by a glow discharge method (also called plasma enhanced chemical

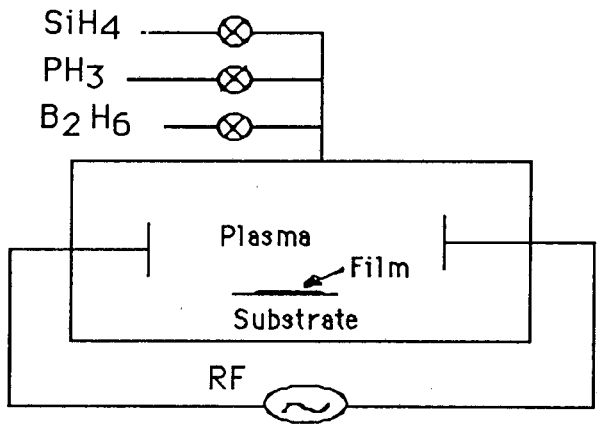

Fig. 2.7. Schematic diagram of glow discharge deposition system. The deposition is commonly done at 13.56 MHz.

vapour deposition). Fig. 2.7 shows a schematic diagram of the deposition system. Intrinsic a-Si:H is deposited using silane gas (SiH_4). Phosphine (PH_3) or Diborane (B_2H_6) gases are introduced for n or p type doping.

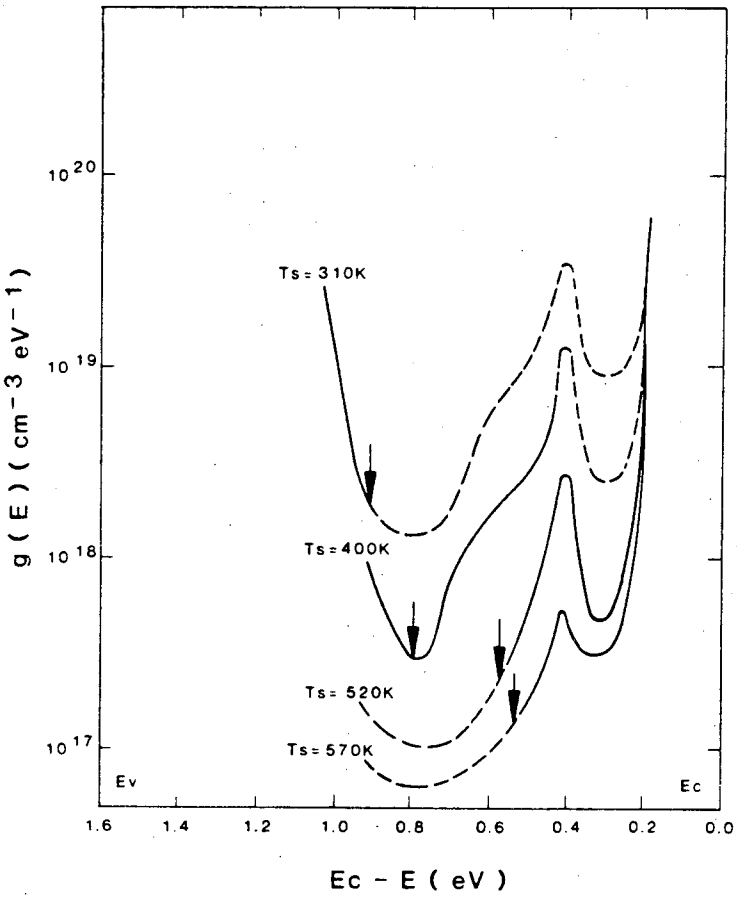

Fig. 2.8. Localized state density, g(E), for glow discharge a-Si:H. T_S is the substrate temperature. Full lines are obtained from the field effect data and the arrows indicate the Fermi level position of the samples. [Madan, 1973; Spear, 1973; Madan et al., 1976].

The density of states (DOS) in the gap of glow-discharge deposited hydrogenated amorphous silicon is critically controlled by the deposition temperature, T_s, of the substrate [Spear et al., 1972]. The DOS decreases by orders of magnitude when T_s is increased from 300° k to 570° k as shown in Fig. 2.8 [Madan, 1988]. The vast change in the DOS with change in T_s is attributed to basic structural changes occuring in the material. The films produced at low T_s generally have more H concentration, in excess of 30%, leading to formation of polymeric type structures with a greater number of Si-H_2 and Si-H_3 groups as shown in Fig. 2.9 [Lucovsky et al., 1979]. It is

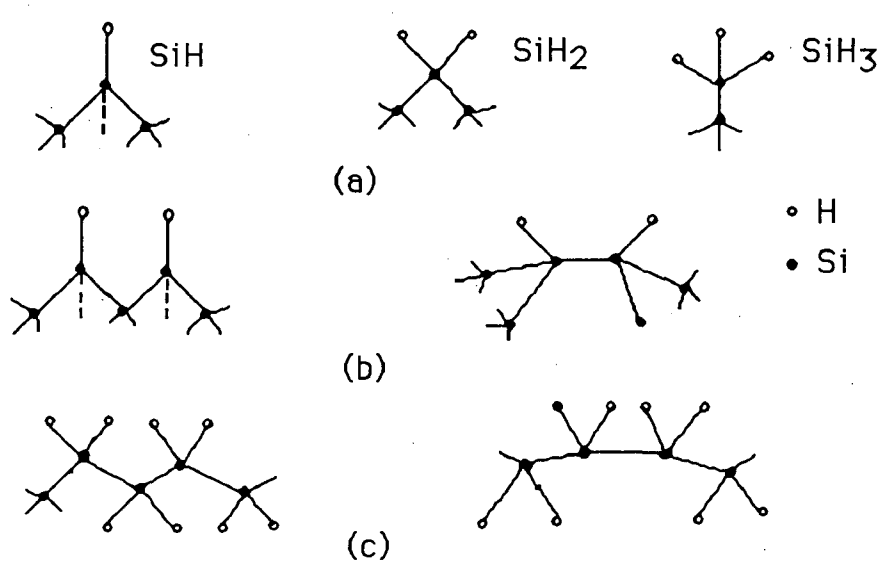

Fig. 2.9. Local bonding geometries. (a) isolated groups, (b) monohydide configurations in which SiH groups are attached to second or nearest neighbor, and (c) polymeric structures based on SiH_2 units [Lucovsky et al., 1979].

the fundamental change from polymeric type structure for films deposited at low T_s to monohydride type at higher T_s that has a major effect on the reduction of the DOS. The best quality a-Si:H has an H concentration of ~ 10%. Hydrogenation decreases the defect density from ~ 10^{19} cm^{-3} in pure amorphous silicon (a-Si) to ~ 10^{15} cm^{-3} in hydrogenated amorphous silicon.

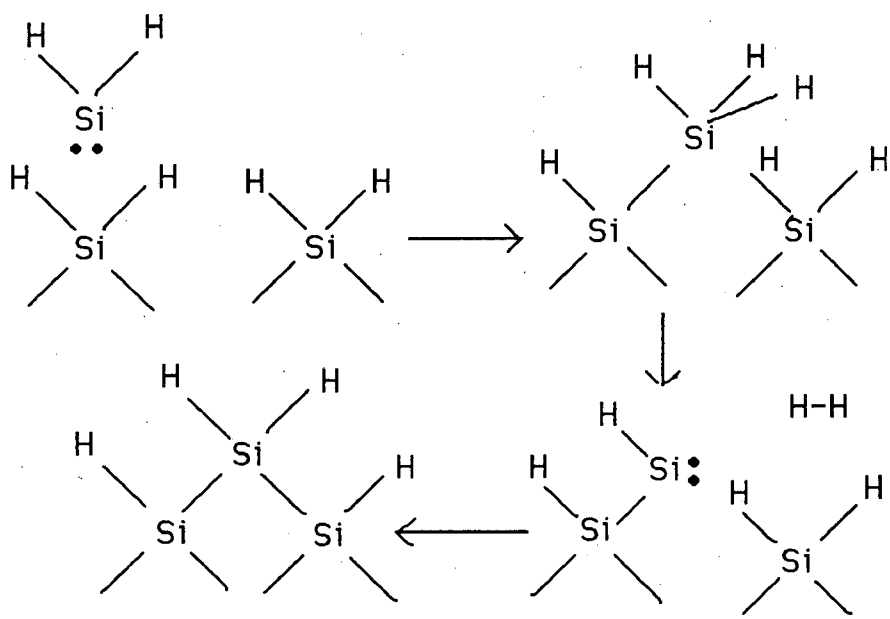

Fig. 2.10. Schematic of the model proposed to explain the hydrogen elimination process from the a-Si:H film during growth [Kampas and Griffith, 1981].

The quality of the film is influenced by the pressure of the gas during deposition since high gas pressure enhances gas phase polymerisation with consequent increase in $Si\text{-}H_2$ and $Si\text{-}H_3$ groupings within the film [Kampas, 1982]. In general the hydrogen content,

C_H, of a-Si based alloy is approximately in the range of 10-30 at% which is much smaller than H/Si ratio (=4) for a pure SiH_4 plasma. Kampas and Griffith [1981] suggested a model for the growth kinetics of a-Si:H film explaining the hydrogen elimination process from the film and the polyhydride formation. According to the model the SiH_2 free radicals react with the Si-H bond on the growing surface and produce an activated complex that can eliminate H_2 molecules. The amount of hydrogen remaining in the film is determined by a competition between H_2 elimination and deactivation of the complex. Further, the authors concluded that changes in the deposition parameters that control the deposition rate also increase the atomic hydrogen flux on the growing surface, which results in a higher hydrogen content in the film. Fig. 2.10 shows a schematic of the SiH_2 addition, H_2 elimination and cross-linking sequence proposed by the authors.

2.4 Electrical transport in amorphous silicon

It is vitally important to understand the processes behind the electrical transport in a-Si:H. As mentioned earlier the transport is strongly influenced by the states in the band gap which can be divided into two parts (a) tail states which result from disorder (b) mid-gap states due to point defects. The role of these states in the conductivity of the material is discussed below.

2.4.1 Conductivity in extended states

Transport in the extended states is a result of carriers excited beyond the mobility edge into states at or around E_c. The conductivity, σ, for a semiconductor can be expressed as

$$\sigma = e\int g(E)\,\mu(E)\,f(E)\,dE \tag{2.1}$$

where g(E) is the density of states, $\mu(E)$ is the mobility and f(E) is the Fermi function.

The extended state mobility in amorphous silicon has been a subject of controversy. It is generally agreed that the directly measurable quantity, the drift mobility, μ_D, is relatively small of the order of 1 $cm^2/V\text{-}s$ for electrons at room temperature. But the drift mobility is only a fraction of the band mobility, μ_o, since it is limited by the trapping of carriers. The two are related by [Tiedje et al., 1980]

$$\mu_D = \mu_0 \frac{n_0}{n_0+n_t} \tag{2.2}$$

where n_0 and n_t are the concentrations of free and trapped carriers respectively. The value of μ_0 extracted from μ_D is ~ 10 $cm^2/V\text{-}s$ [Tiedje et al., 1981] or ~ 500 $cm^2/V\text{-}s$ [Silver et al., 1982] depending upon the inferred density of states g(E). One view is that conduction beyond the mobility edge proceeds with a scattering event every second or third neighbor. The other view is that the band mobility is of the same order as that of crystalline silicon (c-Si) but large den-

sities of traps greatly reduce the drift mobility. The complete absence of geminate recombination; geminate recombination is the name given to the process whereby two thermalized oppositely-charged particles attempt to escape from each other in the presence of their mutual Coulomb attraction [Adler et al., 1985]; indicating extremely rapid separation of photo-generated carriers, and recent work on multilayer structures [Abeles and Tiedje, 1983] suggesting delocalized wave functions with coherence lengths in excess of 30 A° are strong evidence in support of higher values of band mobilities. However, commonly accepted value of μ_0, derived from transient photoconductivity experiments, is of the order of 10.

If it is assumed that conduction is due to carriers within kT of the mobility edge E_c then from eq. (2.1)

$$\sigma = e\int_{E_c}^{E_c+kT} g(E_c)\mu_0 \exp[-(E_c-E_f)/kT]dE \qquad (2.3)$$

$$\approx eg(E_c)\mu_0 \exp[-(E_c-E_f)/kT]\int_{E_c}^{E_c+kT} dE$$

$$\approx eg(E_c)\mu_0\, kT\exp[-(E_c-E_f)_T/kT] \qquad (2.4)$$

The temperature dependence of E_c-E_f can be expressed as

$$(E_c-E_f)_T = (E_c-E_f)_0 - \delta_F T$$

and using eq. (2.4) we have

$$\sigma = eg(E_c)\mu_0\, kTe^{\delta_F/k}\exp[-(E_c-E_f)_0/kT] \qquad (2.5)$$

The pre-exponential factor in eq. (2.6) has been a subject of controversy.

$$\sigma = \sigma_0 \exp[-(E_c - E_f)_T / kT] \tag{2.6}$$

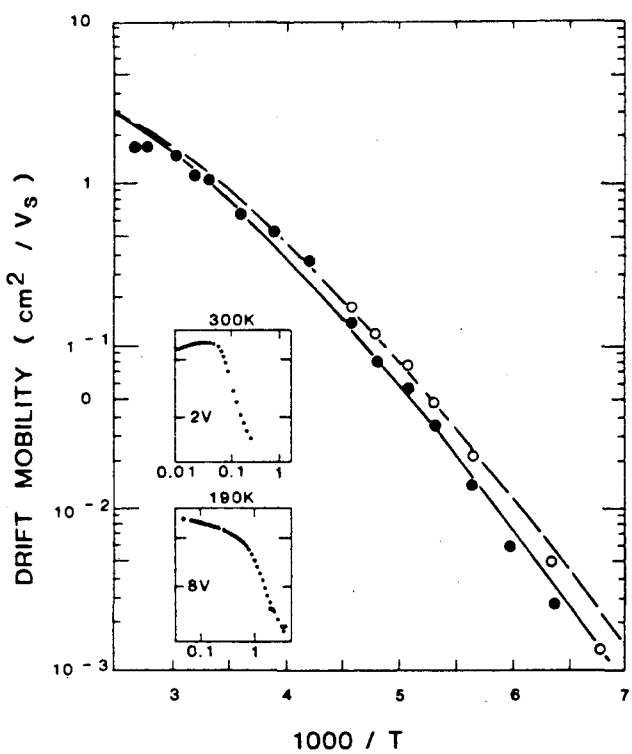

Fig. 2.11(a). Temperature dependence of the electron drift mobility for an electric field of 10^4 V/cm (closed circles) and 2 x 10^4 V/cm (open circles). The solid (broken) line is a fit to the low- (high-) field data with T_c = 312° K, μ_0 = 13 cm^2/V-s and ν = 4.6 x 10^{11} s^{-1}. The insets are representative photocurrent decays at 300° and 190° K plotted as Log I vs Log t; the time scale is microseconds [Tiedje et al., 1981].

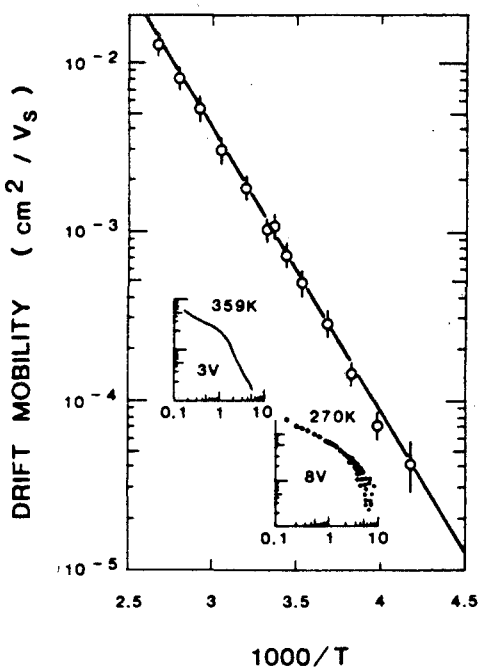

Fig. 2.11 (b). Temperature dependence of the hole drift mobility for an electric field of 5.8 x 10^4 V/cm. The solid line is a fit to the data based on eq. (2.8a) with T = 500° K, μ_0 = 0.67 cm^2/V-s and ν = 1.6×10^{12} s^{-1}. The insets are representative photocurrent decays at 359° and 270° K plotted as Log I vs Log t; the time scale is in microseconds [Tiedje et al. , 1981].

Mott [1985] argues that σ_0 in a non-crystalline semiconductor system should be given by

$$\sigma_0 = 0.03\ e^2/\ \hbar L_i \qquad (2.7)$$

where L_i is the inelastic diffusion length, consequence of electron-

phonon interaction. Using the experimental values of the time between collisions Mott concludes that the pre-exponential factor $\sigma_0 = 16\ \Omega^{-1}\ cm^{-1}$ and the extended state mobility $\mu_0 = 8\ cm^2/V\text{-}s$ which are consistent with most experimental values.

The value of μ_D is obtained from time of flight (TOF) experiments where carrier mobility is measured as a function of temperature [Tiedje et al., 1981]. Fig. 2.11(a,b) shows plot of electron and hole mobility as a function of 1/T respectively and fit to the data based on eq. (2.8).

$$t_T \cong \nu^{-1} \left(\frac{\nu}{1-\alpha}\right)^{\frac{1}{\alpha}} \left(\frac{L^2}{\mu_0 V}\right)^{\frac{1}{\alpha}} \qquad T < T_c \tag{2.8}$$

where $\alpha = T/T_c$ and the drift mobility is $\mu_0\,(1-T_c/T)$ for $T > T_c$. Here, kT_c is an energy which characterizes the width of the exponential band tail. From the fit to the data it is estimated that μ_0 for electrons is ~ 13 $cm^2/V\text{-}s$ and for holes is ~ 0.67 $cm^2/V\text{-}s$. It is also seen that at low temperatures the electron photocurrent transient exhibits the power law decay characteristics of dispersive transport (lower inset in Fig. 2.11 (a)). However, the hole transport is dispersive over the entire temperature range and the activation energy is ~ 0.35 eV.

2.4.2 Conductivity in tail states

The tail states in amorphous semiconductors are the conse-

quence of disorder and lie in the energy range $E_a < E < E_c$ and $E_v < E < E_b$ for the conduction and valence bands respectively as shown in Fig. 2.12.

The conductivity at an arbitrary energy $E = E_x$ for the conduc-

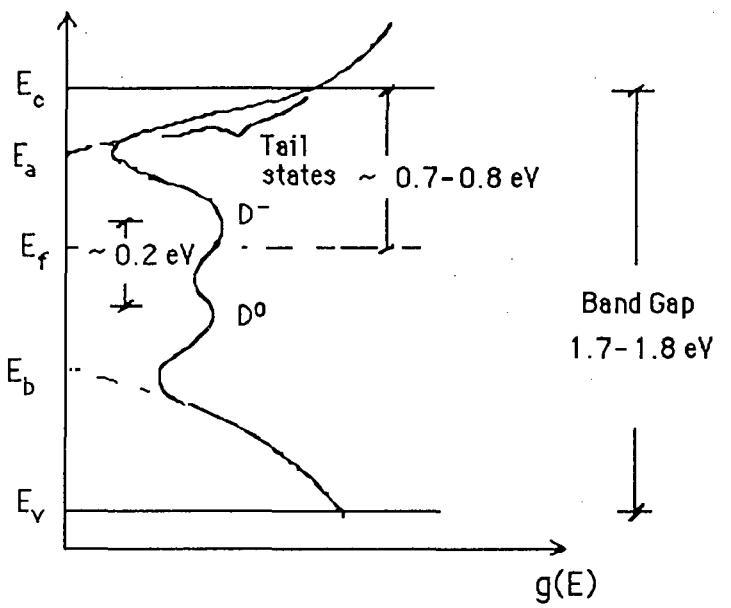

Fig. 2.12. Schematic of the density of states of a-Si:H [Street].

tion band tail can be written as

$$\sigma = e\int \mu(E)\, g(E)\, f(E)\, dE \qquad (2.9)$$
$$= e\mu_{hop} \int_{E_a}^{\infty} g(E_x)\, \exp[-(E_x - E_f)/kT]\, dE$$

where μ_{hop} is the hopping mobility, consequence of transport of carriers in the localized states by tunnelling from an occupied to an

unoccupied state [Adler et al., 1985].

Cohen [1970] showed that hopping mobility, μ_{hop}, is given by

$$\mu_{hop} = \frac{1}{6} \upsilon_{ph} \left(\frac{eR^2}{kT}\right) \exp[-W_1/kT] \qquad (2.10)$$

where R is the hopping distance and W_1 is the energy difference between the initial and final states [see appendix 1].

2.4.3 Variable range hopping conductivity

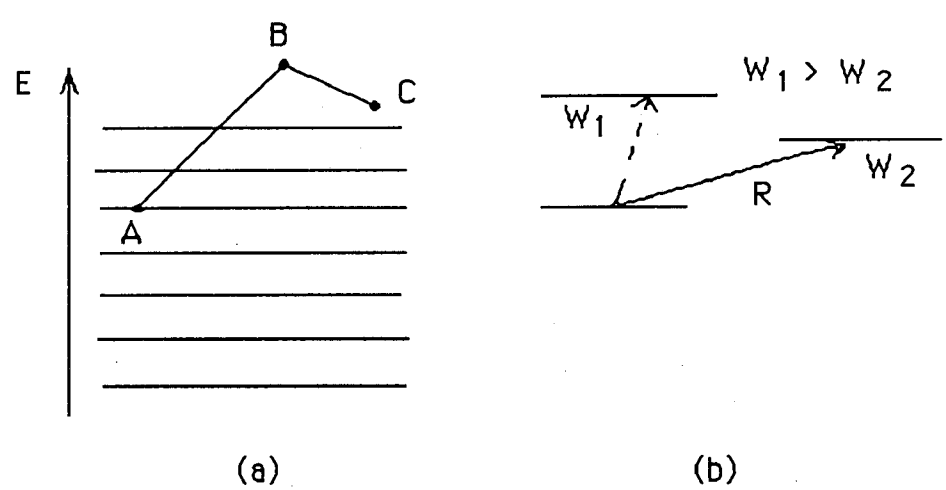

Fig. 2.13. (a) Hopping of a carrier from state A below the Fermi energy to state B above it. (b) At low T, long range less energetic hops are favoured.

Thermally activated hopping conduction of carriers between localized states situated in the mid-gap region $E_b < E < E_a$ occurs at

low T, or at high T in materials with high defect density. Fig. 2.13 shows this kind of transport where a carrier hops from state A below the Fermi energy to state B above it. The hopping conductivity at E_f is given by [appendix 1]

$$\sigma_{hop} = \sigma_0 \exp\left(-\frac{A}{T^{\frac{1}{4}}}\right) \qquad (2.11)$$

Eq. (2.11) is known as Mott's $T^{\frac{1}{4}}$ law [Mott, 1968].

2.4.4 Electrical transport in a-Si:H

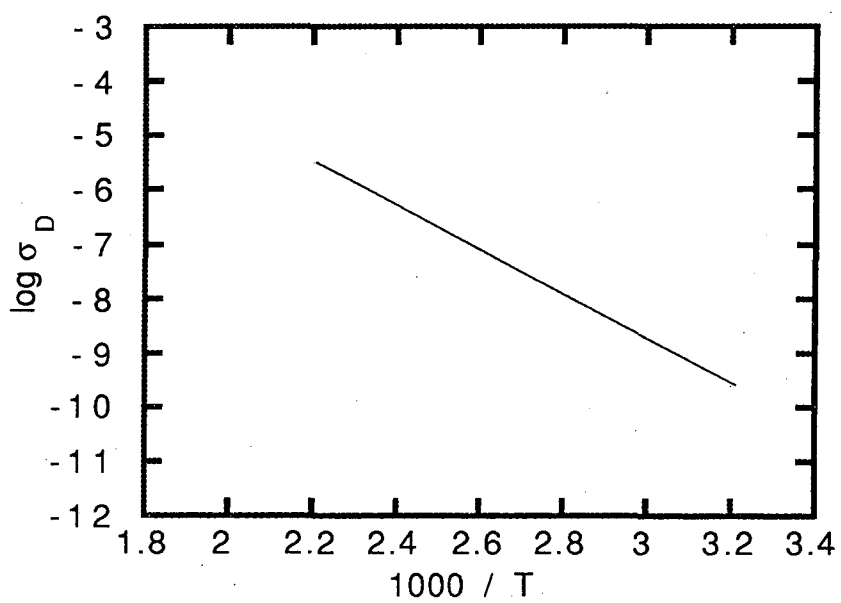

Fig. 2.14. Plot of ln σ_D vs 1/T for typical glow discharge (GD) a-Si:H [Madan, 1988].

Glow discharge a-Si:H has a low defect density, several orders of magnitude lower than a-Si. As seen in Fig. 2.14 the Arrhenius

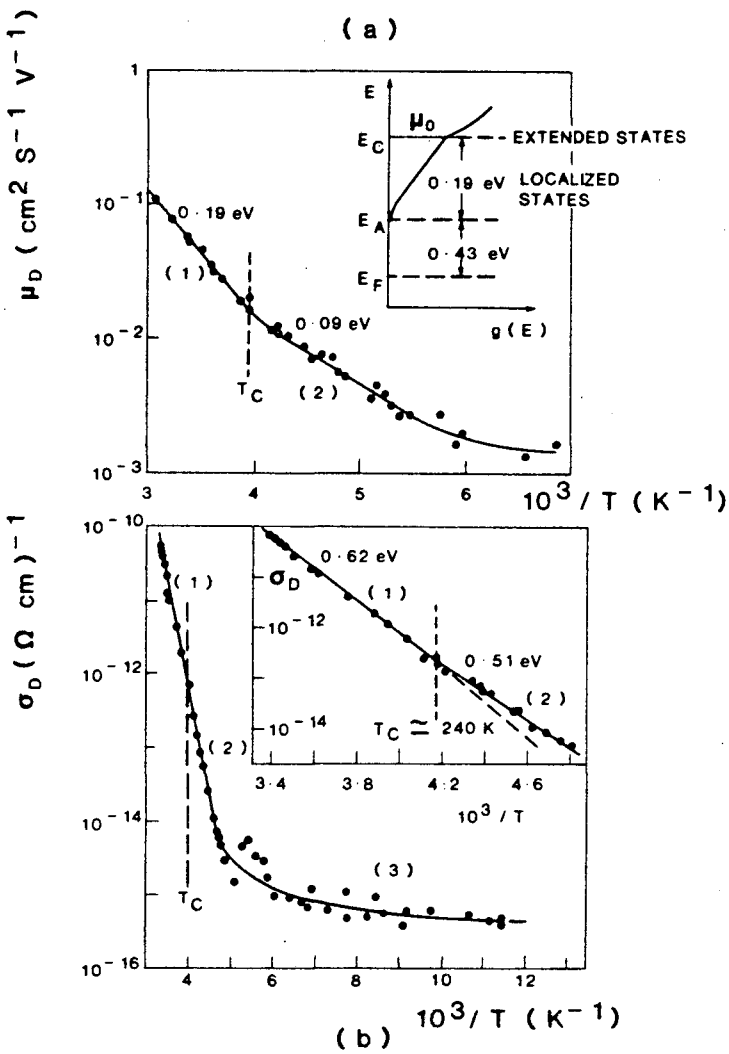

Fig. 2.15. Temperature dependence of (a) Electron drift mobility μ_D. (b) Conductivity σ_D in a glow discharge a-Si:H deposited at T_S = 500° K. T_C is the temperature at which change in transport behaviour is seen [LeComber and Spear, 1970].

plot (dark conductivity σ_D vs 1/T) exhibits a straight line behaviour and a well defined activation energy $E_D = E_c - E_f$ is obtained. The conductivity, σ, can be expressed by eq. (2.6) with activation energy $E_D \sim 0.8$ eV for intrinsic a-Si:H. Intrinsic a-Si:H is slightly n-type and activated behaviour is due to extended state conduction above E_c. This is in contrast to a-Si where unique activation energy is hard to define and conductivity is dominated by thermally activated hopping within the defect states. The change in transport mechanism in a-Si:H from extended states conduction to thermally activated hopping in the tail states was first reported by LeComber et al. [1974] showing that the drift mobility on a ln μ_D vs l/T plot had a kink at T ~ 250° K as shown in Fig. 2.15(a). The same kink was observed in a ln σ_D vs 1/T plot as shown in Fig. 2.15(b). The data was interpreted in terms of the existence of two regions. In the region (1) the conductivity showed activated behaviour with the activation energy $E_D = E_c - E_f$ given by eq. (2.6) and the region (2) where conductivity changed to thermally activated hopping behaviour with the activation energy given by $E_D = E_x - E_f + W$. The ln μ_D vs 1/T plot was also interpreted in terms of the change in conduction from the extended states behaviour with activation energy $E_c - E_a$ (~ 0.2 eV) for region (1) to a thermally activated hopping mode within localized states with the activation energy ~ 0.1 eV for region (2). The photoconductivity measurements of Spear et al. [1974] also showed such a kink.

The evidence of ln σ_D vs $T^{-1/4}$ behaviour predicted by eq. (2.11) is not seen in glow discharge a-Si:H although this behavior is found

in highly defective material such as elemental evaporated Si.

2.5 Material parameters of a-Si:H for device applications

The quantities of interest in using a-Si:H for device applications are carrier mobility, carrier lifetime usually expressed as mobility-lifetime product and the dangling bond density [Qureshi et al., 1988]. While carrier mobility determines device speed and, together with carrier lifetime, determines the charge collection behaviour of a device, the defect density is crucial in shaping the electric field in the device under the influence of which carrier drifts. Therefore, the role of these parameters in a device fabricated from a-Si:H cannot be over emphasized. These parameters bear direct relationship to material quality, and their measurement is crucial in judging the quality of a-Si:H.

2.5.1 Drift mobility by transient photoconductivity method

The drift mobility is measured by time of flight (TOF) where carriers are injected at one point in the sample and their transit under the influence of electric field across the sample is studied by measuring the transit time t_T. An expression for carrier mobility under uniform electric field F is obtained as below.

The carrier velocity, v, is given by

$$v=\mu_D F$$

where μ_D is the drift mobility and F is the electric field. Also

$$v=\frac{d}{t_T}$$

Thus, for uniform electric field F=V/d , we have

$$\mu_D=\frac{d^2}{Vt_T} \qquad (2.12)$$

Some important considerations in drift mobility measurements are :

(a) The mean free path X_0 of light must be short compared to sample thickness, d, so that carriers are generated on one end of the sample and the signal is primarily due to transit of only one type of carrier. This condition is satisfied by using appropriate wave length light. We use 510 nm laser light ($X_0 \sim 0.2$ μm in a-Si:H) to study diodes 12 μm or more thick.

(b) The photo-injected charge must be small so that the electric field in the sample is not perturbed by it [Street, 1983]. This can be ensured by reducing the light intensity. A rule of thumb used to avoid these space charge effects is that the injected charge be approximately an order of magnitude smaller than charge (CV) across the sample.

(c) The relaxation time, $\tau_{rel}=\varepsilon_0\varepsilon_r/\sigma$, where ε_0 is the permitivity of vacuum, ε_r is the dielectric constant of amorphous silicon and σ is the conductivity, must be much larger than the transit time t_T of carriers. This condition is easily satisfied in intrinsic a-Si:H and the

mobility of both types of carriers can be measured by injecting light from the n or p side of a p-i-n diode. The relaxation time for intrinsic a-Si:H is of the order of a milisecond or longer, estimated from eq. (2.13) [Tiedje et al., 1980]

$$t \approx 10^{-12} \exp [E/kT] , \qquad (2.13)$$

where t is the thermal release time and E is the energy (measured from the conduction band) of a state in the gap occupied by an electron. The relaxation time for a-Si:H can also be estimated from

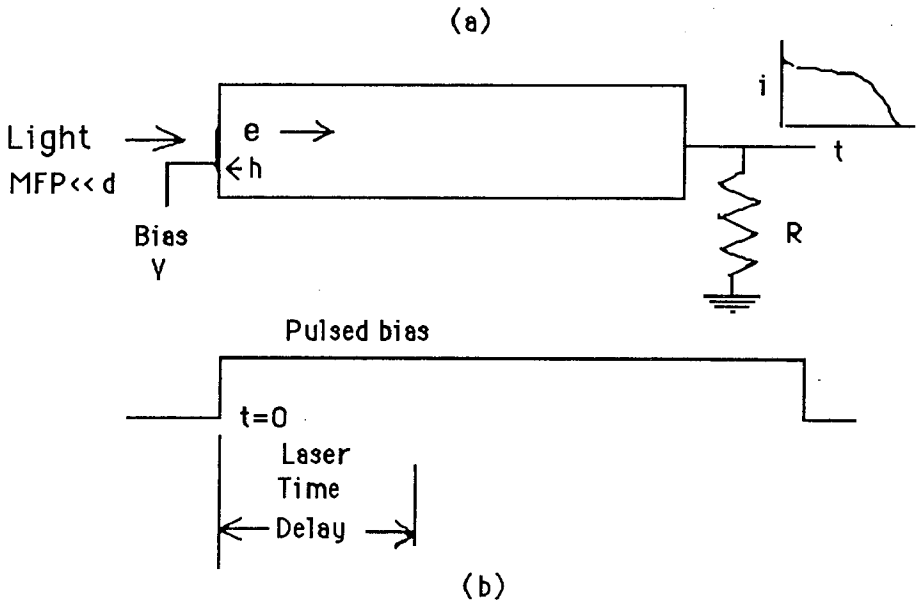

Fig. 2.16. Schematic illustrating the principle behind drift mobility measurement. (a) Drift of electrons across the sample. (b) Time delay between pulsed bias and laser light.

resistivity and the dielectric constant ($\sigma \sim 10^{-10}\ \Omega^{-1}\ cm^{-1}$, $\varepsilon_0\varepsilon_s \sim 10^{-12}$ F/cm). Once relaxation occurs under applied bias, space charge is created in the sample, resulting in the shaping of the electric field. However, in a T.O.F experiment the condition of a uniform electric field is satisfied by pulsing the bias and then injecting the charge several microseconds after the applied bias, as illustrated in Fig 2.16(b). The sample is allowed to reach thermal equilibrium which usually takes several seconds, before the sequence is repeated. Typical electron transient at room temperature is shown in Fig. 2.16(a).

2.5.2 Gaussian transport

Transport of electrons at room temperature is non-dispersive and is described by Gaussian statistics [Scher et al., 1975]. The time development of the injected carriers can be described in terms of mean displacement l from the illuminated surface as shown in Fig. 2.17. The parameter β characterizes the spread of charge sheet about the mean. The charge density as a function of position and time during the transit can be described by [Leal Ferreira , 1977]

$$\rho(x, t) = A\frac{1}{t^{1/2}}\exp[-(x-x_0)^2/B\,t] \qquad (2.14)$$

where x_0 refers to the location where the charge sheet is created. For Gaussian transport, spread of the charge sheet by diffusion about

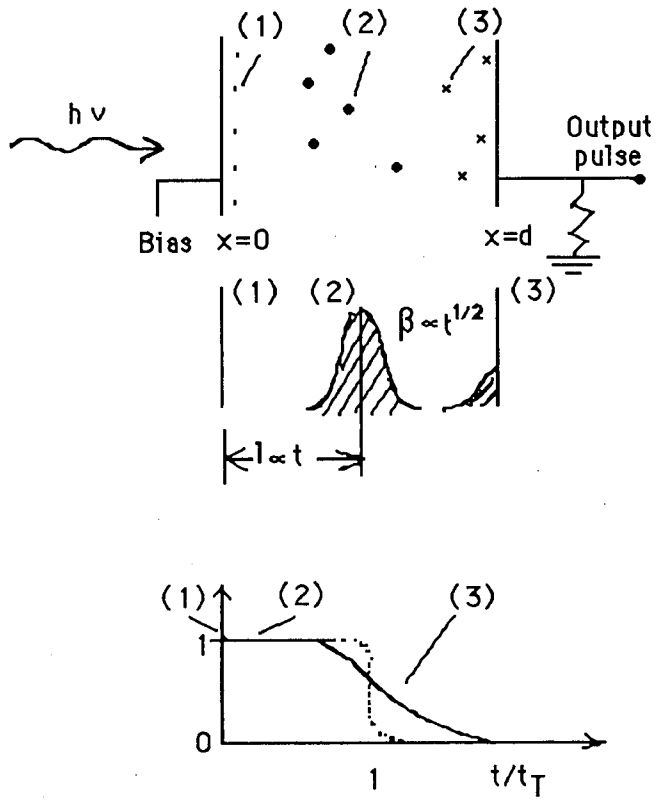

Fig. 2.17. Schematic representation of carrier propagation under Gaussian conditions, Top: Position of representative carriers in the sample bulk at t= 0 (') , $t < t_T$ (•) and $t \sim t_T$ (*). Middle: Charge distribution in sample bulk at t=0, $t < t_T$ and $t \sim t_T$. Bottom: Current pulse in external circuit induced by charge displacement. Units normalized to t_T and $i_T = i(t)$. Dashed line represents transient current for lower applied bias field, i.e. longer transit time. (1) shows charge sheet just after injection, (2) indicates charge is traversing through the bulk but not reached the farther contact and (3) shows that a fraction of injected charge has already reached the farther contact [Pfister and Scher, 1978].

the mean can be written as

$$\frac{\beta}{l} \approx \frac{t^{1/2}}{t} = t^{-1/2} \tag{2.15}$$

Thus at transit time we have

$$\frac{\beta}{l} = t_T^{-1/2} \propto \left(\frac{F}{d}\right)^{1/2} \tag{2.16}$$

For non-dispersive transport transit time is defined as the time at which current drops by 50%. This is the time for the center of the gaussian charge sheet to traverse distance d.

2.5.3 Dispersive (non-Gaussian) transport

In this mode of transport the shape of the current transient is independent of transit time t_T, a property usually referred to as universality [Scher et al. , 1975]. The charge sheet does not grow symmetrically about its mean position. Some of the injected carriers drift rapidly into the sample. A significant fraction of carriers suffer scattering and get immobilized for times of the order of transit time t_T. The charge packet grows asymmetrically where the leading edge penetrates deep into the sample and the maximum point of charge density moves slowly away from the generation point. The spread and the mean position of charge have the same time dependence giving β/l=constant [Scher et al., 1975].

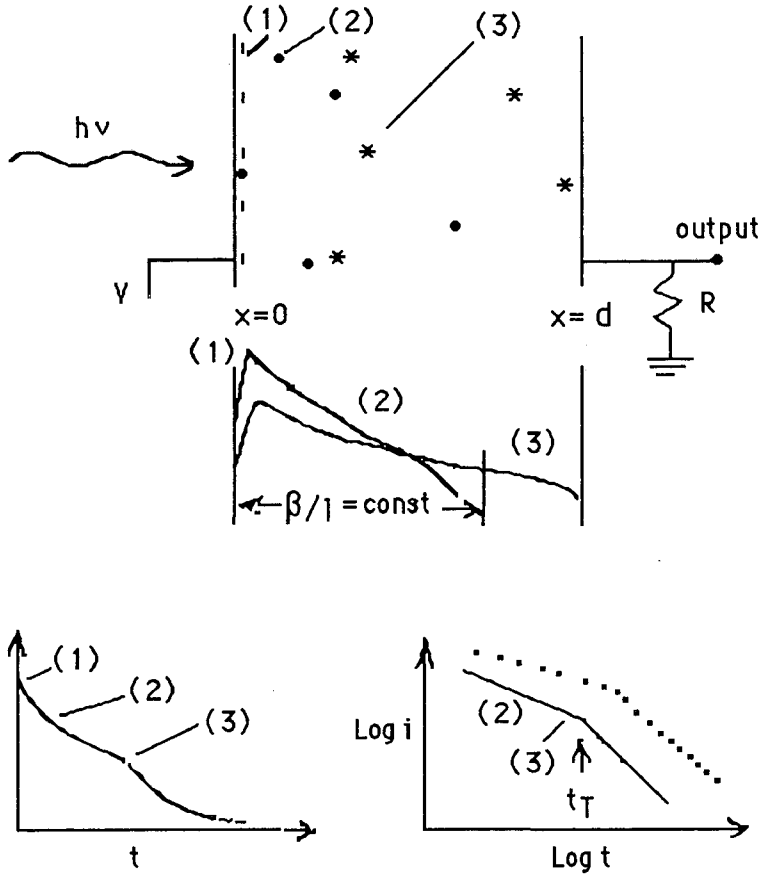

Fig. 2.18. Schematic representation of carrier propagation under ideal non-Gaussian conditions. Top: Position of representative carriers in the sample bulk at t=0 (′), $t<t_T$ (•) and $t \sim t_T$ (*). Middle: Charge distribution in sample bulk at t=0, $t<t_T$ and $t \sim t_T$. Bottom: Current pulse in external circuit induced by charge displacement in linear units (left) and logarithmic units (right). Dashed line represents transient current for lower applied bias field, i.e. longer transit time. (1) shows charge sheet just after injection, (2) indicates charge is traversing through the bulk but not reached the farther contact and (3) shows that a fraction of injected charge has already reached the farther contact [Pfister and Scher, 1978].

The current transient in the case of dispersive transport has two slopes $(1-\alpha)$ and $(1+\alpha)$ when plotted as a log i(t) vs log t plot, as shown in Fig. 2.18. Here α is the dispersion parameter. This behaviour has been modelled by Scher et al. [1975]. The transit time in this case is defined by the point of intersection of two slopes.

2.5.4 Mobility-lifetime product

The mobility-lifetime product $\mu\tau$ is a useful parameter as it determines the mean drift length, $\mu\tau F$, of carriers before capture. It is a directly measurable quantity and is obtained by measuring charge collection as a function of electric field, F. Under uniform electric field the charge collection is given by the Hecht equation [Street, 1983]

$$\int J dt = Q = Q_0 \mu \tau \frac{F}{d}[1-\exp(-\frac{d}{\mu \tau F})] \qquad (2.17)$$

where Q_0 is the injected charge due to one type of carrier and d is the sample thickness. The experiment for $\mu\tau$ measurement is done under pulsed bias conditions and the charge collection data is fitted to the Hecht equation. The $\mu\tau$ product is obtained from the fit.

2.5.5 DC bias transient

The defect centers in a-Si:H release charge causing the electric field in the sample to become nonuniform in a time of the

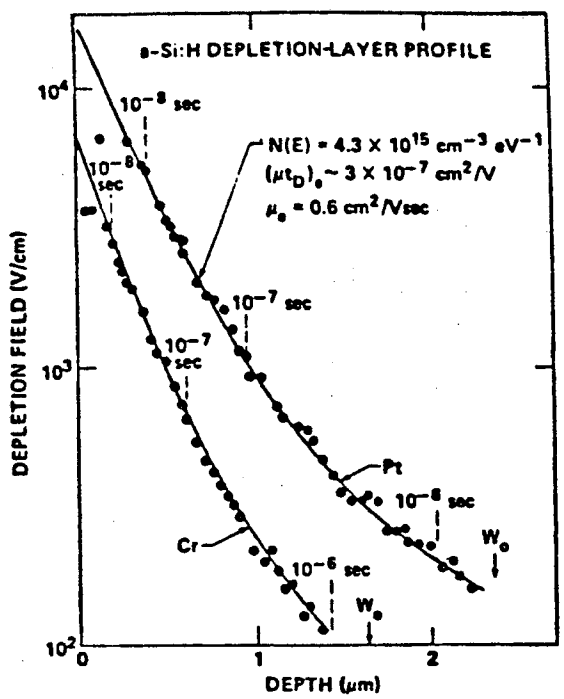

Fig. 2.19. Examples of the internal-electric field profile for Cr and Pt contacts to the same sample. The times marked correspond to those of the transient response. The vaues of W are obtained from the charge-collection measurements. N(E) is derived from the exponential region of the field profile [Street, 1983].

order of a second after DC bias is applied [Street, 1983]. The photo-excited carriers move under the influence of nonuniform electric field which is caused by the presence of space charge. The field follows the drop off given by the Poisson equation ($dF/dx=-\rho/\varepsilon_0\varepsilon_r$)

where ρ is the charge density in the sample. The transient photo-current produced by motion of photo-excited carriers in this nonuniform field is, therefore, a direct measure of the electric field

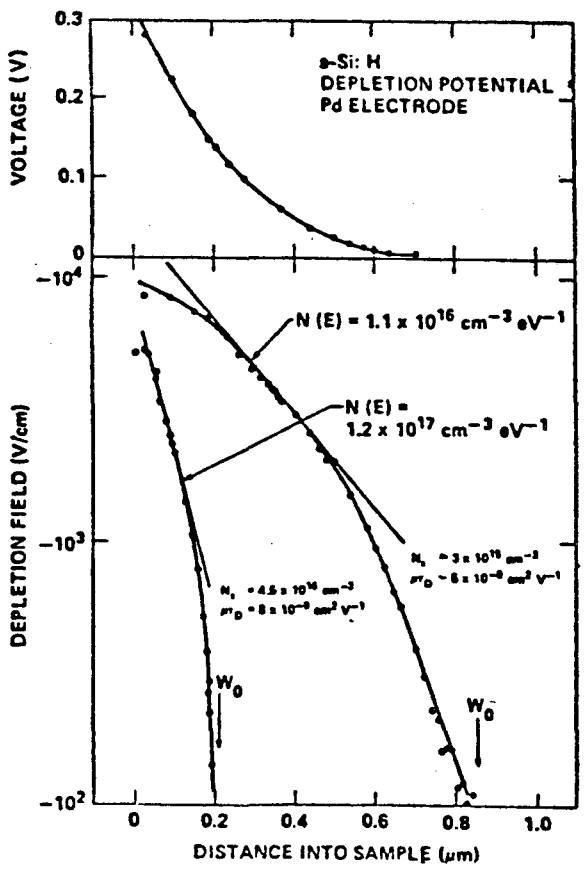

Fig. 2.20. Measurements of the field and potential profiles for two samples with higher defect density and Pd electrodes. The values of N_S are obtained from ESR measurement [Street, 1983].

inside the sample. The transient response under DC bias decreases monotonically as electrons move across the sample.

The shape of the photocurrent transient relates to the shape of the electric field inside the sample and, therefore, to the ionized defect density. This has been demonstrated in the work of Street [1983]. Fig. 2.19 shows the depletion field as a function of depth into sample. The defect density is derived from the exponential region of the field profile.The measurements were done on a-Si:H samples with n+ bottom contact and chromium contact on top of the i layer. Similar measurements made on samples with Pd contacts are shown in Fig. 2.20.

DC photoconductivity measurements on thick p-i-n diodes intended for radiation detection application purposes are of interest to measure the ionized dangling bond density which shapes the electric field in the diode. The electric field, F, is the agent for drifting the charge across the sample and the drift length is given by the product $\mu\tau F$. Since in an a-Si:H detector the electric field is nonuniform, carriers will move across the field region until they reach the low field region. In the low field region motion of charges is determined by diffusion rather than drift and carriers are eventually trapped or they recombine. Therefore, it is safe to assume that the carriers stop at the end of the depletion layer and are not collected. So in an a-Si:H diode the extent of the electric field in the bulk plays a crucial role in its usefulness as a detector.

2.6 Measurement of material parameters

A time of flight experimental setup was built to measure the

material parameters discussed in section 2.5. Fig. 2.21 is a schematic diagram of the setup. My interest was to study the material parameters of thick p-i-n diodes intended for radiation detection applications. Further, these parameters can be measured to better degree of accuracy in thick samples.

The setup consists of a Nitrogen-Dye laser combination. The laser is triggered externally by a trigger pulse from a high voltage pulser. For pulsed bias measurements the trigger pulse is delayed so that laser fires 50-100 μs after bias is applied across the amorphous silicon diode under study. For DC bias measurements

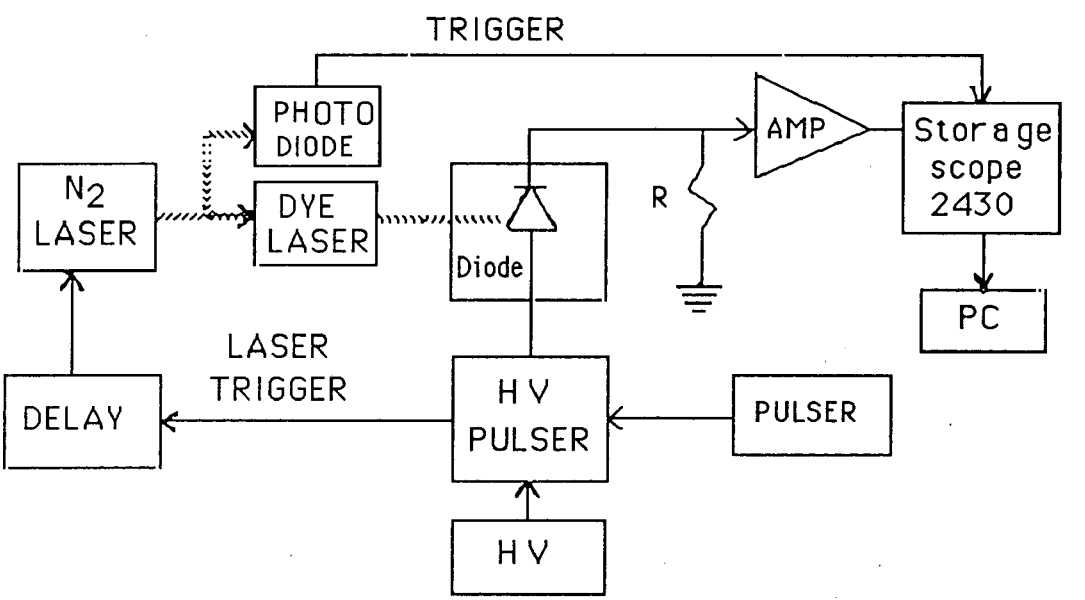

Fig. 2.21. Time of flight experimental setup with Nitrogen-Dye laser unit used to measure material parameters. The laser is 3 ns (FWHM) producing 510 nm light (MFP ~ 0.2 μm in a-Si:H).

diode bias is derived from a regular power supply. The oscilloscope trigger pulse is generated from the light pulse that excites the dye laser by using a photodiode. The signal from the amorphous silicon diode is amplified by a wide-band amplifier before it is fed to oscilloscope for storage and analysis.

2.6.1 Drift mobility measurement

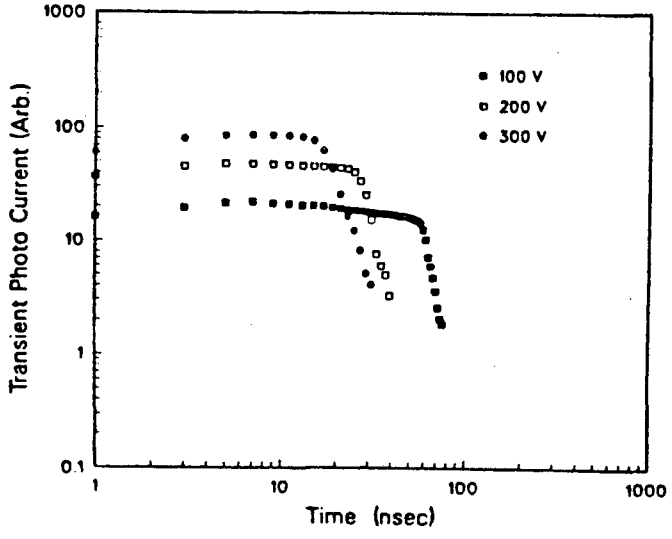

Fig. 2.22 Transient photocurrent electron signal at different pulsed bias voltages using 510 nm light. Non-dispersive transit of electrons across 27 μm p-i-n diode is seen clearly.

Carrier drift mobility is measured by pulsing the bias voltage applied to the diode under study for a duration of ~ 10 ms. The

laser aimed at either the p or n side of the diode is pulsed 50 - 100 microseconds after bias is applied. Pulsing of the bias shortly before the laser pulse is essential to establish a uniform electric field in the diode as explained in section 2.5.1. The transit time for non-dispersive transport where a charge packet spreads by diffusion (electrons at room temperature) is measured from the photocurrent transient as the time when the current falls to 50% value. In this case light is incident on the p side of the sample so that the holes are collected at the same end and the electrons traverse the sample. Fig. 2.22 shows a typical current transient plotted on a log-log plot at different bias voltages.

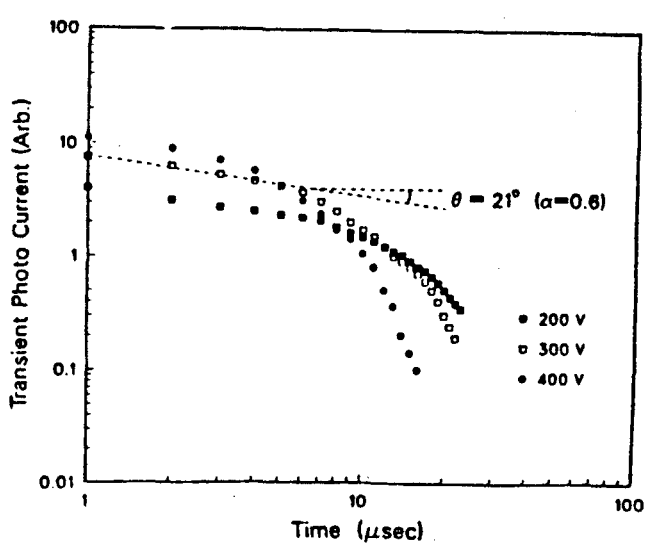

Fig. 2.23. Transient potocurrent hole signal from 27 μm p-i-n diode at different pulsed bias voltages. Hole mobility is dispersive with dispersion parameter $\alpha \sim 0.6$ at 300 V.

Hole transport is dispersive as discussed in section 2.5.3. The transient behaviour in case of dispersive transport is given by eq. (2.18a,b) [Scher et al., 1975]. The transit time is measured by plotting the photocurrent transient on a log-log plot and transit time is taken as the time where the two slopes intersect. Fig 2.23 shows the hole transient at different pulsed bias voltages. A hole dispersion parameter $\alpha \sim 0.6$ was estimated for the sample.

$$I(t) \approx t^{-(1-\alpha)}, \qquad t<t_T \qquad (2.18\ a)$$

$$I(t) \approx t^{-(1+\alpha)}, \qquad t>t_T \qquad (2.18\ b)$$

where the dispersion parameter α is $0 < \alpha < 1$.

2.6.2. Measurement of mobilty-lifetime product ($\mu\tau$)

As discussed in section 2.5.4 the $\mu\tau$ product is measured from a charge collection experiment and fitting collected charge vs bias voltage data to eq. (2.17). Fig. 2.24 shows such a fit to the data. A value of $\mu_e\tau_e = 1.5 \times 10^{-7}$ cm^2/V was obtained.

Similarly, the $\mu\tau$ product of holes is obtained by making a fit to eq. (2.17). A value of $\mu_h\tau_h = 4 \times 10^{-8}$ cm^2/V was obtained for the sample of Fig. 2.24.

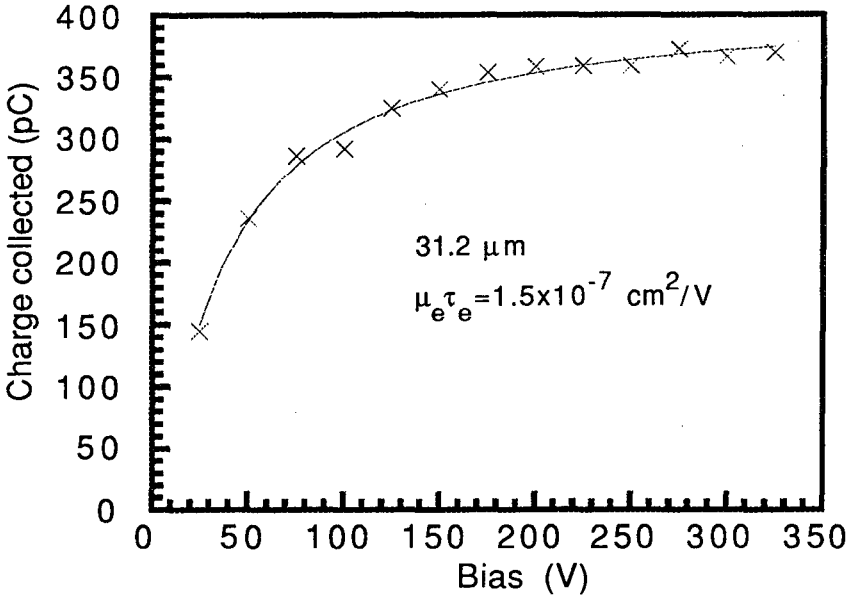

Fig. 2.24. Measurement of electron $\mu\tau$ product through a fit to the Hecht equation.

2.6.3. Defect density measurement

Fig. 2.25 shows a typical DC bias photocurrent transient from which the dangling bond density was calculated using eq. (2.19) [see appendix 2]. For a p-i-n diode values of the ionized defect density were found to be in the range of 6-8x10^{14} cm^{-3}, approximately 1/3 of the defect density measured by ESR.

$$N_d^{\cdot} = \frac{\varepsilon_0 \varepsilon_r}{q\mu} \frac{\ln\,[i_{dc}(t_1) / i_{dc}(t_2)]}{t_2 - t_1} \qquad (2.19)$$

where N_d^* is the ionized dangling bond density. $i_{dc}(t_1)$ and $i_{dc}(t_2)$ are the values of the decaying photocurrent transient at times t_1 and t_2, μ is the mobility, ε_r is the relative permitivity of silicon and q is the electronic charge.

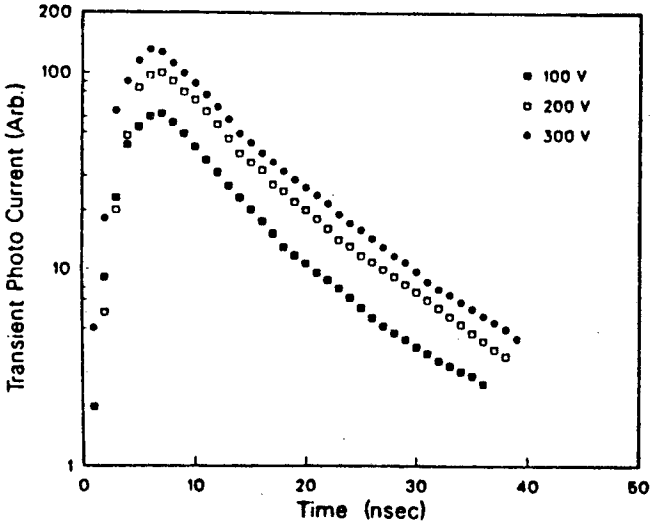

Fig. 2.25. Transient photocurrent electron signal at different DC bias voltages from a 27 μm p-i-n diode using 510 nm light.

Table 2.1 summarizes typical values of material parameters measured on thick a-Si:H p-i-n diodes in a T.O.F experiment. Electron spin density is also listed.

Thickness (μm)	28	27	31.2
Type	Cr-n-i-p	SnO-p-i-n	SnO-p-i-n
μ_e (cm^2/Vs)	1.4	1.2	1.2
$\mu_e \tau_e$ (cm^2/V)	1.1×10^{-7}	1.2×10^{-7}	1.5×10^{-7}
μ_h (cm^2/Vs)	0.003	0.004	0.004
$\mu_h \tau_h$ (cm^2/V)	2.7×10^{-8}	1.2×10^{-8}	4×10^{-8}
N_d^* (cm^{-3}) (TOF)	6×10^{14}	7×10^{14}	-
N_d (cm^{-3})(ESR)	2×10^{15}	-	-

Table 2.1. Typical measured parameters of thick a-Si:H p-i-n diodes from a number of diodes studied using setup of Fig. 2.21. Defect density measurement on 31.2 μm diode could not be done due to large diode capacitance. Carrier mobility and mobility-lifetime product values are in agreement with values reported in literature on thin a-Si:H diodes. ESR measurements were done at Xerox PARC. Cr and SnO represent Chromuim and Tin Oxide contacts.

The value of the ionized defect density, N_d^*, obtained for a-Si:H p-i-n diodes by this method is ~1/3 of the defect density value, N_d, measured by ESR which measures the density of neutral defects in the sample. The same result was obtained by increasing the defect density of a sample by a factor of ~ 2 by heating and then measuring N_d^* and N_d. A comparison of N_d^* and N_d values on subsequent annealing further corroborated the result that only a fraction of the defects (~ 1/3) is ionized when diode is biased into deep depletion.

This result can be explained on the basis of the energy of the defects and on the shift of the Fermi energy which results from the depletion bias. On depletion the Fermi energy must move down towards the center of the band gap of the i layer as it is slightly n type. The observed ionized fraction would correspond to a shift of the Fermi energy of ~ 0.1 eV [Qureshi et al., 1989].

However, the work of Matsuura [1988] who used c-Si-i-n structure for defect density measurement by heterojunction-monitored capacitance (HMC) method shows that the measured defect density is in agreement with the ESR measurement though the work of Street et al. [1990] is in support of the observation that only a fraction of the defects are ionized. This underscores the caution required in interpreting the defect density and field profile measurements by DC photoconductivity method for a-Si:H p-i-n structure. Whether the effect can be the result of the sample structure (e.g. high resistivity of the p layer effecting how rapidly the DC bias transient falls) might be worth further investigation.

A quantity of interest, the $\mu\tau N_d$ product, follows from the basic expression relating the capture processes with the trap-limited transport in amorphous semiconductor. Street [1982, 1984] has shown that this product is given by [appendix 3]

$$\mu\tau N_d \cong \frac{1}{6}\frac{e}{kT}\frac{a}{\sigma} \qquad (2.20)$$

where a is the carrier scattering length (in a-Si:H ~ 10 A° for

electrons and ~5 A° for holes), σ is the capture cross section and T is the temperature. The product $\mu\tau N_d = 2.2 \times 10^8$ $cm^{-1}V^{-1}$ is calculated for electrons from column 2 of Table 2.1.

3 Leakage current and noise of a-Si:H p-i-n diode

The current-voltage (I-V) characteristics of a reversed biased a-Si:H diode is of considerable interest for two reasons.

1. The leakage current is important for noise considerations when the diode is used as a radiation detector.
2. Power dissipation in a diode array especially when used as small high density pixels must be kept to a minimum.

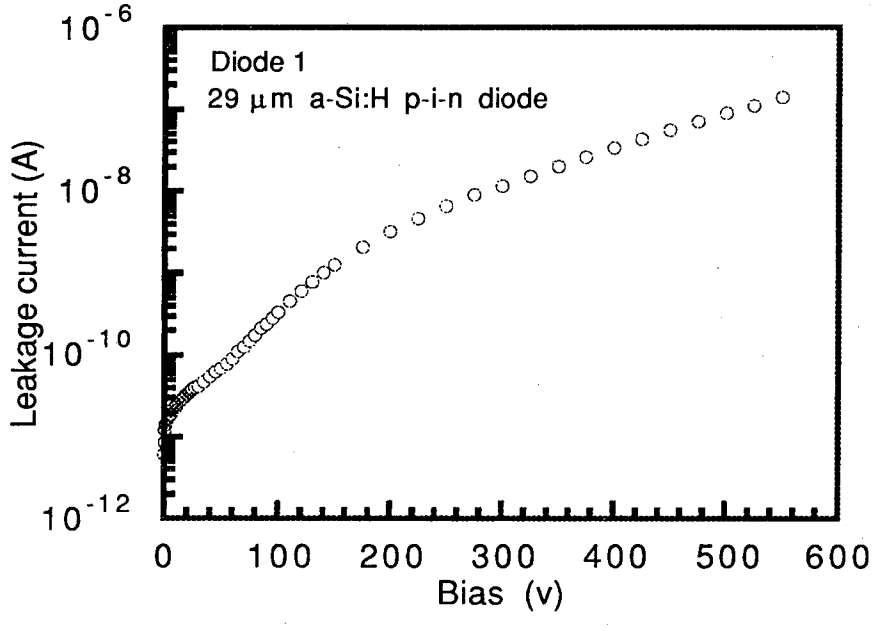

Fig. 3.1(a). Typical I-V curve of an a-Si:H diode under reverse bias. The area around the metallic dot on its face was etched to prevent any surface leakage.

The I-V characteristics of a large number of a-Si:H p-i-n diodes fabricated by glow discharge deposition have been studied. Typical I-V characteristics under reverse bias are shown in Fig. 3.1(a,b). Fig. 3.1(b) is a plot of I vs V on a log-log plot. The plot has

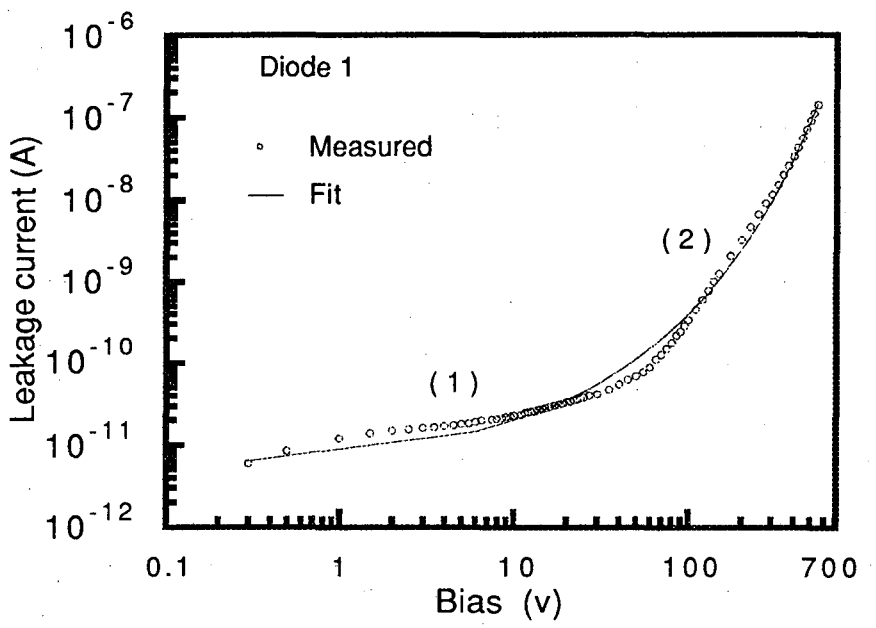

Fig. 3.1(b). I-V curve of diode 1 on log-log plot. Eq. (3.1) fits the data with fitting parameters $k_1 = 5.028 \times 10^{-12}$ and $k_2 = 0.437$.

two distinct regions labelled as (1) and (2). The region (1) is low bias region extending from 0.3 to 50 V. Region (2) extends from 50 to 550 V where current increases monotonically over the voltage range. The measured data is fitted to eq. (3.1).

$$I = k_1 \exp (k_2 \sqrt{V}) \tag{3.1}$$

where V is the bias voltage. k_1 and k_2 are fitting parameters. As is seen in Fig. 3.1(b) the above equation fits the data remarkably well particularly at high bias voltage.

Table 3.1 shows measured and calculated noise (FWHM) of the diode. The leakage current and noise listed in the table were measured on the setup shown in Fig. 3.2. An LBL dual shaping amplifier with CR-$(RC)^4$ (pseudo-Gaussian) shaping [Goulding, 1972] at 3 μs shaping time was used. The charge sensitive preamplifier used was a Tennelec TC 171 with no shaping.

The noise in column 3 of Table 3.1 was calculated from the shot noise equation [Goulding et al., 1982].

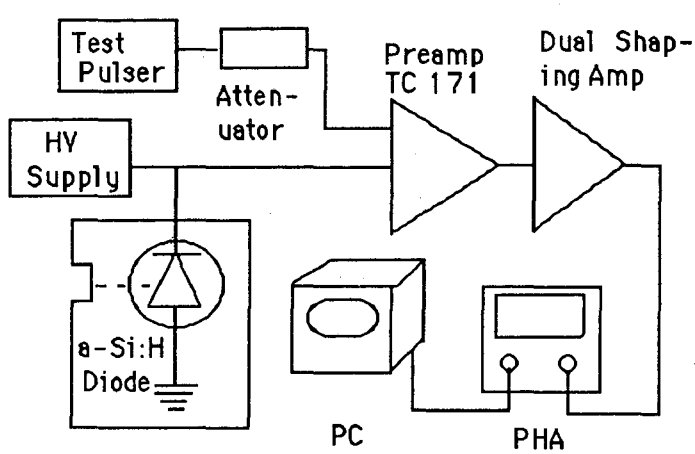

Fig. 3.2. Schematic of experimental set up used for measurement of leakage current and noise listed in Table 3.1.

bias (V)	current (A)	N_{cal} (e-)	N_m (e-)
0	0	-	4000
100	7×10^{-10}	4007	4200
200	6×10^{-9}	4068	4170
300	2.3×10^{-8}	4253	4320
400	6.2×10^{-8}	4652	4650
500	1.5×10^{-7}	5445	5450
550	2.35×10^{-7}	6110	5950

Table 3.1. Measured and calculated noise (FWHM) for 29 μm diode of Fig. 3.1. The noise is calculated from the shot noise equation for the LBL dual shaping amplifier with CR-$(RC)^4$ (pseudo-Gaussian) shaping at 3 μs shaping time as discussed in the text. A remarkable agreement is seen between the measured and calculated noise.

$$\langle N^2_s \rangle = 0.9 \frac{I\tau}{q} \tag{3.2}$$

where τ is the shaping time, I is the leakage current and q is the electronic charge, and the noise component at 0 V bias added in quadrature. It is seen that the measured noise agrees remarkably well with the calculated noise. This shows that for a well behaved a-Si:H p-i-n diode, noise is completely accounted for by the shot noise and the noise component at 0 V bias for CR-$(RC)^4$ (pseudo-Gaussian) shaping at 3 μs shaping time. A sample calculation of the

noise at 400 V bias is given below.

Sample calculation of noise at 400 V bias:
The shot noise equation for CR-RC shaping is given by

$$\langle N^2_s \rangle = \frac{\varepsilon^2}{4q} I\tau$$

where I is the leakage current, τ is the shaping time, q is the electronic charge and ε =2.718. The above equation can be written as

$$\langle N^2_s \rangle = 1.153 \times 10^{13}\ \tau\ (\mu s)\ I(A) \qquad (rms)^2 \qquad (3.3)$$

At 400 V bias I = 6.2×10^{-8} A and τ = 3 μs.
Therefore, $\langle N^2_s \rangle = 3.459 \times 10^{13} \times 6.2 \times 10^{-8} = 2.14 \times 10^6$
For CR-$(RC)^4$ shaping we have [Goulding, 1972]

$$\frac{\langle N^2_s \rangle_{CR-RC^4}}{\langle N^2_s \rangle_{CR-RC}} = \frac{0.9}{1.87} = 0.48$$

Therefore, $$\langle N^2_s \rangle_{CR-RC^4} = 0.9\ \frac{I\tau}{q} = 0.48 \times 2.14 \times 10^6$$

$$\langle N_s \rangle = 0.69 \times 1.463 \times 10^3 \quad (rms)$$
$$= 1009.3\ (rms)$$
$$= 1009.3 \times 2.35 = 2372\ e^- \quad (FWHM)$$

Therefore, $$N_{cal} = \sqrt{[4000^2 + 2372^2]} = 4650\ e^-\ (FWHM)$$

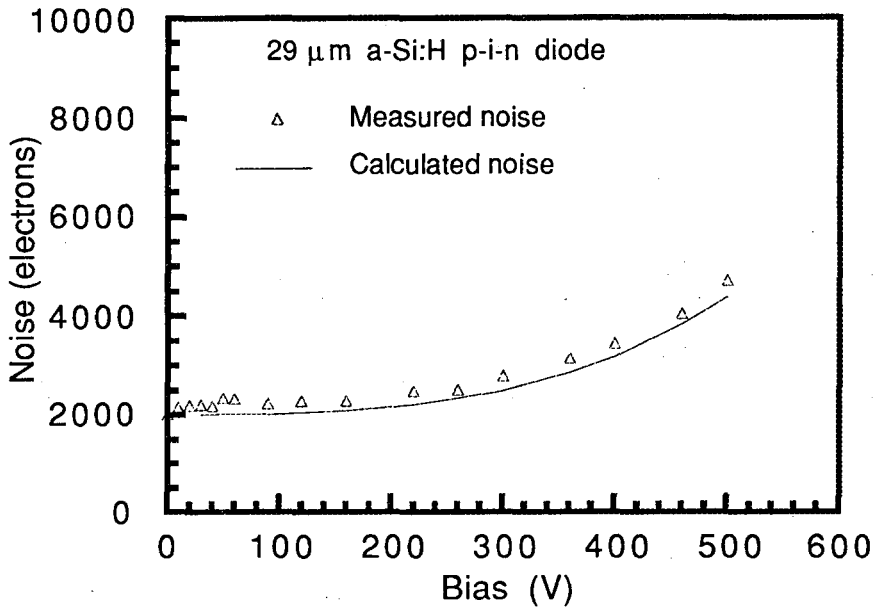

Fig. 3.3. Measured and calculated noise (FWHM) on another 29 μm diode from the same production run as diode 1 for 3 μs shaping time and CR-$(RC)^4$ shaping. Here noise at 0 V bias is lower by a factor of 2.

Fig. 3.3. shows the calculated and measured noise of a 29 μm p-i-n diode having smaller noise component at 0 V. It is seen that the calculated noise closely follows the measured noise over the operating voltage range of the diode. The noise data is listed in Table 3.2.

bias (v)	current (nA)	N_{cal} (e^-)	N_m (e^-)	bias (v)	current (nA)	N_{cal} (e^-)	N_m (e^-)
0	0	-	2005	160	3.6	2085	2284
10	-	-	2157	220	9.5	2209	2482
20	-	-	2190	260	15.7	2334	2517
30	0.1	2007	2205	300	24.6	2501	2799
40	0.1	2007	2172	360	45.3	2853	3158
50	0.2	2010	2341	400	67	3180	3443
60	0.3	2011	2325	460	117	3839	4046
90	0.7	2020	2224	500	167	3897	4382
120	1.6	2041	2288				

Table 3.2. Calculated and measured noise at 3 μs shaping time for a 29 μm a-Si:H p-i-n diode using an LBL dual shaping amplifier with CR-$(RC)^4$ shaping.

The I-V curve of the diode is shown in Fig. 3.4. The eq. (3.1) is fitted to the data as shown in the figure. The increase in leakage current with bias described by eq. (3.1) has the same dependence on voltage as one would expect if this increase were due to the Poole-Frenkel effect [Hill, 1971] involving excitation of carriers from neutral defects. In the Poole-Frenkel effect the ionization energy of a defect center is decreased by the applied field F, in the direction of the field by $\beta F^{1/2}$. Electron emission can take place over

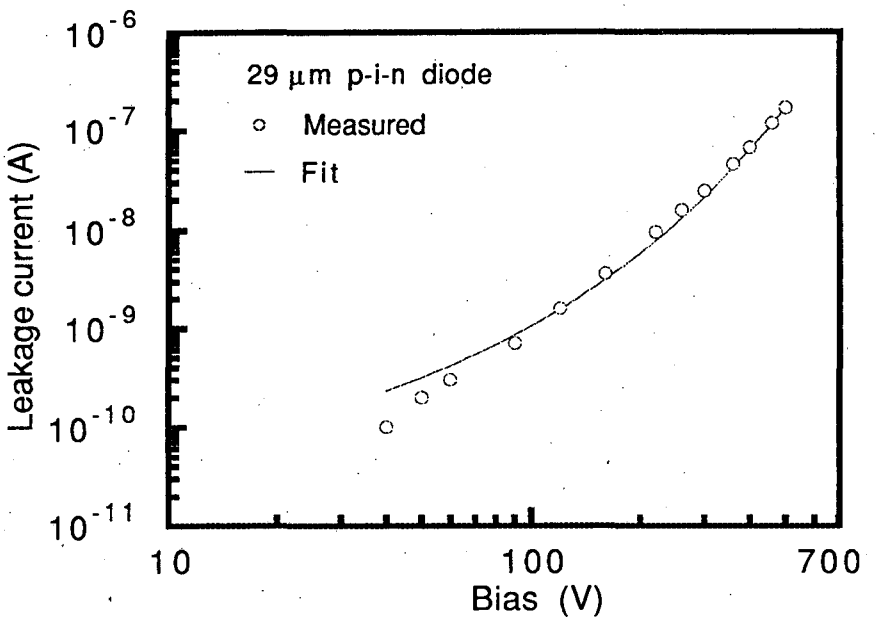

Fig. 3.4. I-V curve of a 29 μm diode under reverse bias. The noise data is listed in table 3.2. The data is fitted to eq. (3.1). The fitting parameters are $k_1 = 1.745 \times 10^{-11}$ and $k_2 = 0.41$.

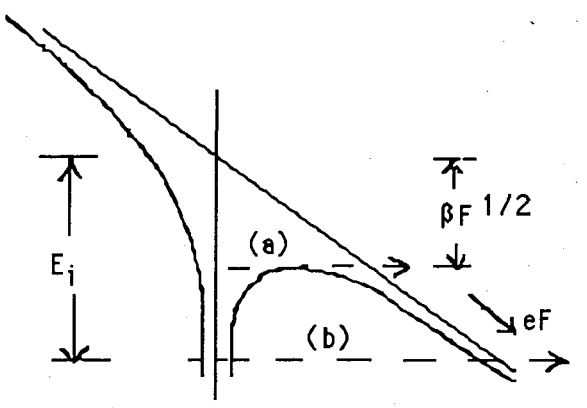

Fig. 3.5. The Poole-Frenkel effect. The ionization energy, E_i, of a defect center is decreased by the applied field F, in the direction of the field. The coefficient β is the Poole-Frenkel constant [Hill, 1971].

the top of the reduced barrier as in (a), or by tunnelling as in (b) of Fig. 3.5.

These measurements clearly suggest that in real devices the detector leakage current for a well behaved diode at the operating bias is the dominant contributor to noise in the form of shot noise for CR-$(RC)^4$ shaping.

The noise at 0 V bias is contributed by two factors. One is the result of loading of the diode capacitance on the charge sensitive amplifier commonly known as the delta noise, given by [Goulding et al., 1982].

$$\langle N^2_\Delta \rangle = \frac{kT\, C^2\, \varepsilon^2}{2q^2\, \tau\, g_m} \tag{3.4}$$

where C is the equivalent capacitance of the diode and the amplifier input stage, τ is the shaping time , g_m is the transconductance, k is the Boltzman constant and q is the electronic charge. The second noise component is due to thermal noise. This noise component needs to be probed further.

Further, as diode area is reduced , say by a factor of 10, one expects from equations (3.3) and (3.4) a reduction in the step (shot) and delta noise approximately by factors of 3.16 and 10 respectively making the contribution of step noise component more dominant.

4 Radiation hardness of a-Si:H

Radiation hardness is an important consideration when a device is to be used in a high radiation environment. Crystalline Si radiation detectors are known to degrade in their performance on prolonged exposure to radiation. One important consequence of irradiation is the introduction of energy levels in the band gap which then act as traps for the carriers causing a reduction in the carrier lifetime and change in the electrical resistivity of the device. The reverse leakage current increases and so does the noise of the device. These effects are seen in crystalline silicon detectors at particle (neutron) fluences $\sim 10^{12}$ cm^{-2}. This degradation of the device in a high radiation environment is undesirable from performance and economic considerations. It is of particular concern in high energy accelerator applications.

Hydrogenated amorphous silicon diodes have been shown to be significantly less susceptable to radiation damage owing to their inherent disorder. Most of the early studies were done on thin diodes (~ 1 μm) for solar cell applications.

4.1 Radiation damage by electrons and alpha particles

Street [1979] has shown that the damage caused by 1 Mev electrons and 100 Kev alpha particles is predominantly in the creation of singly occupied D^0 dangling bonds and the broadening of the tail

state distribution. Both of these effects can be annealed out. The radiation induced effects were studied by electron spin resonance and luminescence. It was found that the electron or ion bombardment introduced defects which were predominantly singly occupied dangling bonds (D^0) which acted as recombination centers and quenched the photoluminescence in a-Si:H. The trend was seen to reverse on annealing.

The damage due to energetic electrons and ions is primarily the displacement of nuclei. The maximum fractional energy transfer is given by $4mM/(m+M)^2$. Since a-Si:H has two types of atoms (hydrogen ~ 10%) collision with both types of atoms results although energy transfer in electron-hydrogen collision is more than in electron-silicon collision. The removal of hydrogen results in a single dangling bond and because of small size of hydrogen atom reconstruction of Si bonds is less likely to occur. Due to the strength of the Si-H bond hydrogen will bond to the Si network. On the other hand a displaced Si atom is likely to leave behind a divacancy and a weak bond which results in localized energy states in the gap [Street ,1979].

4.2 Radiation damage by gamma rays

Recently gamma ray irradiation effects on undoped a-Si:H from 10^{16}-10^{17} photons cm^{-2} using a Co^{60} source have been reported by Imagawa et al. [1989]. This study showed a significant increase of D^+ defect centers on irradiation which could partly be annealed out.

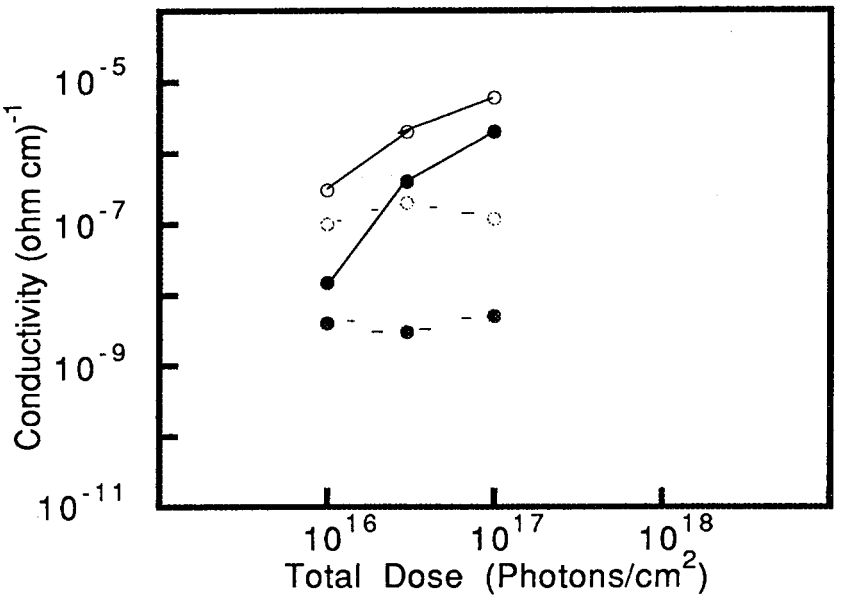

Fig. 4.1. Dark conductivity (closed circles) and photo conductivity (open circles) as a function of gamma ray total dose. Solid line : after irradiation; broken line : after annealing at 180° C for 2 hours [Imagawa et al., 1989].

The photo and dark conductivities increased by two orders of magnitude after irradiation as shown in Fig. 4.1. The activation energy (see section 2.4.4) decreased from 0.7 eV to 0.4-0.5 eV by gamma ray irradiation as shown in Fig. 4.2 and the samples were found p type which meant that the Fermi energy moved down towards the valence band and this behavior was due to the change of charge states of the defects from D^0 to D^+. Table 4.1 shows the dependence of the D^0, D^-, D^+, and total defects on the total dose . The data listed in the table shows that the total defects and the neutral dangling

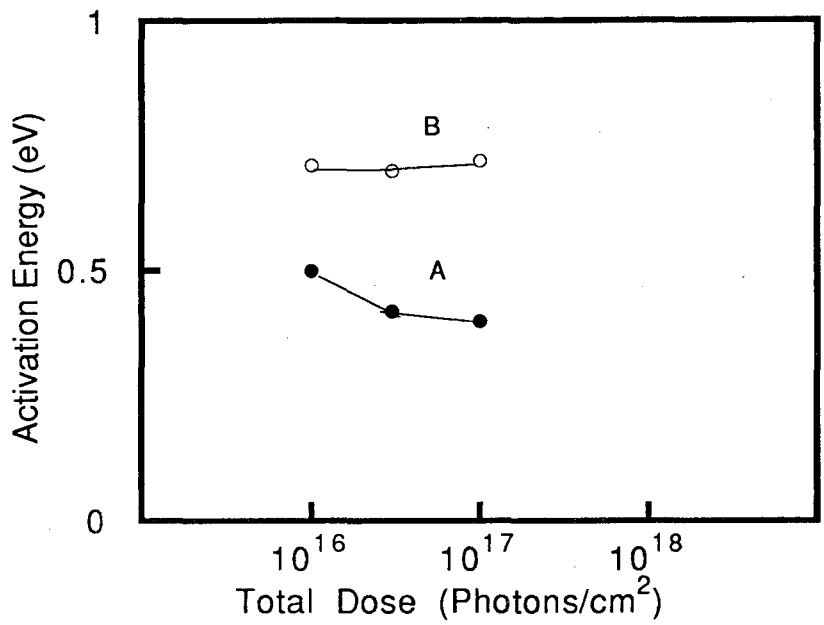

Fig. 4.2. Activation energy of the dark conductivity as a function of gamma ray dose. Curve A: After irradiation; curve B: after annealing at 180° C for 2 hours [Imagawa et al., 1989].

Total dose (photons/cm^2)	Gap states (cm^{-1} eV^{-1})				
	THS ($D^0 + D^-$)	TES ($D^0 + D^+$)	$D^- - D^+$	$D^+ + D^-$	Total defects
0	1.9×10^{16}	1.3×10^{16}	6×10^{15}	-	3.2×10^{16}
10^{16}	1.2×10^{15}	2.6×10^{16}	-	1.4×10^{16}	3.8×10^{16}
10^{17}	8.4×10^{15}	3.2×10^{16}	-	2.4×10^{16}	4×10^{16}

Table 4.1. The dependence of the D^0, D^-, D^+, and total defects on the total dose. THS is trapped hole states and TES is trapped electron states [Imagawa et al., 1989].

bonds D^0 do not change appreciably after irradiation although D^+ defects increase. This feature is consistant with the lowering of the Fermi energy for p-type behaviour and the increase in conductivity on irradiation with gamma ray photons.

The defect creation mechanism due to energetic gamma rays is expected to be due to electronic excitation and direct atomic displacement although the effect due to the latter should be less dominant because of no direct momentum transfer. The increase in the D^+ defect centers is interpreted as the result of change in the charge states of already existing dangling bonds (D^0 and D^-) by the processes $D^0 \rightarrow D^+ + e$ and $D^- \rightarrow D^0 + e$ and since the increase in the D^0 states is small it is believed that the dominant effect of gamma ray irradiation is due to electronic excitation unlike the case of electron or ion irradiation which cause atomic displacement.

4.3 Radiation damage by neutrons

Radiation damage of a-Si:H p-i-n diodes was studied using 1 Mev neutrons from the Triga reactor facility at U. C. Berkeley. Neutron irradiation causes displacement damage in the material. An elastic or inelastic collision with a nucleus can result in displacement of an atom from its position. The threshold energy for displacement in Si is ~ 15 eV [Sandia report, 1985]. In many collisions the energy transferred to a knock-on atom is large so that its collision with other atoms causes secondary displacements. The total displacement cross section, σ_d, of neutrons for Si is shown in

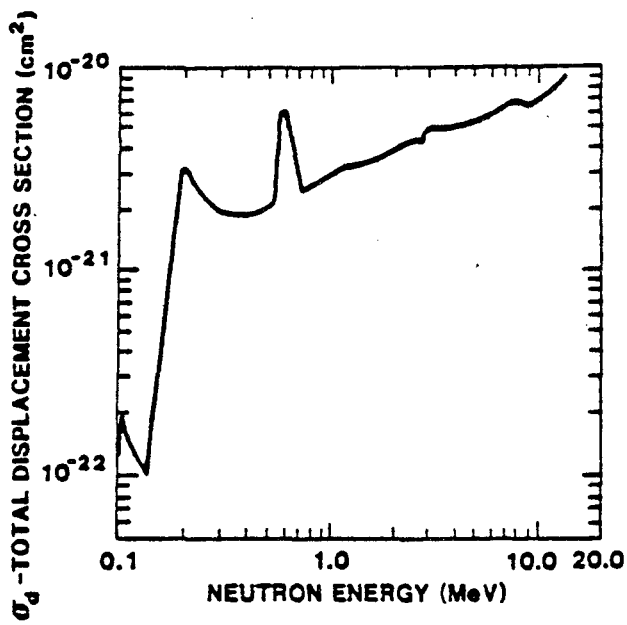

Fig. 4.3. Displacement cross section (including primary and secondary displacements) vs neutron energy for silicon [Sandia report, 1985].

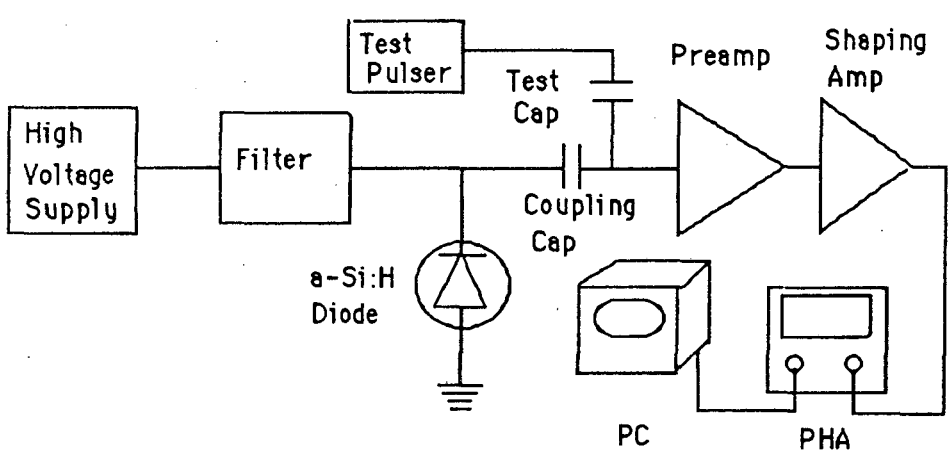

Fig. 4.4. Schematic of the setup used for leakage current and noise measurement.

Fig 4.3.

The total number of displacements n per unit volume is given by

$$n = \Phi N_A \sigma_d$$

where Φ is the particle fluence, N_A is the atom density and σ_d is the total displacement cross section.

Neutron fluences were measured by standard Ni activation techniques. The damage studies were done on 5 μm and 12 μm thick a-Si:H p-i-n diodes, irradiated with neutron fluences ranging from 10^{12} to ~ $4x10^{14}$ cm^{-2}. The damage was studied in terms of changes in leakage current, noise, and ability to detect alpha particles. The effect on defect density could not be measured because the tin oxide coating on glass substrate of the samples masked the ESR signal.

Experimental setup used for leakage current, noise and signal measurement is shown in Fig. 4.4. The noise calibration was done using two test pulse amplitudes superimposed on each measurement of signal and noise. The 5 μm diodes were exposed in steps to fluences of 10^{12} cm^{-2} and 10^{13} cm^{-2}. The pulse height spectrum of the alpha signal before irradiation and after 10^{13} cm^{-2} exposure is shown in Fig. 4.5(a,b). It is clear that there is no appreciable degradation of signal and noise of the diodes.

A more detailed experiment was done on 12 μm diodes exposing them in steps to fluences ranging from $5x10^{12}$ cm^{-2} to ~ $4x10^{14}$ cm^{-2}. The leakage current, noise and alpha signal from 6 Mev alpha

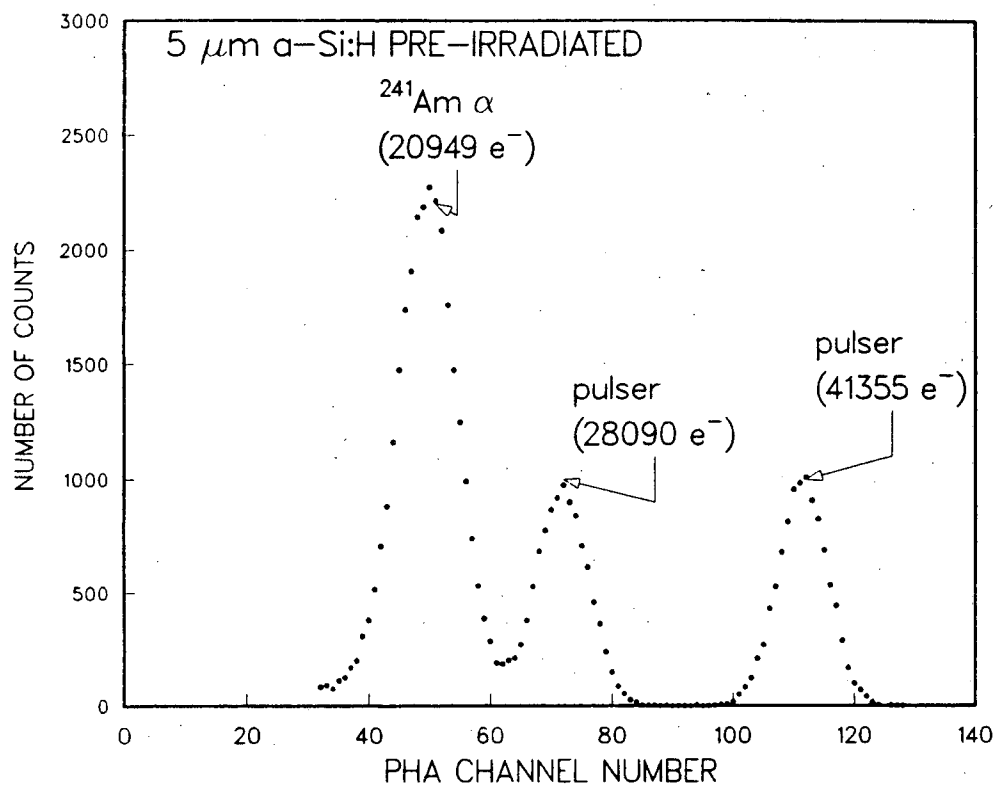

Fig. 4.5(a). Pulse height spectrum of 6 Mev alpha signal before irradiation.

source measured after each exposure are shown in Fig. 4.6(a,b). There is no degradation in noise while a 20% change in alpha signal is seen. The leakage current increases by a factor of 10 at low bias voltage. The samples were annealed at 180° C for two hours. The diodes fully recovered after annealing and their performance was indistinguishable from that before irradiation. An intermediate ann-

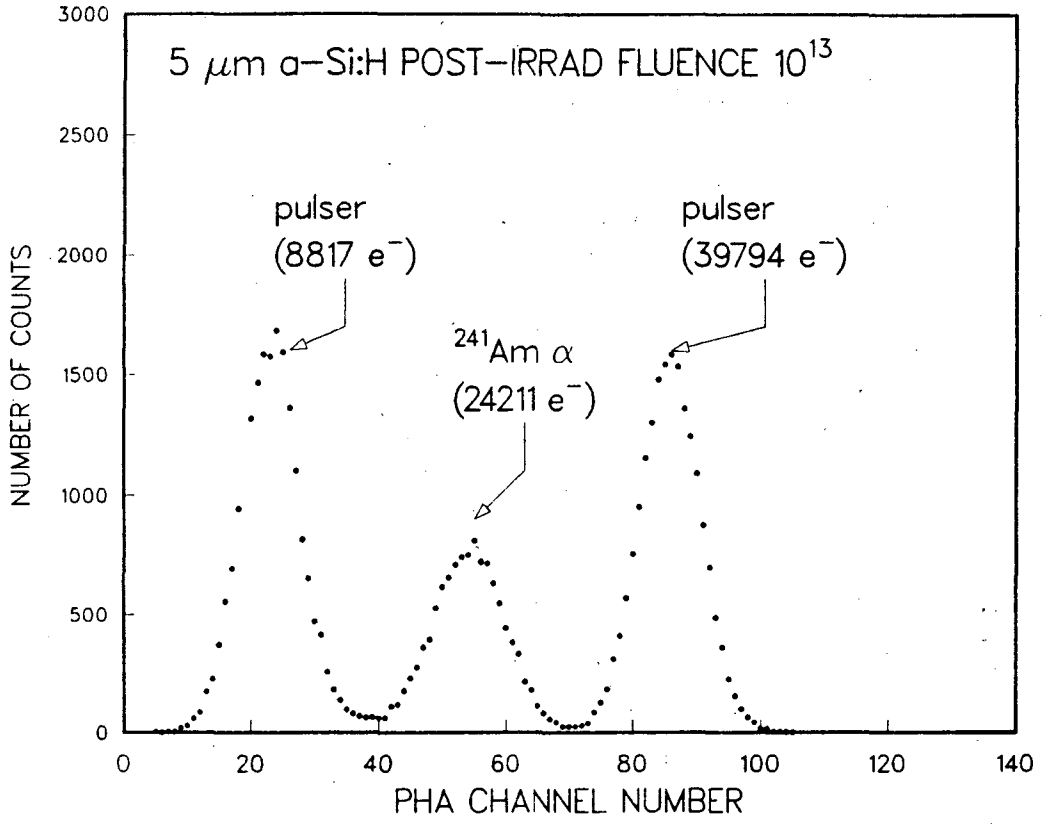

Fig. 4.5(b). Pulse height spectrum of 6 Mev alpha signal after 10^{13} cm^{-2}, 1 Mev neutron exposure. The signal pulse width broadened by a factor of 2. The detector was mounted at 60° to the alpha particle direction. The 20% difference in alpha signal from pre-irradiated value is probably due to uncertainty in angular orientation.

ealing procedure done after 8.9×10^{13} cm^{-2} fluence did not influence the result. It is believed that annealing enhances motion of hydrogen in the network and facilitates reconstruction of broken bonds [Crandall, 1989].

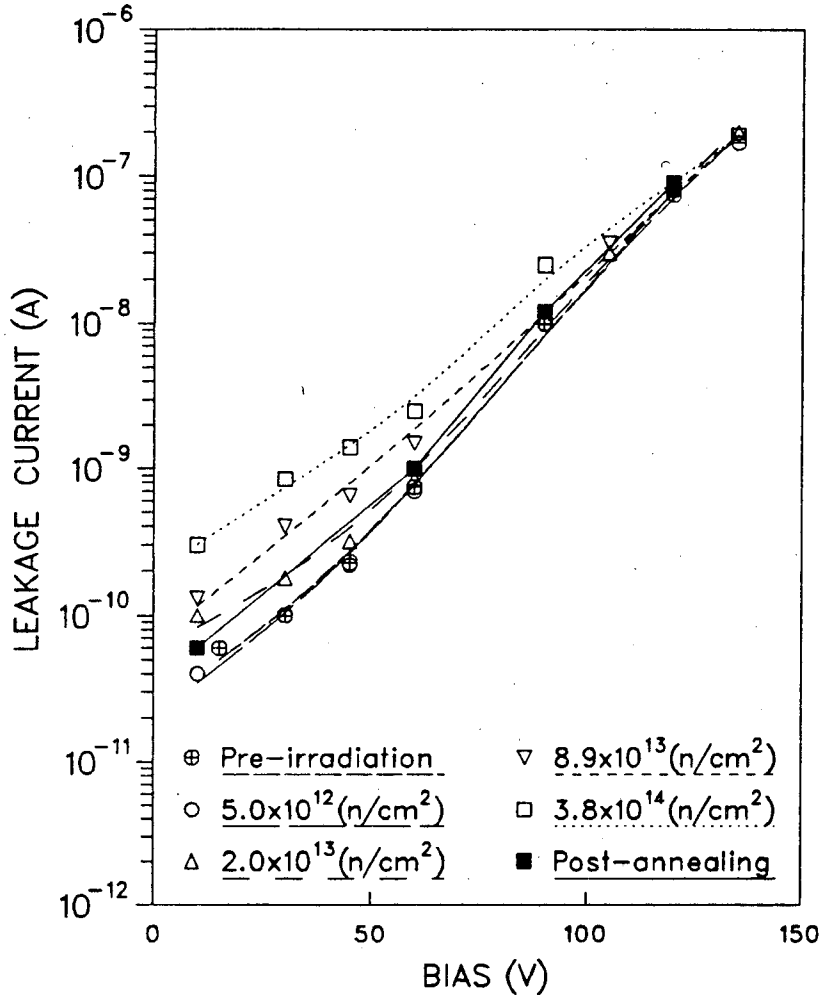

Fig. 4.6(a). Degradation in leakage current of a 12 μm p-i-n diode on exposure to 5×10^{12} - 4×10^{14} cm^{-2} fast neutron fluences. The curves are drawn with the smoothing routine of CA-Tellagraf [Computer Associates, San Diego, CA].

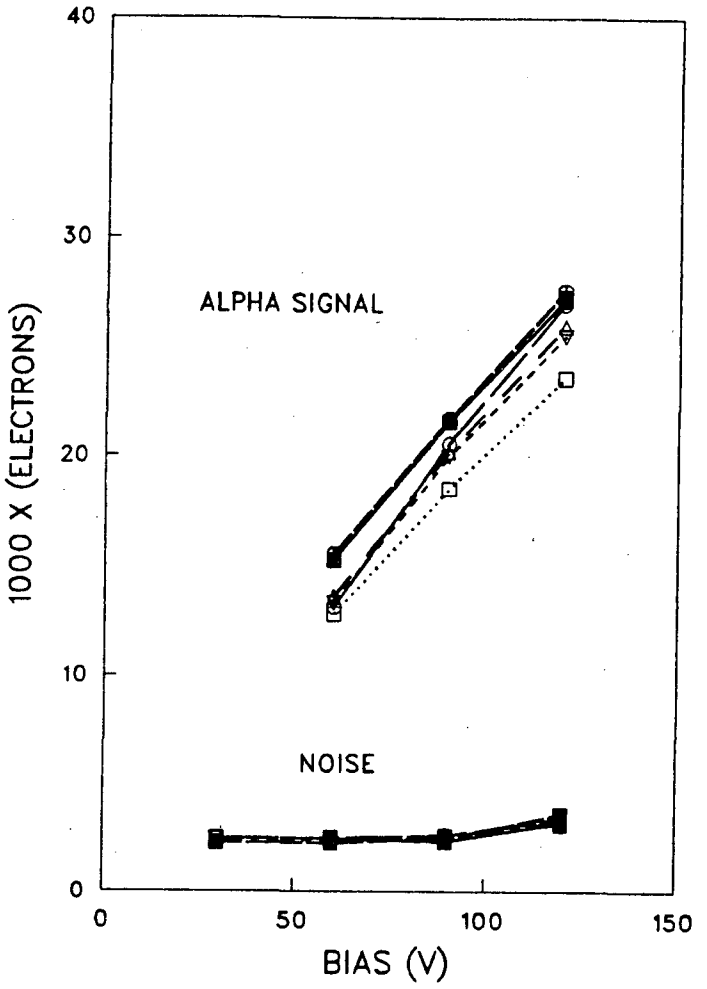

Fig. 4.6(b). Degradation in noise of a 12 μm p-i-n diode on exposure to $5x10^{12}$ - $4x10^{14}$ cm^{-2} fast neutron fluences. Effect of exposure on 6 Mev alpha signal is also seen. The curves are drawn with the smoothing routine of CA-Tellagraf [Computer Associates, San Diego, CA].

For comparison, a crystalline diode, 255 μm thick, was irradiated under identical circumstances. The effects on leakage current, noise and alpha signals were studied. Fig. 4.7 shows the degradation in leakage current at 10^{12} and 10^{13} cm^{-2} fluences.

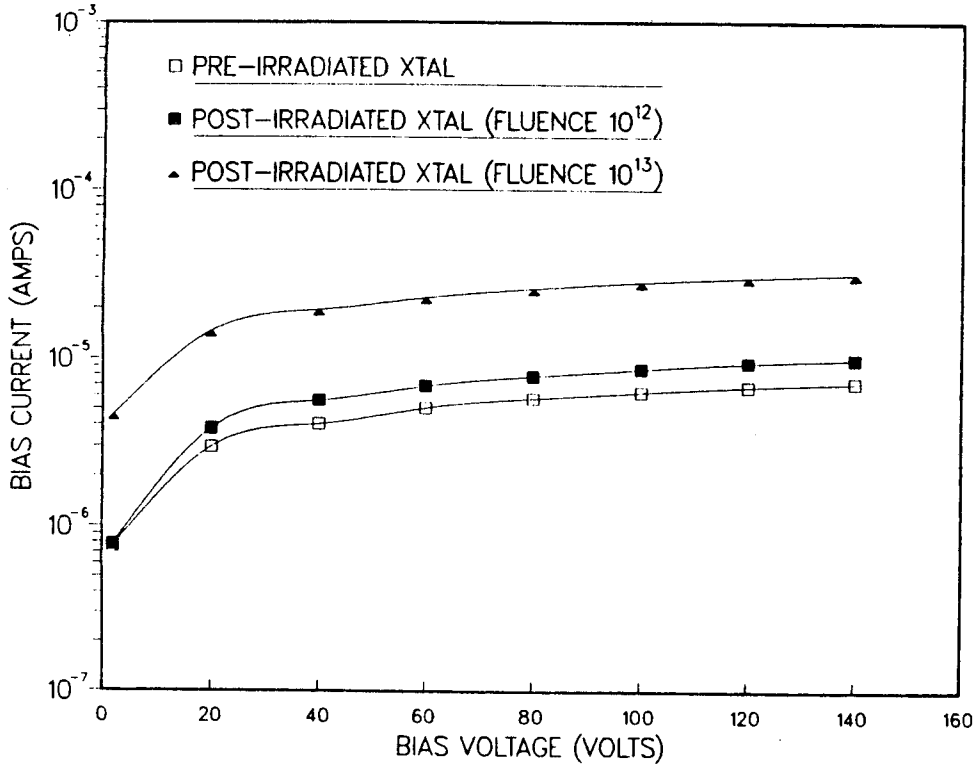

Fig. 4.7. Effect of $1x10^{12}$ and $1x10^{13}$ cm^{-2} fast neutron fluences on leakage current of a 255 μm crystalline diode. Leakage current increases by about a factor of 5 for $1x10^{13}$ cm^{-2} fluence. The curves are drawn with the smoothing routine of CA-Tellagraf [Computer Associates, San Diego, CA].

Fig. 4.8(a,b,c) shows the effect on noise and alpha signal at 10^{12} and 10^{13} cm^{-2} fluences. Some degradation in noise and signal was seen at 10^{12} cm^{-2} fluence. However, at 10^{13} cm^{-2} fluence the diode failed. No alpha signal was detected. The experiment was repeated with another crystalline diode and the effects were reproducible.

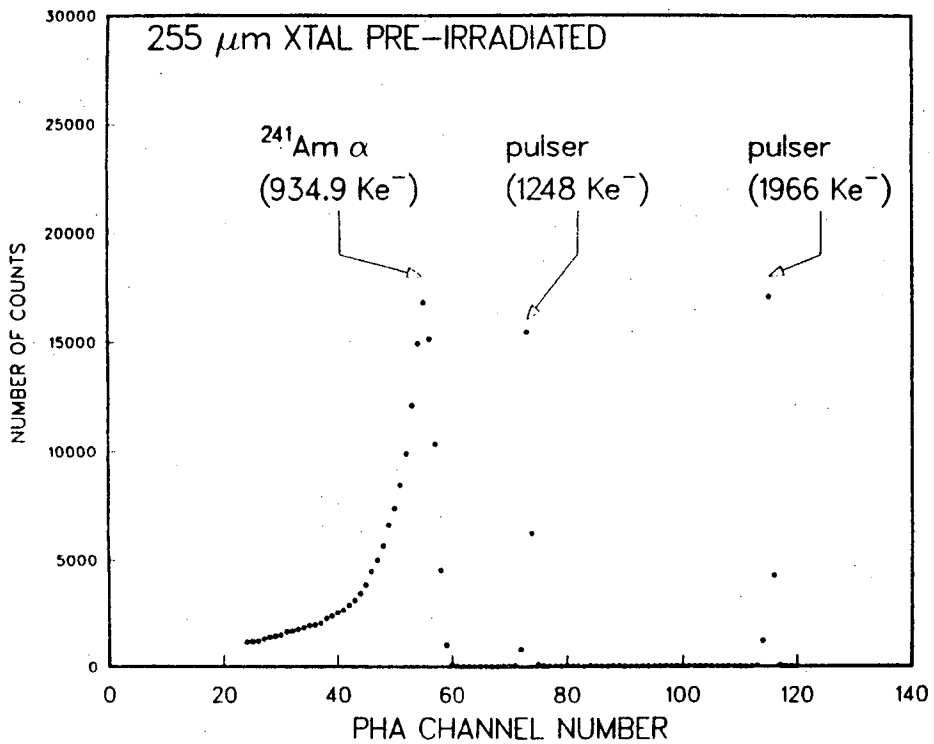

Fig. 4.8(a). Alpha signal in a 255 μm crystalline diode before irradiation.

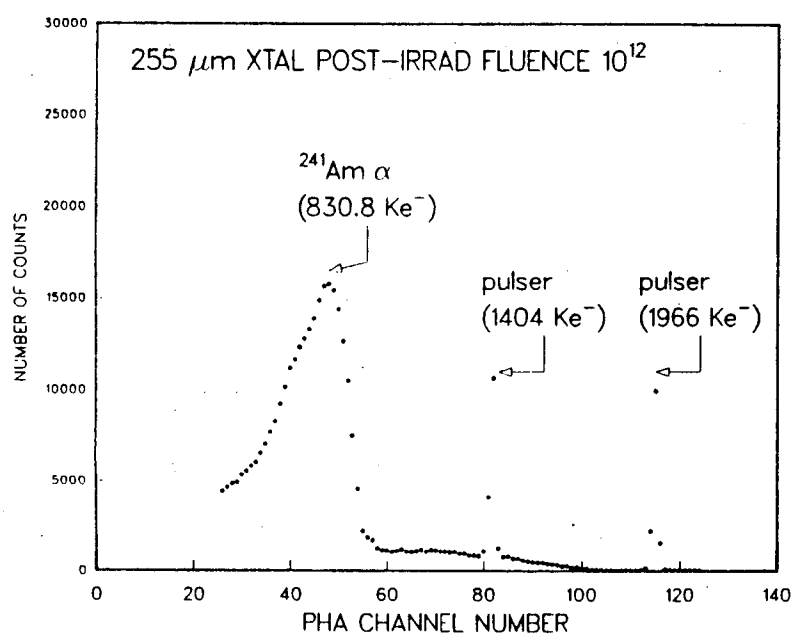

Fig. 4.8(b). Alpha signal after irradiation with 1×10^{12} cm^{-2} fast neutron fluence. About 10% degradation in signal size was observed.

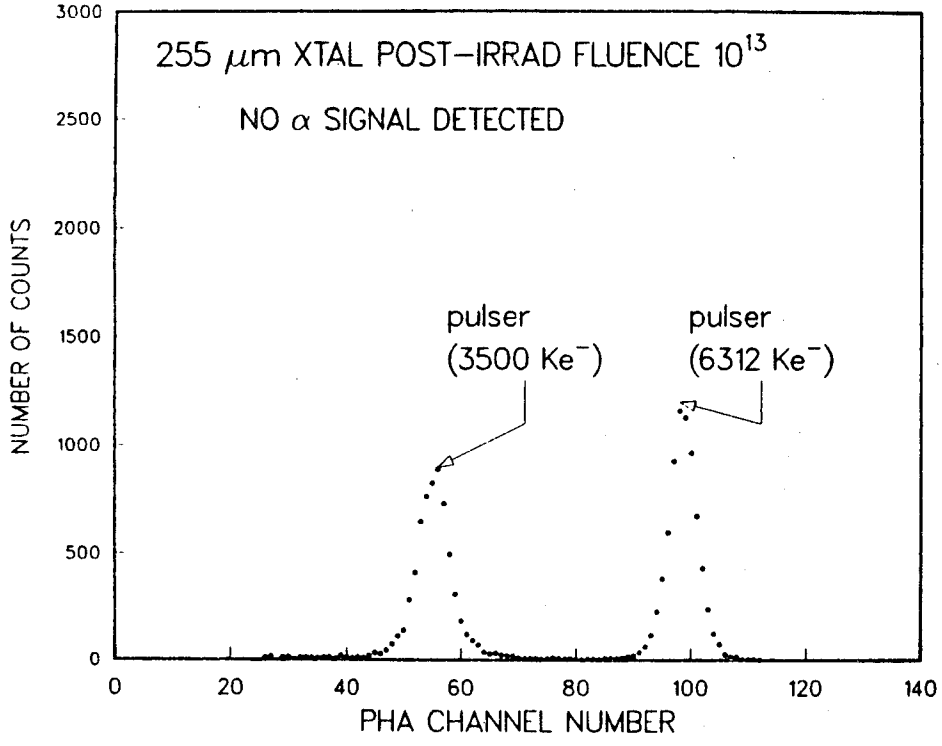

Fig. 4.8(c). No alpha signal is detected after irradiation with 10^{13} cm^{-2} neutron fluence. Significant degradation in diode noise is observed.

In conclusion, the neutron irradiation experiment revealed that a-Si:H diodes are appreciably radiation resistant to 1 Mev neutron fluences in excess of $4x10^{14}$ cm^{-2}. This was not found to be the case with crystalline diodes which failed at 10^{13} cm^{-2} fluence. These results were published in part in [Perez-Mendez et al., 1987] and [Perez-Mendez et al., 1988].

4.4 Radiation damage by protons

It is known that protons have higher total cross section for displacement as compared to neutrons. Fig. 4.9 shows total displacement cross section of protons as a function of energy for Si.

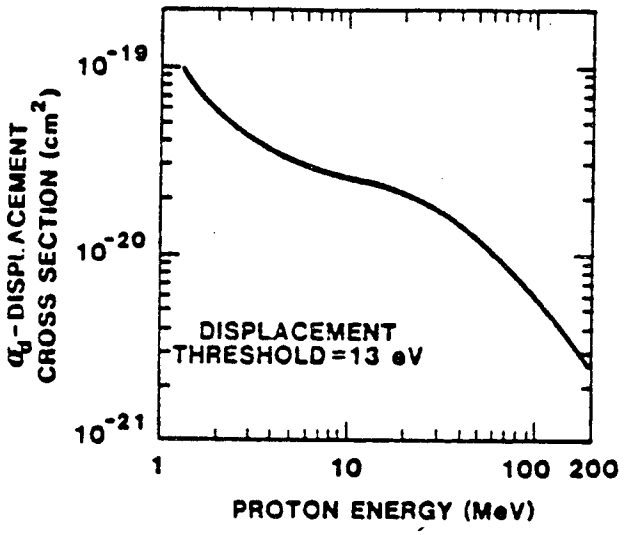

Fig. 4.9. Displacement cross section (including primary and secondary displacements) vs proton energy for silicon [Sandia report, 1985].

For instance a comparison with Fig. 4.3 shows that the total displacement cross section for 1 Mev protons is about 50 times larger than 1 Mev neutrons. Therefore, one would expect more damage from proton irradiation of a-Si:H than from neutrons as the number of broken bonds would be larger. Hanak et al. [1987] , using 1

Mev protons, concluded that a-Si:H diodes (solar cells) were 50 to 100 times more radiation resistant than c-Si and GaAs cells. It was concluded that nuclear collisions by 1 Mev protons with Si was the primary mechanism for defect creation in a-Si:H diodes. The cross

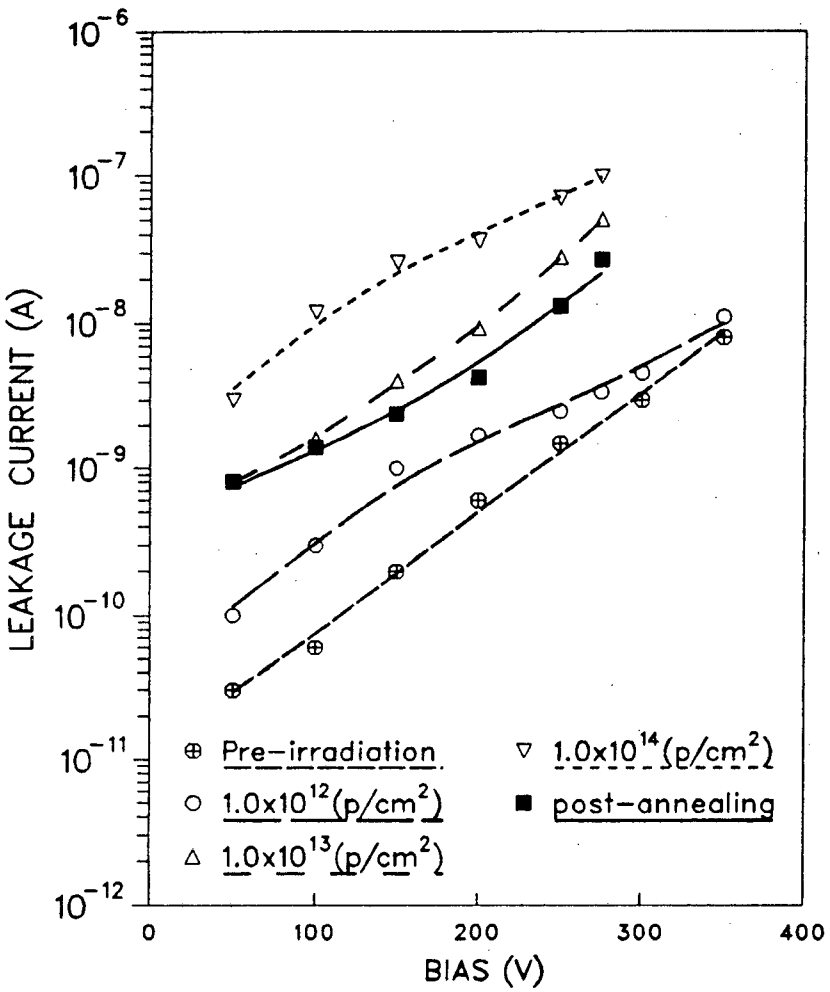

Fig. 4.10(a). Effect of 1.4 Mev proton irradiation on leakage current of a 12.6 μm n-i-p diode exposed to $1x10^{12}$ - $1x10^{14}$ cm^{-2} fluences. The leakage current increases by two orders of magnitude over the fluence range. Annealing at 180° C lead to partial recovery. The curves are drawn with the smoothing routine of CA-Tellagraf [Computer Associates, San Diego, CA].

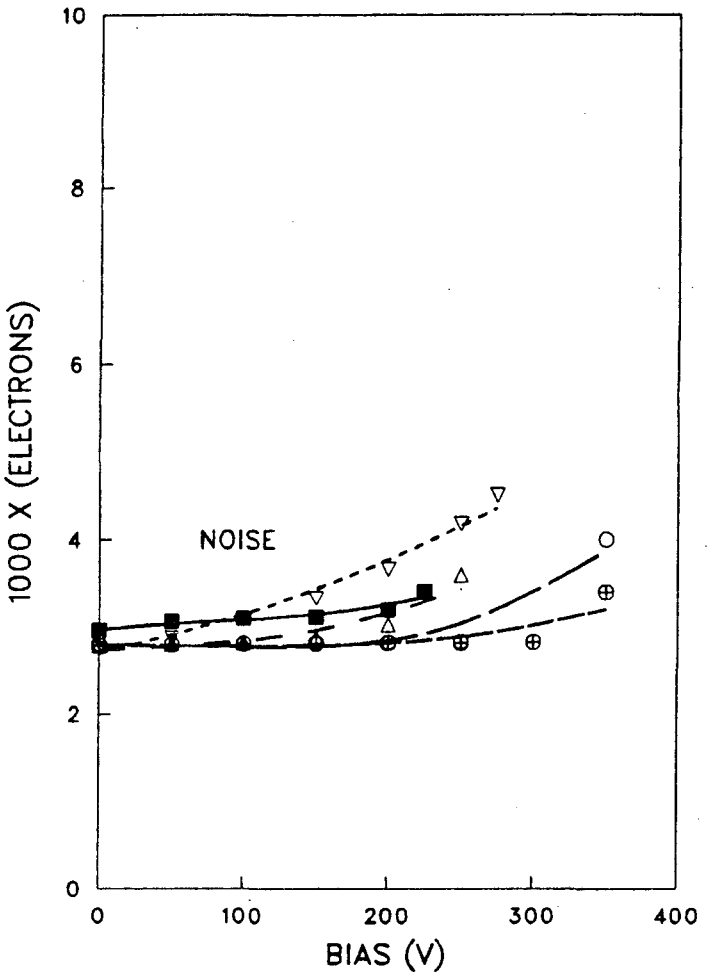

Fig. 4.10(b). Effect of 1.4 Mev proton irradiation on noise of diode described in Fig. 4.10(a). Annealing at 180° C lead to partial recovery. The curves are drawn with the smoothing routine of CA-Tellagraf [Computer Associates, San Diego, CA].

section for (p,Si) collision for displacement, 3.4×10^{-20} cm^{-2}, is a factor of two larger in comparison to (p,p) collision which is 1.9×10^{-20} cm^{-2}. However, in a device grade a-Si:H the concentration of hydrogen is about 10%. Therefore, the number of Si primary knock

-ons is twenty times larger than the number of hydrogen knock-ons.

Radiation damage of a-Si:H diodes by 1.4 Mev protons from Van de Graaff accelerator at LBL was studied in terms of leakage current and noise. An a-Si:H p-i-n diode was subjected to 1.4 Mev proton fluences ranging from 10^{12} cm^{-2} to 10^{14} cm^{-2}. The results of this study are shown in Fig. 4.10(a,b). The damage is seen to be appreciably greater in comparison to neutrons of comparable energy discussed in section 4.3. Annealing at 180° C for 2 hours lead to partial recovery.

The damage in a thick a-Si:H p-i-n diode (27 μm with etched top surface to prevent surface leakage) by 1.4 Mev protons is shown in Fig. 4.11. Little degradation in leakage current and noise is seen at 10^{12} cm^{-2} fluence. However, at proton fluence of 10^{13} cm^{-2} leakage current and noise behaviour of the diode is significantly degraded. Table 4.2 shows the calculated and measured noise after 1×10^{13} cm^{-2} fluence. The experimental setup of Fig. 3.2 (setup 2) was used for this measurement. A remarkable agreement between the calculated and measured noise is seen in accordance with the discussions in Chapter 3 and the increased noise contribution is primarily from the increase in the shot noise component.

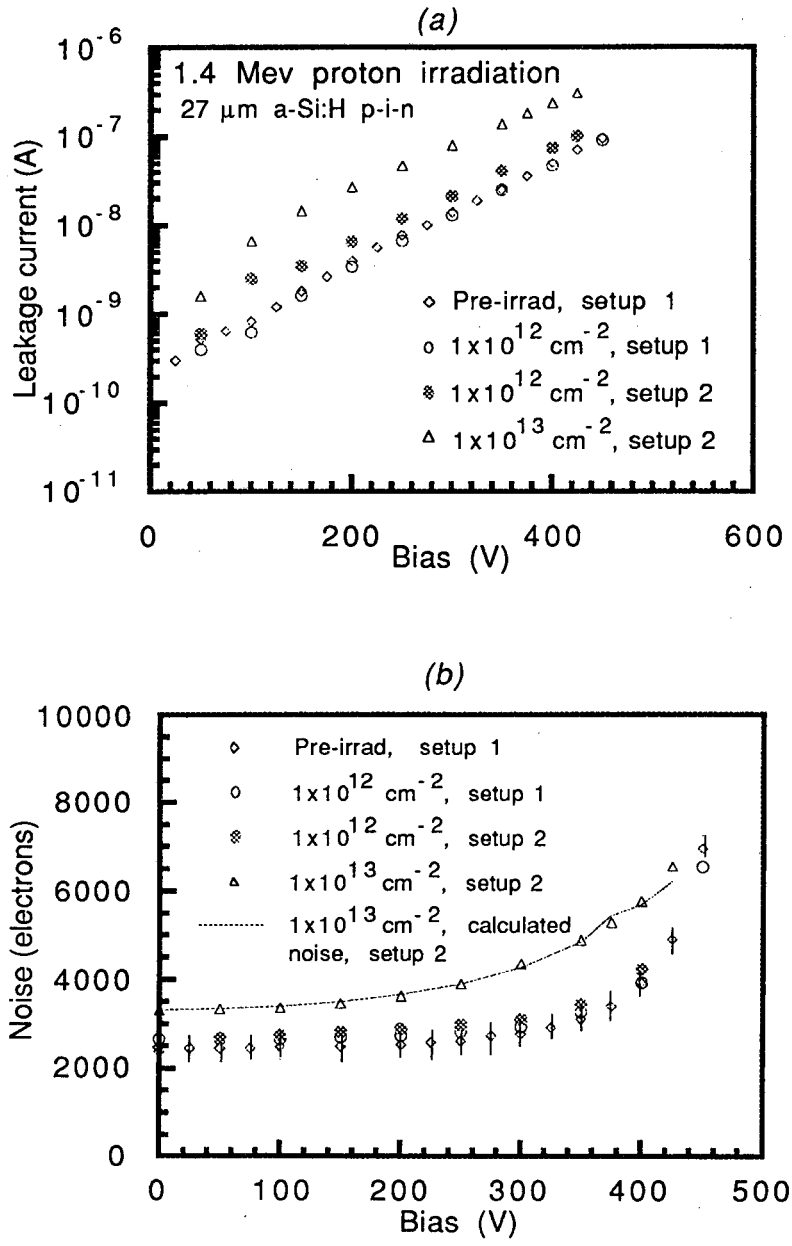

Fig. 4.11. (a) Leakage current (diode surface etched). (b) Noise after 1.4 Mev proton irradiation. Setup 1 used an Amptek A225 preamplifier with 2.5 µs shaping time (shaping function not known). Setup 2 is the same as described in Fig. 3.2. The noise calculated from the measured leakage current (Chapter 3) for $1x10^{13}$ cm^{-2} fluence agrees well with the measured noise.

bias (v)	current (nA)	N_{cal} (e^-)	N_m (e^-)
0	0	-	3309
50	1.6	3330	3328
100	6.6	3398	3358
150	14.4	3501	3454
200	26.7	3658	3629
250	46.5	3896	3902
300	79.8	4267	4349
350	137.8	4846	4883
375	182	5444	5285
400	235	5685	5760
425	303.5	6209	6549

Table 4.2. Calculated and measured noise (FWHM) after 10^{13} cm^{-2} proton irradiation. Set up of Fig. 3.2 was used at 3 μs shaping time and CR-$(RC)^4$ shaping. Diode was 27 μm thick from the same production run as shown in Table 3.1. Irradiation was done using Van de Graaff accelerator at LBL.

A comparison between 1 Mev neutron and 1.4 Mev proton irradiation shows that ~ $5x10^{14}$ cm^{-2} neutron fluence produces less than 10% degradation in leakage current and noise. Irradiation with $1x10^{13}$ cm^{-2} proton fluence degrades leakage current by a factor of ~ 25. The noise at the operating bias is degraded by ~ 40%. No significant degradation in noise is seen at 10^{12} cm^{-2} fluence.

4.4.1 Effect of proton irradiation on carrier mobility and lifetime

Protons of 1.4 Mev energy were used to study the effect of successive irradiations at 10^{12} , 10^{13} and 10^{14} cm^{-2} fluences on carrier mobility and lifetime in a 27 μm a-Si:H p-i-n diode. Fig. 4.12 shows the change in the shape of the electron photocurrent transient after each irradiation obtained by performing a time of flight experiment using the setup of Fig. 2.21.

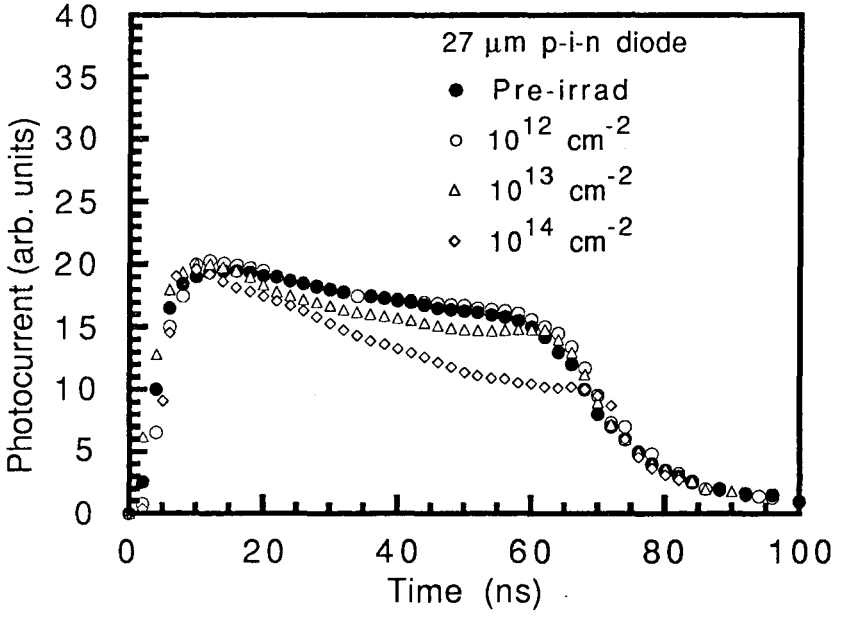

Fig. 4.12. Electron photocurrent transient from 510 nm laser light after various proton irradiation fluences at 100 V pulsed bias using time of flight experimental setup of Fig. 2.21.

Measurements show how carrier mobility and lifetime are affected by irradiation as in Fig. 4.13(a,b,c,d). The current transient was fitted to a drift-diffusion equation given below.

$$I(t) = A\,[\exp(-c_1 t)]\ \mathrm{erfc}\ \left[\frac{c_2(t-c_3 x)}{\sqrt{t}}\right] \qquad (4.1)$$

where the fitting parameter c_1 is inverse of lifetime , c_2 defines the width of the Gaussian and c_3 is inverse of velocity.

Proton irradiation changed electron mobility from pre-irradiated value of 1.03 $cm^2/V\text{-}s$ to 0.98 $cm^2/V\text{-}s$ at 1×10^{14} $cm^2/V\text{-}s$, a decrease of less than 5%. However, electron lifetime decreases from its pre-irradiated value of 232 ns to 60.8 ns at 1×10^{14} cm^{-2} fluence by about a factor of 4. This decrease in electron lifetime is expected as irradiation increases defect density in the material.

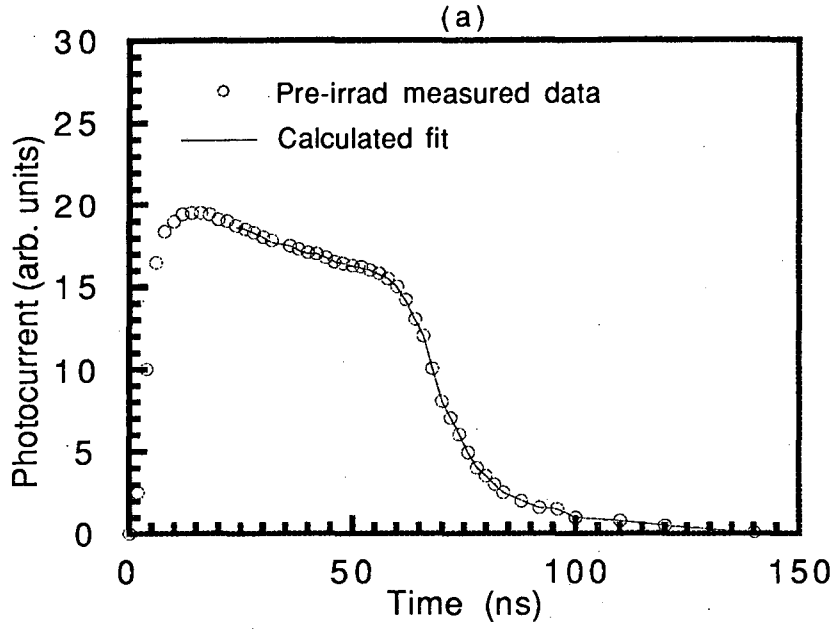
(a)
Pre-irrad measured data
Calculated fit
Photocurrent (arb. units)
Time (ns)
0
5
10
15
20
25
30
0
50
100
150

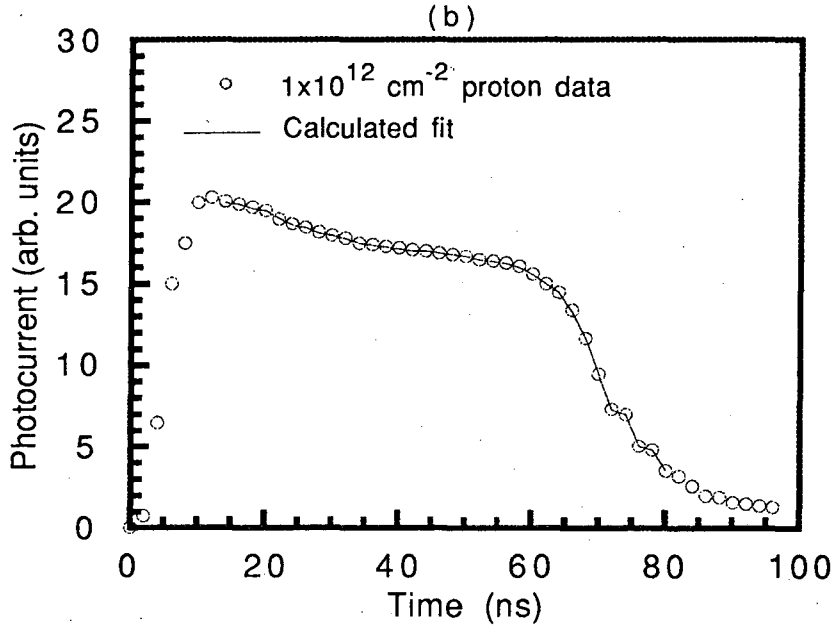
(b)
1x10^12 cm^-2 proton data
Calculated fit
Photocurrent (arb. units)
Time (ns)
0
5
10
15
20
25
30
0
20
40
60
80
100

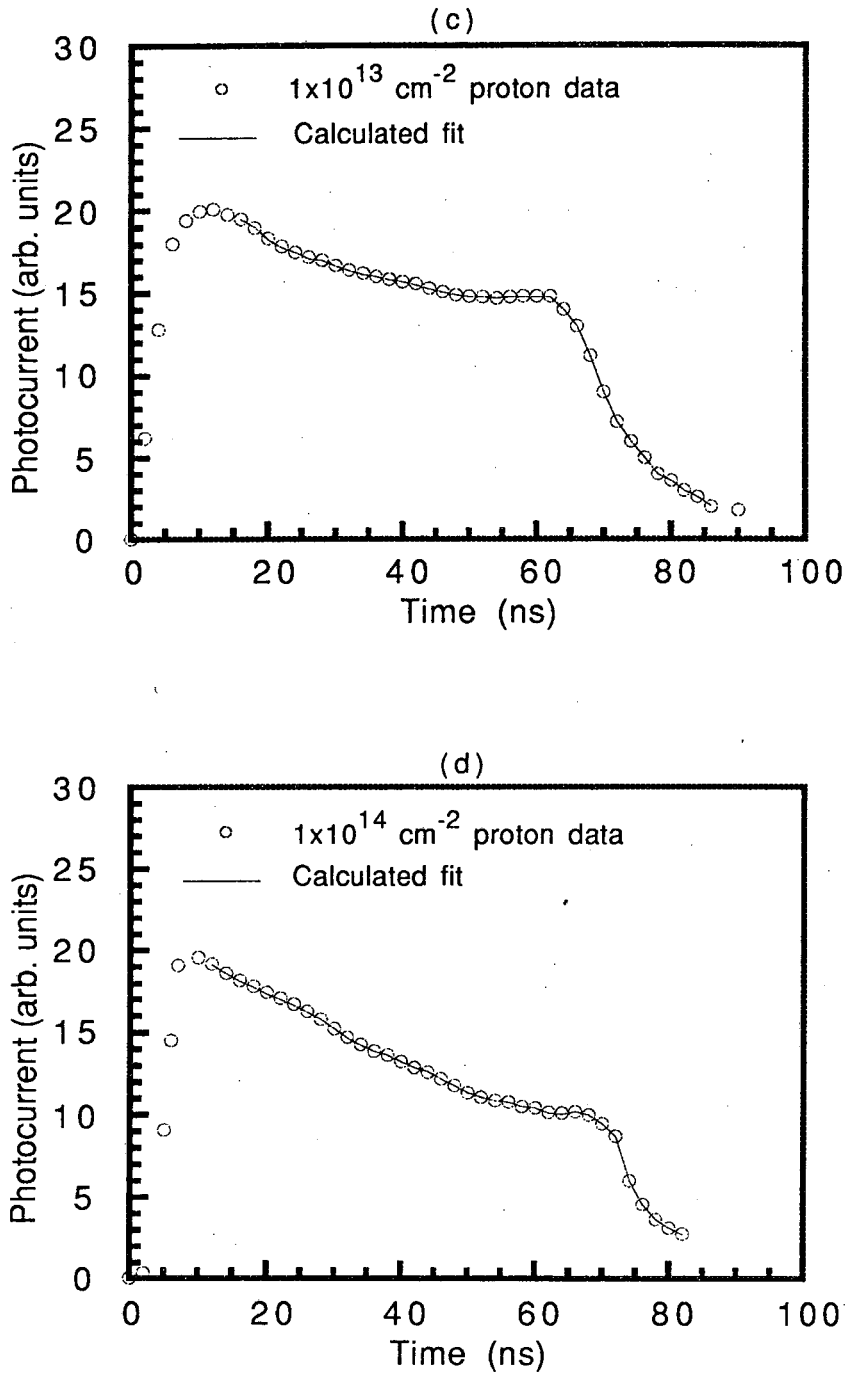

Fig. 4.13. Photocurrent signal at various fluences and fitted data. (a) μ=1.02 cm^2/V-s, τ= 232 ± 29 ns, (b) μ=1.03 cm^2/V-s, τ=160 ± 9 ns, (c) μ=1.02 cm^2/V-s, τ=140 ± 10 ns (d) μ=0.98 cm^2/V-s, τ=61 ± 1 ns.

5 Charge collection

The induced charge dQ in an external circuit produced when a charge q is displaced by a distance dx in a semiconductor detector bounded by two parallel plane electrodes with separation d is given by [Tove et al., 1964]

$$dQ=\frac{q.dx}{d} \tag{5.1}$$

The total distance moved by an excited electron or a hole is given in terms of the electric field F, the lifetime τ and the mobility μ as

$$x_{max}=\mu\ \tau\ F \tag{5.2}$$

Complete collection of charge occurs when x_{max} is larger than the detector thickness. Therefore, three key factors in the collection of charge in a detector are carrier mobility, μ, carrier lifetime, τ, and the electric field, F,. In an a-Si:H p-i-n diode i layer being the active detector region, the electric field distribution in this region is of paramount interest. As pointed out in section 1.1, the fact that a large density of charged centers exist in the i layer when the diode is under DC bias, the electric field would no longer be uniform, unlike a crystalline p-i-n diode where the electric field in the intrinsic layer is uniform. The field configuration in the i layer of an

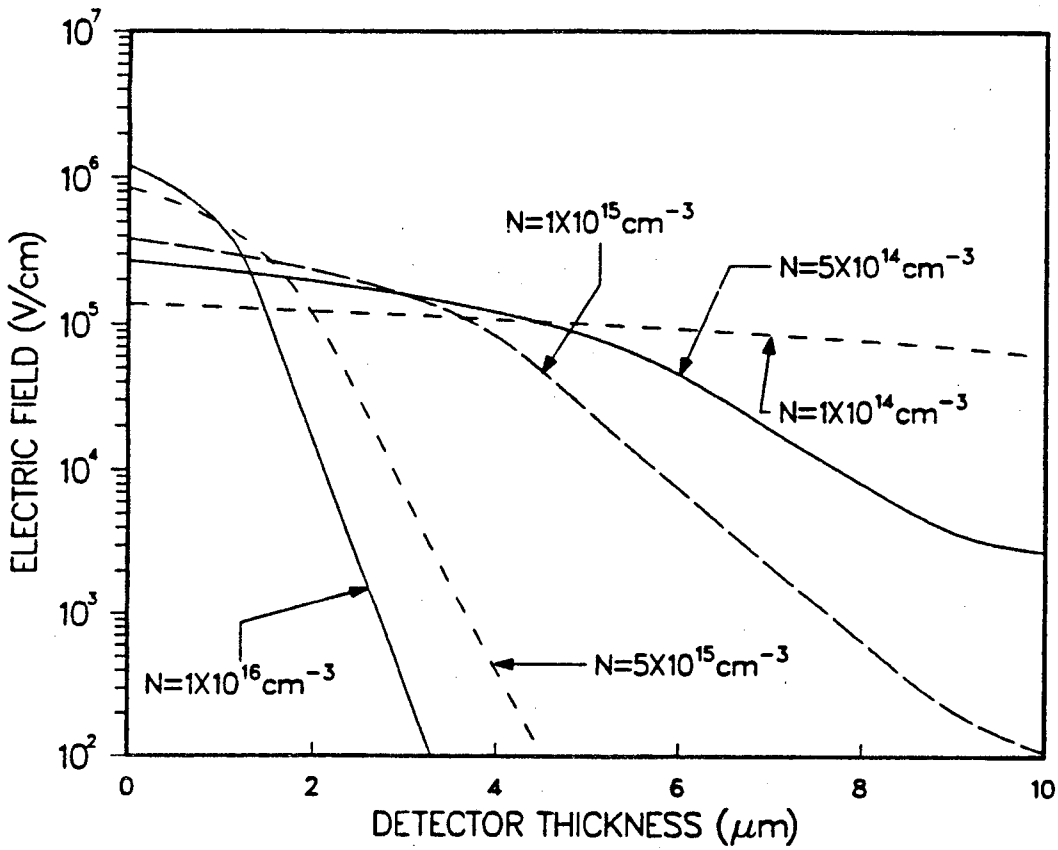

Fig. 5.1. Electric field profile, calculated from eq. (5.3a,b), across a 10 μm a-Si:H diode assuming various ionized dangling bond densities and a D.C. bias of 100 V. The calculations assumed V_c =10 V [Perez-Mendez et al., 1987].

a-Si:H p-i-n diode is obtained by solving the Poisson equation. The model calculations in [Kaplan et al., 1986] assume that the charge density, ρ_0, is constant when voltage is above a certain critical value V_c (deep depletion region). The Poisson equation then has the form

$$\frac{d^2 V}{dx^2} = - \frac{\rho_0}{\varepsilon_0 \varepsilon} \qquad V \gg V_c \qquad (5.3a)$$

where $\rho_0 = eN_d^*$; N_d^* being the density of ionized defects. If N_d^* is constant, then the electric field falls off linearly. At low potential, the gap states are only partially ionized and the Poisson equation is of the form

$$\frac{d^2V}{dx^2} = -\frac{\rho(V)}{\varepsilon_0\varepsilon} \qquad V < V_c \qquad (5.3b)$$

where $\rho(V) = en'V$ and $n' = \frac{N_d^*}{V_c}$; V_c being the critical voltage.

Based on the above model the calculated electric field distribution in a 10 μm a-Si:H diode is shown in Fig. 5.1.

5.1 Experimental studies on charge collection in a-Si:H diodes.

The earliest experiments on the detection of charged particles in hydrogenated amorphous silicon were done at LBL when 2-15 μm a-Si:H diodes were used to detect alpha particles [Kaplan et al., 1986]. The charge collection in these diodes did not plateau as bias was increased. It was soon realised that particles with large dE/dx, e.g. 4.6 Mev alpha particles with dE/dx ~ 150 Kev/μm, produced heavily ionized column of charge (e,h pairs) along the particle track [Perez-Mendez et al.,1987]. Because of low mobilities of carriers in a-Si:H the electrons and holes would tend to recombine before the electric field separated them and caused them to drift across the diode for collection. This effect is known to exist in crystalline

semiconductor diodes when fission fragments comprise the incident radiation [Knoll, 1979]. A clear demonstration of this effect in amorphous silicon diodes (some authors call it plasma effect [Equer et al., 1988]) was seen by turning the detector at an angle to the incident particle which helped the charge separation by the electric field and resulted in higher charge collection. The increase in charge collection on turning a 5 μm diode at 60° to the alpha beam (for particle range > diode thickness) was found to be larger than the geometrical increase in path length. Similar effects were seen in

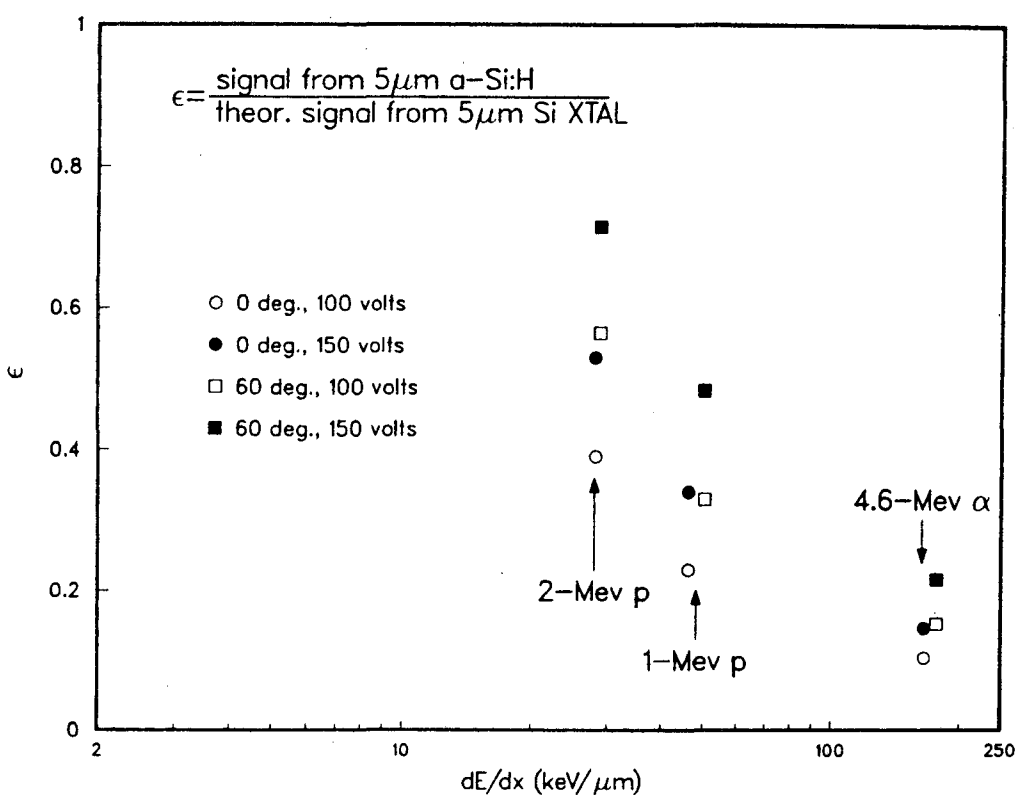

Fig 5.2. Charge collection efficiency vs dE/dx of particles for a 5 μm p-i-n diode.

the detection of 1 and 2 Mev protons in 5 μm a-Si:H p-i-n diodes although the plasma effect was not found to be as severe as in the

Particle	Energy (Mev)	Q/q (e-h pairs)	dE/dx (Kev/μm)	ε (d= 5μm)
Protons	2	20470	26	0.57
	1	20372	40	0.37
Alphas	4.6	33170	147	0.16

Table 5.1(a). Charge collection efficiency, ε, as a function of dE/dx for protons and alpha particles. The data was taken at LBL.

Particle	Energy (Mev)	Q/q (e-h pairs)	dE/dx (Kev/μm)	ε (d=0.5 μm)
Protons	1.8	2400	29	0.58
	1.2	1475	33	0.32
	0.9	1030	45	0.16
	0.8	940	47	0.14
	0.58	600	56	0.078
	0.4	640	67	0.068
Alphas	1.6	1570	250	0.046
	1.2	1550	280	0.040
	0.81	1680	305	0.040
	0.45	1640	305	0.038

Table 5.1(b). Charge collection efficiency, ε, as a function of dE/dx for protons and alpha particles [Equer et al. ,1988].

case of alpha particles the reason being the smaller dE/dx of 1 and 2 Mev protons in Silicon (1 Mev protons, dE/dx ~ 39 Kev/μm ; 2 Mev protons, dE/dx ~ 25 Kev/μm) in comparison with alpha particles. Fig. 5.2 shows the charge collection efficiency as a function of dE/dx of various particles at 0° and 60° angles for a 5 μm diode.

A more detailed study of the charge collection characteristics of a-Si:H diodes with alpha particles and protons of energy in the range of 400 Kev to 5.8 Mev was subsequently done by Equer et al. [1988].

Table 5.1 shows the charge collection efficiency of protons and alpha particles of various energies and how the charge collection efficiency significantly decreases with increase in dE/dx. Some analysis of the plasma effect is given in [Fujieda, 1990].

5.2 Minimum ionizing particle detection

In high energy physics applications amorphous silicon technology was thought to offer promising possibilities as a large area low cost radiation detector. For high energy physics applications, detection of minimum or near minimum ionizing particles is of interest. However, detection of minimum ionizing particles above noise requires thicknesses of tens of microns which could be depleted at reasonable bias. Initially, a-Si:H diodes of only a few micron thickness were available. It is appropriate here to throw some light on what is meant by a minimum ionizing particle in

general.

5.2.1 Minimum ionizing particle

If stopping power, dE/dx, of a particle going through some medium is plotted as a function of energy, E, a plot similar to one shown in Fig. 5.3 is obtained from what is known as Bethe formula given by [Segre, 1977]

$$-\frac{dE}{dx} = \frac{4\pi z^2 e^4}{mv^2} n_e \left[\ln\frac{2mv^2}{I(1-\beta^2)} - \beta^2\right] \qquad (5.4)$$

where

z = particle z
v = particle velocity
m = electron mass
n_e = electron density in the medium
I = ionization potential
β = v/c
e = electron charge

At very low energies, when particle energy is comparable with the orbiting electron energy, the incident electron gets bound to a site resulting in rapid fall off of ionization. On the other hand ionization increases at high energies due to relativistic effects. At

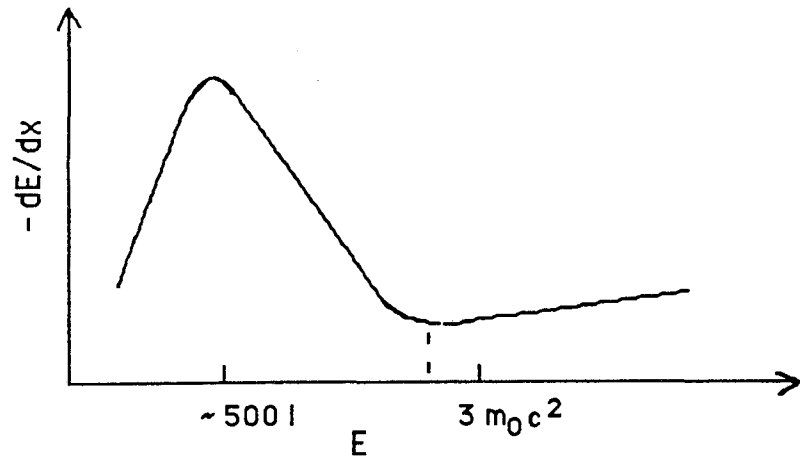

Fig. 5.3. Variation of stopping power with particle energy [Marmier and Sheldon, 1969].

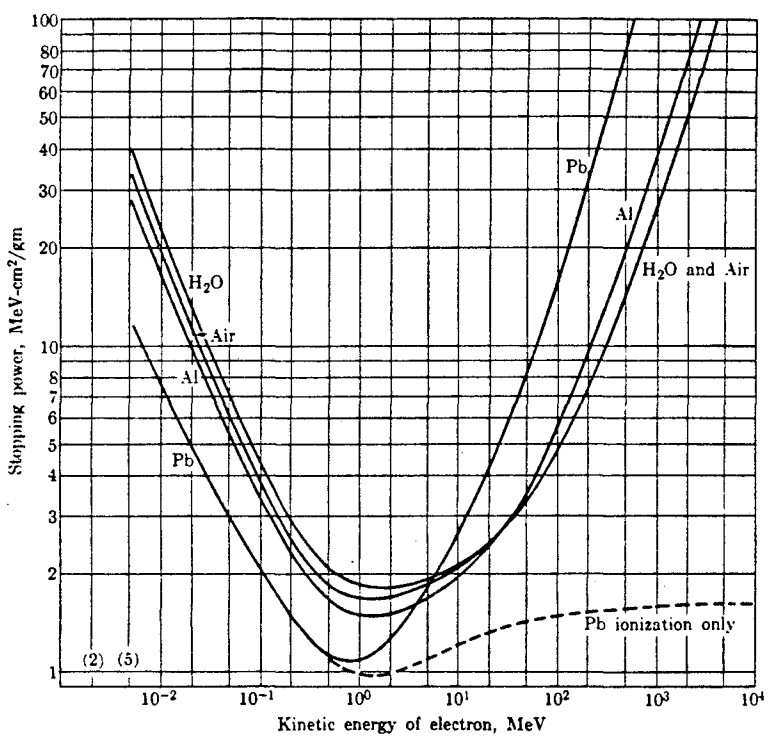

Fig. 5.4. Total (ionization and radiation losses) stopping power for electrons in air, water, aluminum and lead. For Lead, the contribution from ionization is also shown [Heitler,1954].

medium energies the stopping power falls off as $1/v^2$ or $1/E$. A broad minimum in stopping power is seen around 2-3 x the rest mass of the particle. This is a useful rule of thumb to estimate the energy of a minimum ionizing particle. For example protons whose rest mass is 938 Mev are minimum ionizing at ~ 2 Gev. An alpha particle (m_0c^2 = 3727 Mev) at ~ 7 Gev is 4 x minimum. For comparison tabulated value of minimum ionizing proton is 2.3 Gev in Si and the minimum energy loss is 1.67 Mev-cm^2/g. An electron (m_0c^2 = 0.511 Mev) is minimum ionizing at 1-2 Mev energy. Fig. 5.4 shows the stopping power of electrons in various media [Enge, 1966]. It is seen that a minimum ionizing electron has energy between 1-2 Mev in Al which will also be the case for Si as its z and density is similar to Al.

5.2.2 Charge creation by interacting particle in a-Si:H

One important step towards realising the goal of using a-Si:H for minimum ionizing particle detection was to demonstrate that such particles could be detected by it. Considering the magnitude of trap density, ~ 10^{15} cm^{-3}, present in the material, one could wonder if particles with small dE/dx would be detected. That is, are there threshold effects that limit the minimum detectable pulse of charge in hydrogenated amorphous silicon diodes ?

The minimum ionizing particles deposit the least amount of energy, $(\Delta E)_{min}$, per unit track length of the particle. Therefore, the average number of electron-hole pairs, n_{min}, created in the process

would be the bare minimum and is given by

$$n_{min} = \frac{(\Delta E)_{min}}{W} \tag{5.5}$$

where W is the average energy required to produce an electron-hole pair in the medium. The minimum energy loss of protons in silicon is 1.67 Mev-cm^2/g which is 0.38 Kev/μm using density of 2.3 g/cm^3 for silicon.

The average energy required to produce an electron-hole pair in a-Si:H has been of considerable interest over the last few years. Klein [1968] showed that there exists a remarkable correlation between the W value and the band gap of crystalline semiconductors. This correlation is shown in Fig. 5.5 and can be expressed as

$$W = 2.8\, E_G + r(\hbar\omega_R) \qquad 0.5 \leq r(\hbar\omega_R) \leq 1.0 \text{ eV} \tag{5.6}$$

The second term in the equation is attributed to phonon loss. Whether this correlation is applicable to amorphous silicon has been an open question. Spear [1969] studied W value of a-Se and found W $\approx$ 18 eV. This meant for a-Se W is $\approx$ 7 E_G instead of $\approx$ 2.8 E_G (E_G < 3 eV) according to the above correlation. More recently Pochet et al. [1989] have put a conservative limit on the W value of a-Si:H between 3.4 eV and 4.5 eV. Assuming that the correlation of Klein is applicable and W is $\approx$ 4.8 eV, the average number of e-h pairs produced from a minimum ionizing proton is $\approx$ 80 per micron. This

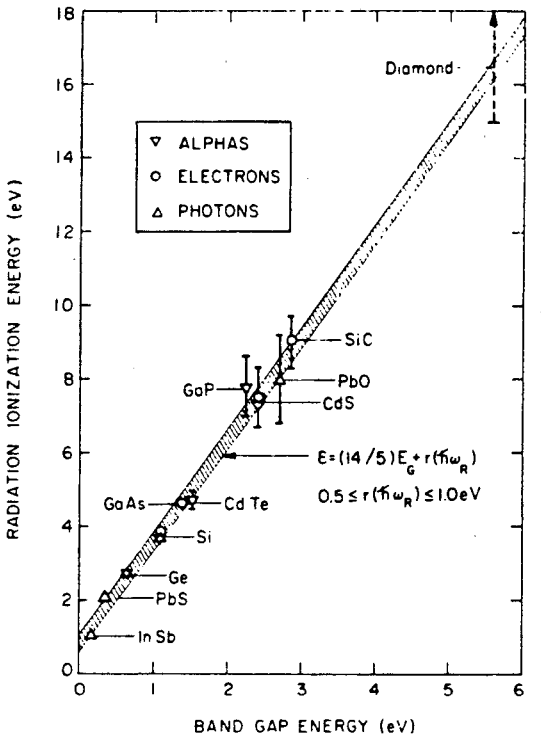

Fig. 5.5. The average energy required to form one electron-hole pair W vs bandgap for different crystalline semiconductor materials [Klein, 1968].

number would be ≈ 105 e-h pairs per micron if the W value of crystalline silicon is used. Based on these numbers, in an a-Si:H diode 30 μm thick the total expected number of e-h pairs produced by a minimum ionizing proton would be about 2400 - 3000. In a diode with noise between 3000 to 4000 electrons (diode noise discussed in chapter 3) signal this size would be buried in noise. Therefore a minimum ionizing particle in thinner diodes could not be ordinarily detected.

A signal-averaging technique was used to make the minimum ionizing particle observable. In such an averaging process the signal, S, averaged N times remains S while random noise is reduced by square root of N thus improving the overall signal to noise by square root of N (see, for example, Tektronix Oscilloscope 2430 manual; [Knoll, 1979])

5.2.3 Minimum ionizing particle measurement

The signal averaging technique was implemented by using a Tektronix 2430 Oscilloscope. The schematic of the experimental setup used is shown in Fig. 5.6.

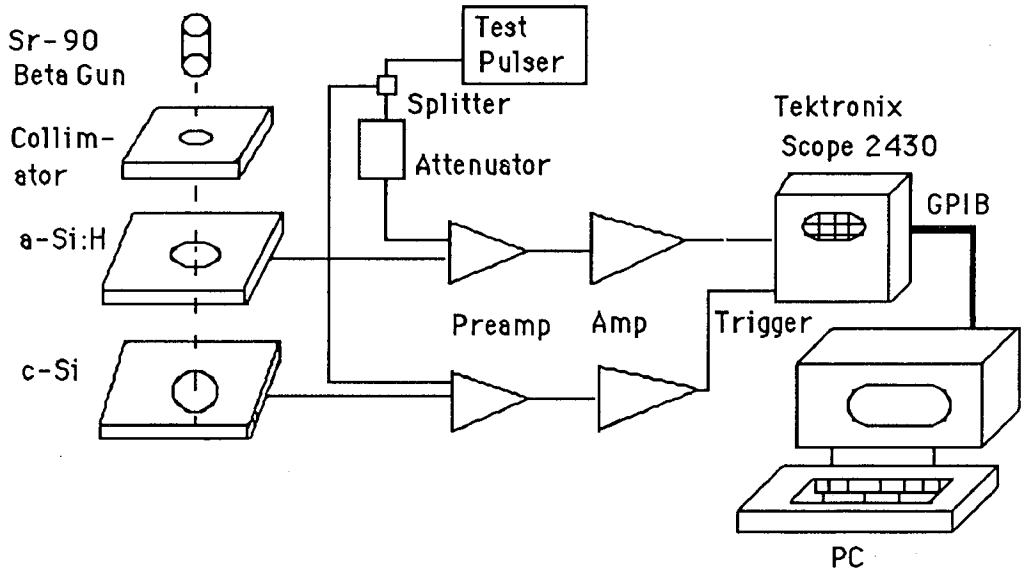

Fig. 5.6. Experimental setup used for the detection of minimum ionizing particles by a-Si:H diode. Sr-90 gun source was used.

Beta particles from a 4 mCi Sr-90 gun source were used in a coincidence experiment between an a-Si:H diode and a crystalline diode. As seen from Fig. 5.4 a 2 Mev beta particle from Sr-90 is close to a minimum ionizing particle. A beta particle going through the a-Si:H diode and the crystal diode produced a trigger pulse in the crystal diode. This pulse was used to trigger the oscilloscope which then acquired the signal produced by the a-Si:H diode.

As a check on the measurement technique a 150 μm crystalline

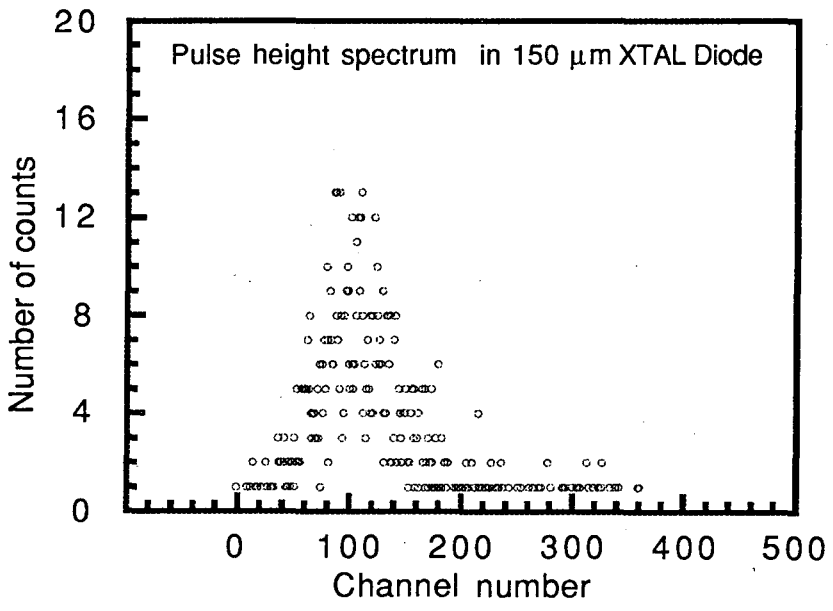

Fig. 5.7. Pulse height spectrum from beta particles in 150 μm crystalline diode using setup of Fig. 5.6. The oscilloscope was used in normal mode and amplifier shaping time was 0.5 μs.

silicon diode was used in place of the a-Si:H diode. Crystalline silicon being well understood provided a useful check on the measurement technique. The coincidence experiment was done between the two crystalline diodes using beta particles from Sr-90 source. To ensure that each particle that produced a trigger went through the front diode, the size of the diode was made larger in diameter compared to the rear diode in addition to using a fine collimator. Fig. 5.7 shows pulse height spectrum obtained by using two crystalline silicon diodes in the coincidence experiment with 2430 Oscilloscope in normal mode (no averaging). For almost every trigger a signal in the front crystalline diode is seen above background. The calibrated signal from a beta particle in its transit through 150 μm diode was 14,914 ± 56 e^- which amounts to signal of 99.4 ± 0.37 electron-hole pairs per micron of crystalline silicon, a number one would expect.

The beta signal in a-Si:H diode was measured at 3 μs shaping time and 256 signal-averages were used. A desk-top microcomputer was used for pulse height analysis. Signal amplitude was determined from the digitized trace by averaging four channels at the pulse peak time and subtracting the average base-line counts per channel. The resultant amplitude was then accumulated for many signals until pulse-height spectrum was obtained. Test pulser pulses were used to calibrate the signal. Fig. 5.8 shows pulse height distribution of 256-signal averaged pulses on a 31 μm diode at 300 V bias. The signal is seen clearly above background. Fig. 5.9 shows beta signal in this diode as a function of bias.

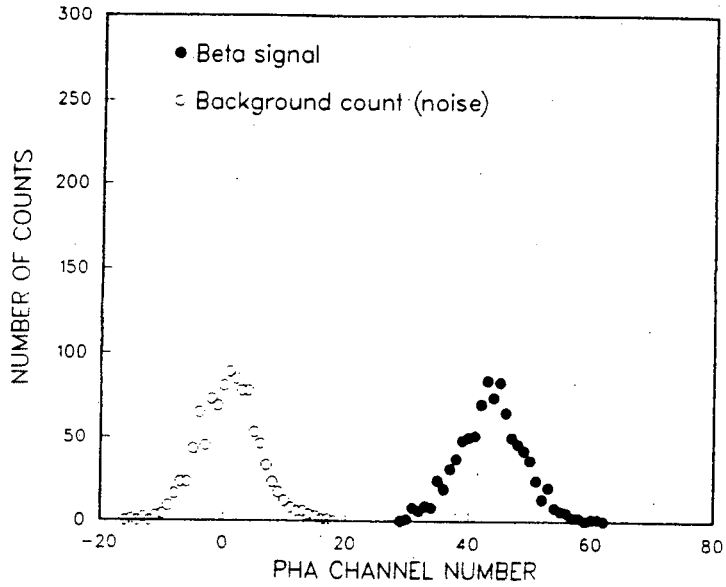

Fig. 5.8. Pulse height distributions of 256 signal-averages, for source in as shown in Fig. 5.6, and source out with pulser triggering the system.

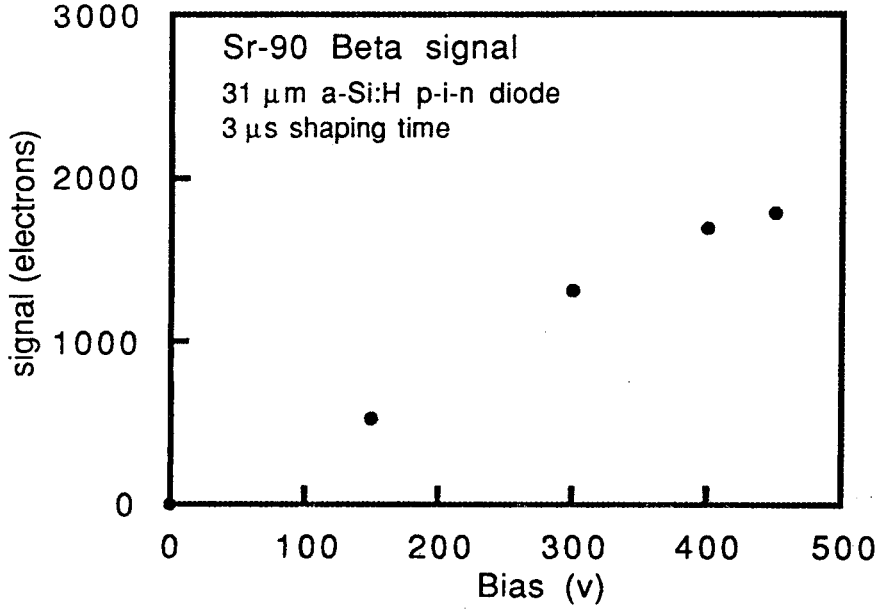

Fig. 5.9. Beta signal as a function of voltage for a 31.2 μm a-Si:H p-i-n diode. The diode noise was ~ 4000 electrons at 400 V; diode capacitance ~ 125 pF. Signal averages of 256 were used.

5.2.4 Beta signals at short shaping times ranging from 20 ns - 500 ns

As pointed out in chapter 1 the mobility of electrons and holes in a-Si:H is small; ~ 1 $cm^2/V\text{-}s$ for electrons and < 0.01 $cm^2/V\text{-}s$ for holes. Consequently, one would expect that for short shaping times and reasonable electric fields only electrons are collected. A measurement was done to study the charge collection from beta particles as a function of shaping times ranging from 20 ns to 500

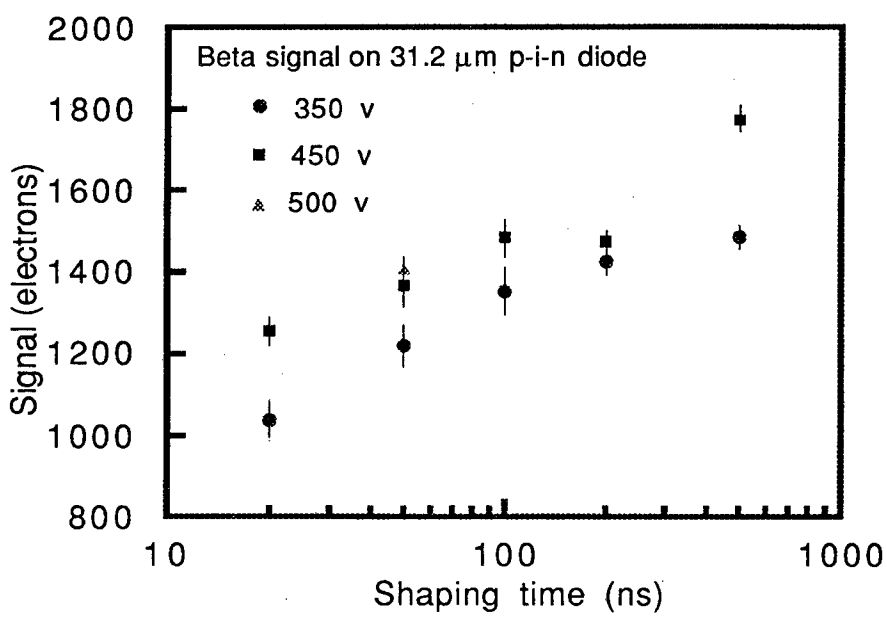

Fig. 5.10. Sr-90 beta signal as a function of shaping time. The shaping time used were 20, 50, 100, 200 and 500 ns. Tennelec TC 171 was used as preamp and the amplifier was timing filter amplifier (EG&G). The measurements were done using the setup of Fig. 5.6.

ns. A 31.2 μm p-i-n diode described in the previous section was used. The charge collection data using light showed that the diode was fully depleted at ~ 350 V bias [Fujieda et al., 1988]. The measurements were done at 350 and 450 V bias. Fig. 5.10 shows the measured beta signal on this diode as a function of shaping time.

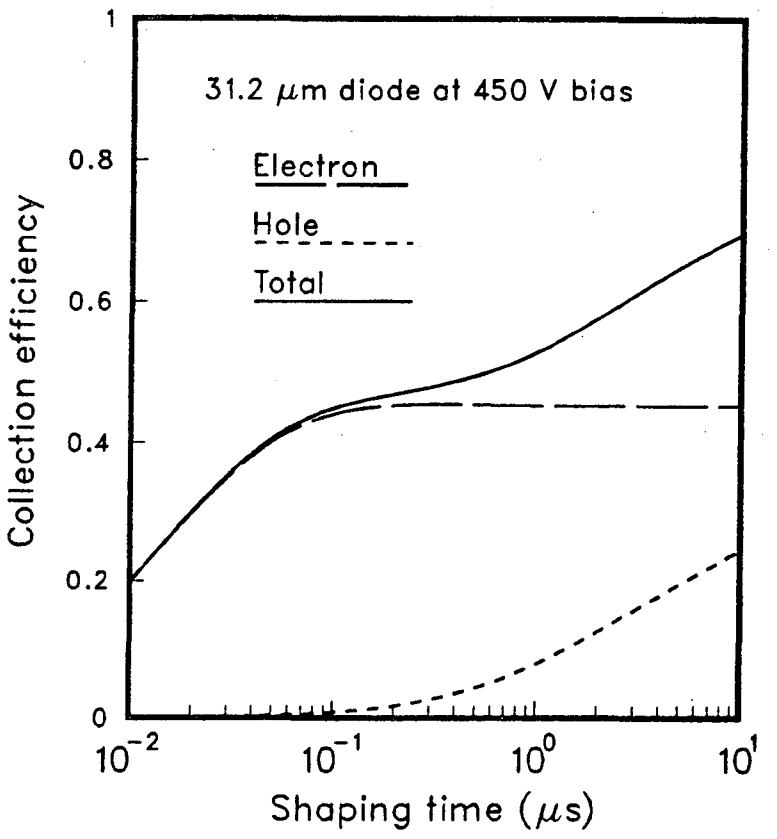

Fig. 5.11. Charge collection efficiency as a function shaping time in a 31.2 μm a-Si:H p-i-n diode at 450 V bias. Calculation assumes uniform energy deposition by a minimum ionizing particle with no plasma effect and uses measured values of material parameters from Table 2.1 and the ionized defect density of 6 x 10^{14} cm^{-2}. Details of calculation are in [Perez-Mendez et al., 1990].

It is seen from Fig. 5.10 that a sizeable electron signal (1400 to 1500 e^-) is collected at shaping times ranging from 50 to 100 ns. At these shaping times the contribution from holes is expected to be small as shown in Fig. 5.11 where the fraction of charge collected is ploted as a function of shaping time in a 31.2 μm diode at 450 V bias. Measured values of material parameters tabulated in column 3 of table 2.1 were used. Charge collection as a function of bias at 50 ns shaping time is shown in Fig. 5.12. A small increase in signal is seen from 450 V to 500 V bias and the charge collected is approximately 1400 electrons. It is also interesting to see from Fig. 5.9 and

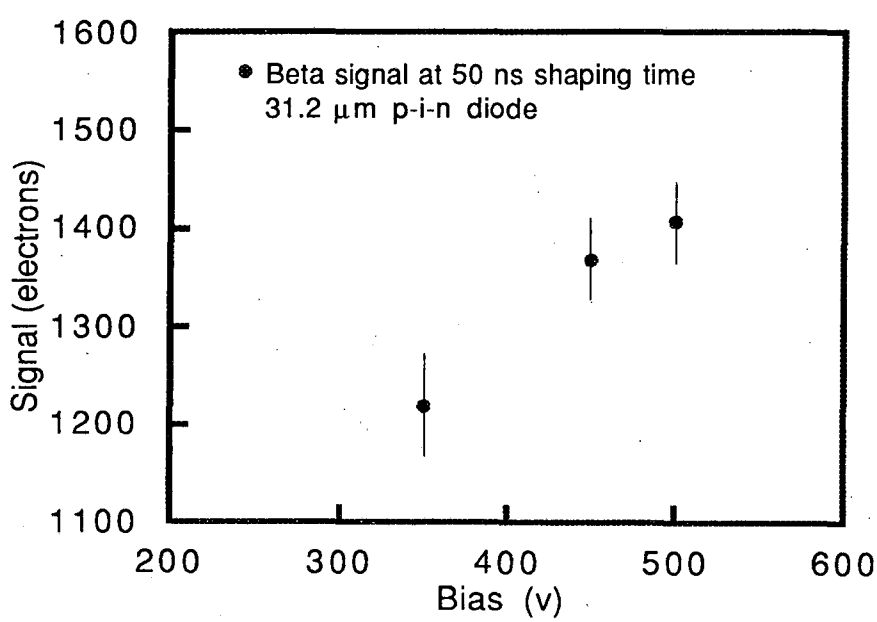

Fig. 5.12. Beta signal at 50 ns as a function of bias.

Fig. 5.10 that the charge collected at 450 V bias does not increase appreciably when shaping time is increased from 0.5 μs to 3 μs. Using the measured value of signal size at 100 ns shaping time (i.e. 1486 ± 43 e^-) from Fig. 5.10 and the calculated fraction of charge collected (i.e. 0.45 ± 0.02) from Fig. 5.11, the charge created by a beta particle going through the material is estimated to be 106 ± 6 e-h pairs per micron. This number is similar to what one expects in the case of crystalline silicon.

5.2.5 Recent experiment with beta particles

Recently beta pulses with signal amplitudes exceeding noise by a factor of 4 or more have been observed at shaping times ranging from 0.5 μs to 6 μs. These large pulses form about 15% of the total count rate. The experimental set up used for signal and noise measurement is shown in Fig. 5.13. The pulses were first detected on a 29 μm a-Si:H p-i-n diode described in Fig. 3.2. The pulse-height spectrum of beta signal from Sr-90 beta gun source at 300 V bias and 3 μs shaping time is shown in Fig. 5.13. Beta pulses were seen at bias voltage as low as 150 V. An oscilloscope trace of such a beta

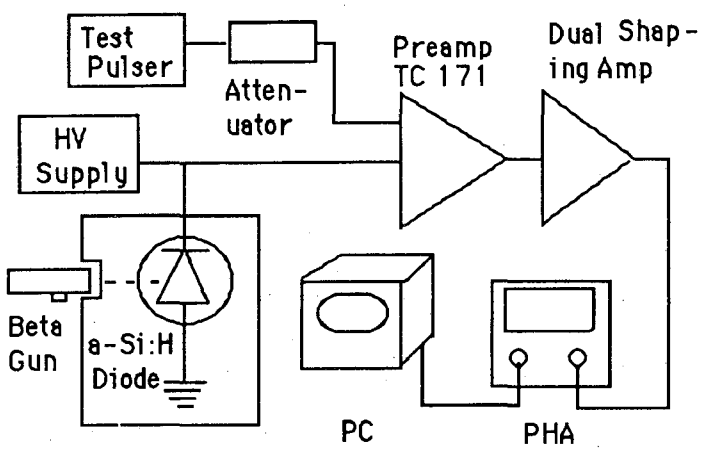

Fig. 5.13. Schematic of experimental setup used to measure beta signal and diode noise. The preamp has no shaping and the dual amp has (pseudo-Gaussian) CR-(RC)^4 shaping.

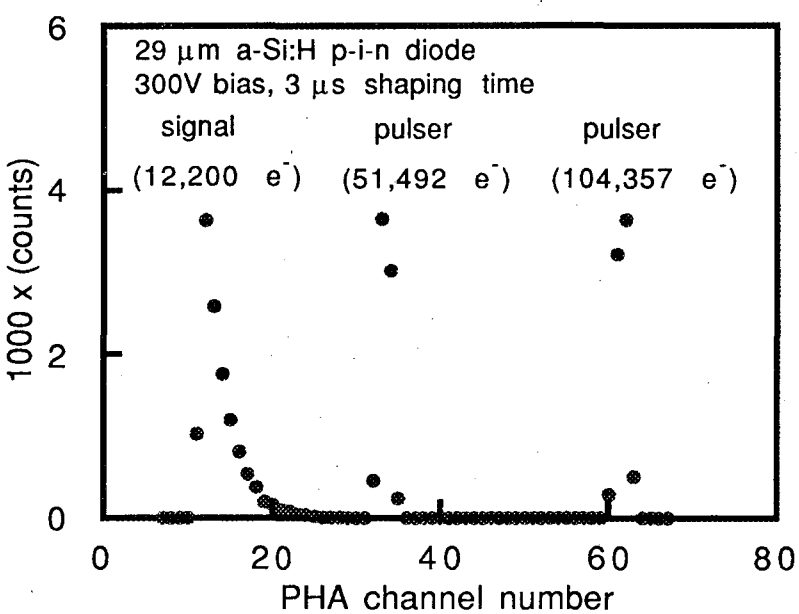

Fig. 5.14. Pulse height spectrum of beta pulses with two calibration pulses measured on a 29 μm a-Si:H p-i-n diode. Detector noise is 2960 electrons. Calibration: 1876 electrons per channel; PHA lower level discriminator set to 0.

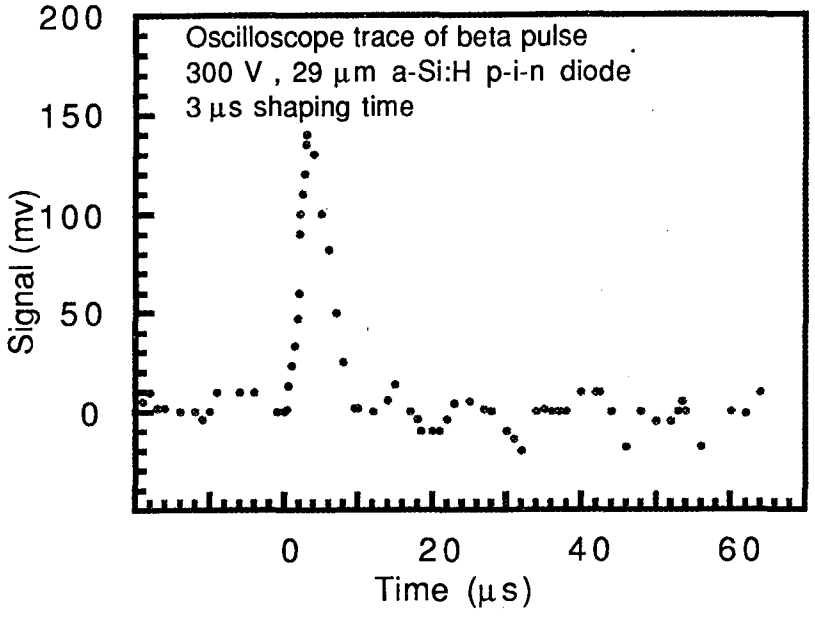

Fig. 5.15. Digital oscilloscope trace of a beta pulse at 300 V, 3 μs shaping time detected in a 29 μm a-Si:H p-i-n diode.

pulse is shown in Fig. 5.15.

The pulse-height spectrum with the beta source removed is shown in Fig. 5.16. No signal was observed.

A coincidence experiment was done to verify that large pulses were truly associated with beta particles. A 150 μm crystalline diode and the a-Si:H diode were used for the coincidence experiment shown in Fig. 5.17. The large pulses from the a-Si:H diode were used as trigger. A beta ray traversing the crystalline diode and also producing a large beta pulse in the a-Si:H diode caused the system to trigger. No trigger pulses were seen with beta source removed from the detector box. The signal size in the crystalline detector agreed

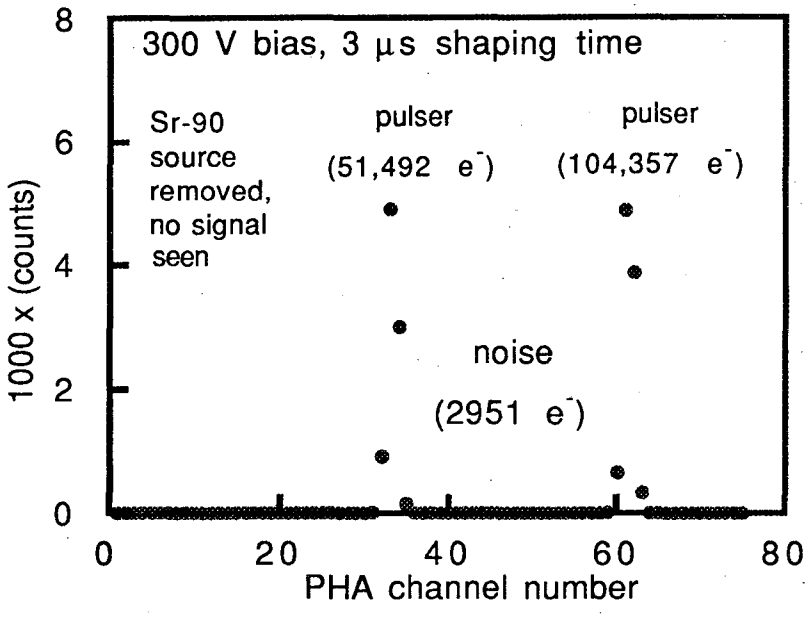

Fig. 5.16. Pulse height spectrum with Sr-90 beta source removed. All settings were same as in Fig. 5.14.

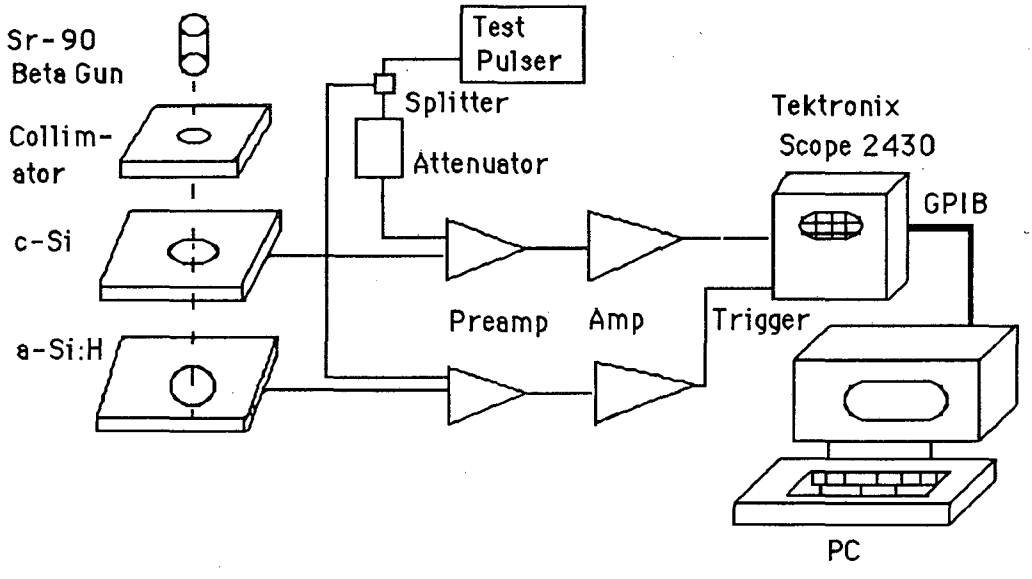

Fig. 5.17. Experimental set up used for coincidence between xtal and a-Si:H diodes.

reasonably well with the energy deposited in the diode by a beta ray traversing through the diode and producing a trigger pulse in the a-Si:H diode.

It is not yet clear what mechanism is responsible for producing these large pulses from beta particles in a-Si:H diode. One possible explanation is that the energy deposited by an electron traversing a thin target is distributed asymmetrically about the most probable value. The distribution is essentially Gaussian on the lower energy side, but has a tail on the higher energy side and is known as Landau distribution [Segre, 1977 p 51; Lindhard et al. , 1963; Goldwasser et al. , 1952]. The pulses could also be from low energy electrons which have higher dE/dx (Fig. 5.4).

5.3 High energy alpha experiment

This experiment was designed to measure signals produced in a-Si:H detectors by energetic particles and demonstrate the usefulness of a-Si:H detectors in high energy particle detection applications. The signals produced in a-Si:H diodes by high energy alpha

beams (860 Mev) from Bevatron accelerator at LBL were measured at short shaping times (50 and 100 ns). The choice of energy was purely based on the availability. The 860 Mev alpha particles have dE/dx (~ 13.9 Mev-cm^2/g or 3.2 Kev/μm) which is about eight times the minimum ionizing alpha particle. The signal at these shaping times is expected to be primarily from electron collection while the contribution from the holes is anticipated to be small. This is due to the large difference in the mobility of electrons and holes. The hole mobility is a factor of 100 or so smaller than the electron mobility. The mobilty-lifetime product of holes is a factor of 3 to 4 smaller compared to that of electrons. A sizeable fraction of hole signal is lost even for shaping times as large as several microseconds [Pochet et al, 1989].

Fig. 5.18 shows the measured signal as a function of bias at 50 and 100 ns shaping times when an 860 Mev alpha particle traverses through a 12.5 μm a-Si:H p-i-n diode in a coincidence experiment. The experimental setup used was similar to one shown in Fig. 5.6. To check for consistancy the 860 Mev alpha signal was measured by the setup of Fig. 5.6 when the a-Si:H diode was replaced by a 150 μm crystalline diode. The measured signal in a fully depleted xtal diode at 0.5 μs shaping time was 137,044 ± 39 electrons. Using dE/dx value of 13.95 Mev-cm^2/g for 860 Mev alpha particles in 150 ± 5 μm thick diode gives a W value of 3.51 ± 0.16 eV. .

Fig. 5.18 shows measured signal in a 12.5 μm a-Si:H diode at 50 and 100 ns shaping times as a function of bias when an 860 Mev alpha particle goes through the diode.

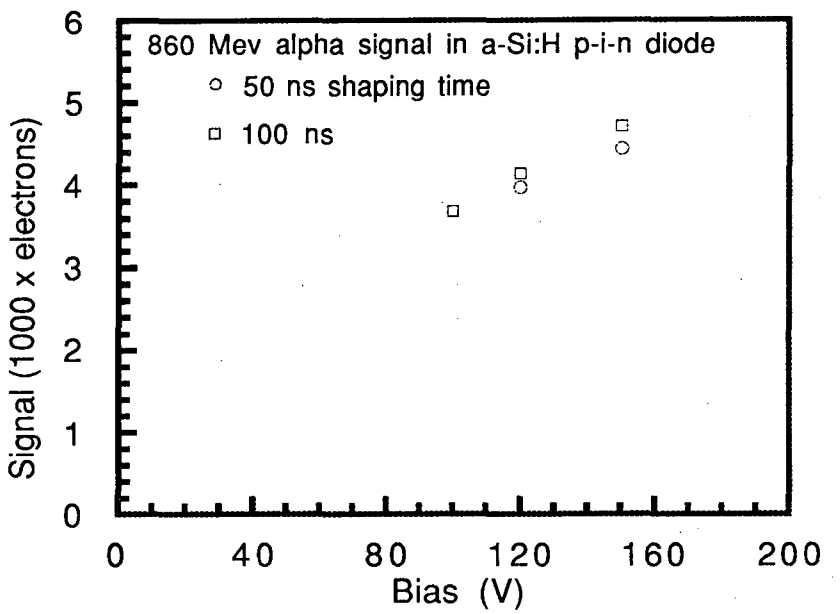

Fig. 5.18. Measured signal when an 860 Mev alpha particle goes through a 12.5 μm a-Si:H p-i-n diode.

The preliminary experiment with thicker a-Si:H diode (31.2 μm) using 860 Mev alpha beam showed probable presence of plasma

Bias (V)	Signal (Ke-)	
	0°, (d=31.2 ± 0.2 μm)	60° ± 2°, (d=62.4 ± 4μm)
450	9.9 ± 0.3	23.3 ± 0.7

Table 5.2. 860 Mev alpha signal at 0° and 60° to the beam. Increased signal size at 60° by a factor greater than 2 is probably due to presence of some recombination effects.

effect discussed in section 5.1. The measured signal at 0° and 60° ± 2° inclination to the beam is shown in Table 5.2. The increase in 60° signal was seen to be more than a factor of 2, an indication of the probable presence of recombination effects at 13.9 Mev-cm^2/g dE/dx value.

The alpha signal was seen above system noise without averaging. Table 5.3 shows alpha signal measured at 350 V bias and 100 ns shaping time in normal mode and averages of 16 at 60° inclination to the beam. The two values were found to be in good agreement.

Bias (v)	Signal (Ke^-), 60° inclination	
	Normal	16 averages
350	21.0 ± 1.7	20.4 ± 0.5

Table 5.3. 860 Mev alpha signal measured in normal and averaging mode to check for consistancy. The agreement evidently is quite good.

The loss of signal due to recombination effects at ~ 8 x dE/dx of minimum ionizing particle needs to be ascertained and further experimentation is required before the W value is inferred from these measurements. The measurements, without taking into consideration recombination effects, showed a spread in the effective W value ranging from 3.9 to 4.7 eV.

Conclusion

Properties of hydrogenated amorphous silicon diodes relevant to radiation detection applications were studied. The interest in using hydrogenated amorphous silicon for radiation detection applications in physics and medicine was motivated by the fact that hydrogenated amorphous silicon can be deposited over large area at relatively low cost compared to crystalline silicon.

1. Material parameters

The material parameters of interest namely, carrier mobility, μ, lifetime, τ, and the defect density, N_d, of thick a-Si:H p-i-n diodes were studied by time of flight (transient photoconductivity) experiments. The mobility and mobility-lifetime product values on thick diodes were comparable to values reported on thin diodes for solar cells. The ionized defect density, N_d^*, of p-i-n diodes measured by transient photoconductivity method under DC bias was found to be only ~1/3 of the total defect density as measured by ESR.

2. Leakage current and noise

The leakage current under reverse bias of well behaved a-Si:H p-i-n diodes was studied. The leakage current is important from noise and power dissipation considerations. The increase in leakage

current with bias has the same dependence on voltage as one would expect if this increase were due to the "Poole-Frenkel effect" involving excitation of carriers from neutral defects. The noise of the diode over the operating voltage range is completely explained in terms of the "shot noise" component and the noise component at 0 V bias (delta and thermal noise) added in quadrature. The leakage current makes dominant contribution to noise in the form of shot noise for CR-$(RC)^4$ (pseudo-Gaussian) shaping at 3 μs.

3. Radiation damage

The irradiation effects of 1 Mev neutrons and protons on thick a-Si:H p-i-n diodes were studied in terms of degradation in leakage current and noise. This study showed that a-Si:H diodes were radiation resistant to neutron fluences in excess of 4×10^{14} cm^{-2}. No appreciable change in leakage current and noise was seen while alpha signal degraded by about 20%. The diodes fully recovered after annealing at 180° C for two hours.

Proton irradiation (1.4 Mev) produced little degradation in leakage current and noise at 10^{12} cm^{-2} fluence. However, at proton fluence of 10^{13} cm^{-2} leakage current and noise was significantly degraded.

A comparison between 5×10^{14} cm^{-2} neutron fluence and 10^{13} cm^{-2} proton fluence reveals that leakage current in case of neutrons increases by 10-20% with neglegible increase in noise. Proton irradiation increases leakage current by a factor of 10 to 25 with

significant increase in noise as a result of increase in shot noise contribution.

Proton irradiation was also used to study effects on electron mobility and lifetime with increasing fluence. The diode subjected to 1.4 Mev proton fluence ranging from 10^{12} cm^{-2} to 10^{14} cm^{-2} showed that no appreciable change was seen in electron mobility on irradiation. However, electron lifetime decreased from 232 ns by about a factor of 4 to 60 ns at 10^{14} cm^{-2}. This decrease in carrier lifetime is associated with an increase in defect centers on irradiation.

4. Charge collection

Minimum ionizing particles, for example 1-2 Mev electrons, were detected in thick (~ 31 μm) a-Si:H p-i-n diode at 3 μs shaping time. These particles were detected by signal averaging technique implemented to improve the signal to noise ratio in a diode with large capacitance. It was demonstrated that if one were to rely on signal from electrons alone the device speed could be much higher as most electrons are collected in shaping time ranging from 50 to 100 ns with small contribution to signal from hole collection. This result was also confirmed by measurements with 860 Mev alpha particles at short shaping times. As thicker fully depleted diodes are realised more energy is deposited in the diode with increase in signal to noise ratio due to reduced capacitance. In such a device electrons alone would produce large enough signal making a faster

device more realistic.

Measurements showed a minimum ionizing beta particle produced ~ 104 e-h pairs per micron of a-Si:H, consistant with the value for crystalline silicon. Measurements with 860 Mev alpha particles (~ 8 x minimum ionizing dE/dx) showed that the energy expended per e-h pair, W value, in a-Si:H is smaller than predicted from the Klein's curve for crystalline semiconductors. Preliminary measurements with 860 Mev alpha particles showed a spread in the effective W value ranging from 3.9 to 4.7 eV. These estimates were obtained from signal measurements at short shaping times (100 ns) and model calculations of the fraction of electrons and holes collected using measured values of material parameters. Further work is required to determine a better value of the W value of a-Si:H.

Heavily ionizing particles, e.g. alpha particles, produce a saturation effect (plasma effect) in hydrogenated amorphous silicon diodes. This phenomenon is similar to the effect produced by fission fragments in crystalline silicon detectors. As a consequence of this effect the collected charge is not proportional to the energy deposited in the diode. The effect is neglegible for minimum ionizing particles.

The work reported in this thesis shows that hydrogenated amorphous silicon p-i-n diodes hold good promise for radiation detection applications.

Appendix 1

The probability p that electron jumps from state A to state B through scattering with a phonon depends on

(1) The probability of finding a phonon with an excitation energy W and is given by the Boltzman factor ~ exp(-W/kT), where W is the energy difference between the two states.

(2) Attempt to escape frequency ν_{ph}.

(3) The probability of electron transfer from one state to another

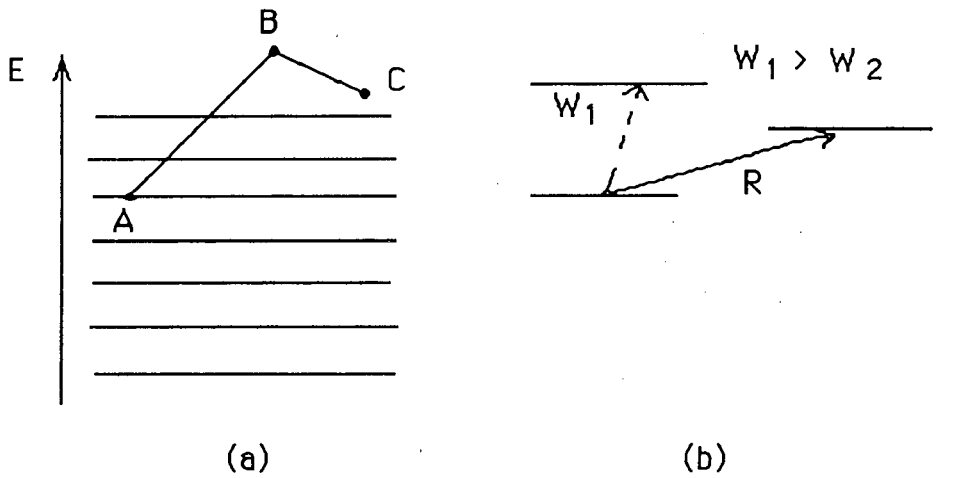

Fig. 2.13. (a) Hopping of a carrier from state A below the Fermi energy to state B above it. (b) At low T, long range less energetic hops are favoured.

which depends on the overlapping of wave functions and is given by exp(-2αR). R is the jump distance and α is a quantity representing rate of fall of wave function at a site.

Total probability p is given by

$$p = \upsilon_{ph} \exp(-2\ \alpha\ R\text{-}W/kT)$$

From Einstein's relation,

$$\mu = \frac{eD}{kT},$$ and using an expression for diffusion coefficient , $$D = \frac{1}{6}pR^2$$ [Cohen, 1970], we have

$$\mu = \frac{e}{6}\frac{pR^2}{kT} \text{ and } \sigma = ne\mu = \frac{e^2}{6} pR^2 N(E_f)$$

where $N(E_F)$ is the density of states at the Fermi energy.
Substituting for p we have

$$\sigma = \frac{e^2}{6}\upsilon_{ph} R^2 N(E_f) \exp(-2\alpha R - \frac{W}{kT})$$

As T is lowered the energy of phonons decreases and more energetic phonon assisted hops become less favourable. Carriers tend to hop larger distances.

To find the most probable hopping distance let

N(W) = No. of states per unit volume per unit energy, then the number of states within energy W and within distance R is given by

$$\frac{4}{3}\pi R^3 N(W) W$$

For electron to hop from a state just below the Fermi energy to a state just above it this number should be at least 1.
Therefore,

$$W \approx \frac{3}{4\pi R^3 N(E_f)}$$

and $$p = \upsilon_{ph} \exp[-2\alpha R - \{\frac{4}{3}\pi R^3 N(E_f) kT\}^{-1}].$$

The most probable jump distance R_{min} is given by minimizing the exponent with respect to R.

Let,

$$X = -2\alpha R - \{\frac{4}{3}\pi R^3 N(E_f) kT\}^{-1}$$

and $$\frac{dX}{dR} = 0 ,$$

we have $$R_{min} = [\frac{9}{8\pi \alpha N(E_f) kT}]^{\frac{1}{4}}$$

$$\therefore \quad p = \upsilon_{ph} \exp(-\frac{A}{T^{1/4}})$$

where $$A = 2.1 \times [\frac{\alpha^3}{k} N(E_f)]^{\frac{1}{4}}$$

and the hopping conductivity is given by

$$\sigma_{hop} = \sigma_0 \exp(-\frac{A}{T^{\frac{1}{4}}}) \qquad (2.1\ 1)$$

Eq. (2.1 1) is known as Mott's $T^{\frac{1}{4}}$ law.

Appendix 2

Let

v_{pb} = Pulse bias signal
$v_{dc}(t)$ = DC bias signal
t_T = Transit time
μ = Mobility = $d/E_0 t_T = d^2/V_0 t_T$
R = Resistance across which signal is measured
n = Carrier density
A = Diode area
q = Electronic charge
$I_{dc}(t)$ = Signal current under DC bias
I_{pb} = Signal current under pulsed bias
V_0 = Pulsed bias across diode
E_0 = Pulsed field = V_0/d

Let

$$v_{pb} = R\, I_{pb} = R\, q\, A\, n\, v = R\, q\, A\, n\, \mu\, E_0 = R\, Q\, \mu\, E_0 \qquad (1)$$

where Q = n q A.

Under DC bias

$$v_{dc}(t) = R\, I_{dc}(t) = R\, q\, A\, n\, v = R\, q\, A\, n\, \mu\, E_{dc}(t)$$

or

$$v_{dc}(t) = R\, Q\, \mu\, E_{dc}(t) \qquad (2)$$

From eq.s (1) and (2) we have

$$E_{dc}(t) = E_0\, v_{dc}(t)/v_{pb} \qquad (3)$$

$$\frac{dx}{dt} = \mu E_{dc}(t)$$

or

$$x = \mu \int_0^t E_{dc}(t_1)\, dt_1$$

$$x = \mu \int_0^t \frac{E_0 v_{dc}(t_1)}{v_{pb}}\, dt_1$$

$$= \frac{d}{v_{pb}\, t_T} \int_0^t v_{dc}(t_1)\, dt_1 \qquad (4)$$

Assuming the electric field falls off linearly we can write the depletion thickness as

$$x_d = \sqrt{\frac{2\, V_0 \varepsilon_0 \varepsilon_r}{q\, N_d}} \qquad (5)$$

$$\frac{dE}{dx} = -\frac{q\, N_d}{\varepsilon_0 \varepsilon_r}$$

$$E(x) = -\frac{q\, N_d}{\varepsilon_0 \varepsilon_r}\, x + c_1$$

For $E(x) = 0$ at $x = X_d$

$$c_1 = \frac{q\, N_d}{\varepsilon_0 \varepsilon_r}\, x_d$$

Therefore,

$$E(x) = -\frac{q\, N_d}{\varepsilon_0 \varepsilon_r}\, (x - x_d) \qquad (6)$$

$$v = \frac{dx}{dt} = \mu E(x) = -\mu \frac{q N_d}{\varepsilon_0 \varepsilon_r} (x - x_d)$$

$$\frac{\varepsilon_0 \varepsilon_r}{q N_d \mu} \frac{dx}{x - x_d} = -dt$$

$$\frac{\varepsilon_0 \varepsilon_r}{q N_d \mu} \ln \left(\frac{x_d - x}{x_d}\right) = -t$$

Using eq. (6) we have

$$\frac{\varepsilon_0 \varepsilon_r}{q N_d \mu} \ln \left[\frac{\varepsilon_0 \varepsilon_r E(x)}{q N_d} \frac{1}{x_d}\right] = -t$$

Using eq.s (3) and (5)

$$\frac{\varepsilon_0 \varepsilon_r}{q N_d \mu} \ln \left[\frac{\varepsilon_0 \varepsilon_r E_0}{q N_d \sqrt{\frac{2 V_0 \varepsilon_0 \varepsilon_r}{q N_d}}} \frac{v_{dc}(t)}{v_{pb}}\right] = -t$$

$$\frac{\varepsilon_0 \varepsilon_r}{q N_d \mu} \ln \left[\frac{v_{dc}(t)}{v_{pb}}\right] + \frac{\varepsilon_0 \varepsilon_r}{q N_d \mu} \ln \left[\frac{V_0}{d}\right] - \frac{\varepsilon_0 \varepsilon_r}{q N_d \mu} \ln \left[\frac{q N_d}{\varepsilon_0 \varepsilon_r} \sqrt{\frac{2 V_0 \varepsilon_0 \varepsilon_r}{q N_d}}\right] = -t$$

For time duration t_1 and t_2 we have

$$N_d \approx \frac{\varepsilon_0 \varepsilon_r}{q \mu} \frac{\ln \left[\frac{v_{dc}(t_1)}{v_{dc}(t_2)}\right]}{t_2 - t_1} \qquad (7)$$

where $\varepsilon_0 \varepsilon_r = 12 \times 8.85 \times 10^{-14}$ F/cm.

Expressing result in terms of current signal we have eq. (2.19).

Appendix 3

In crystalline semiconductors, deep trapping is described in terms of a capture cross section σ, with carriers at the edge of the band having a thermal velocity v, and N_d is the defect density.

$$\tau_F^{-1} = \sigma \, v \, N_d \tag{1}$$

where τ_F is the free-carrier lifetime. Eq. (1) assumes that the scattering length, a, is larger than the capture radius d ($\sigma = \pi d^2$). If instead a<d, then capture is dominated by diffusion and the rate is given by the formula [Waite, 1957]

$$\tau_F^{-1} = 4\pi \, dDN_d \tag{2}$$

where D is the diffuson coefficient. In amorphous semiconductors of interest, a and d are likely to have similar magnitudes.

Another difference is that free carriers in an amorphous semiconductor are not at the bottom of a band, with thermal velocity. Instead they move at the mobility edge E_c with minimum metallic conductivity, σ_{min}, given by [Mott and Davis, 1979]

$$\sigma_{min} = 0.025 \, e^2 / \hbar a$$

Free carrier mobility at the mobility edge E_c is given by

$$\mu_0 = \frac{eD}{kT}$$

$$D = \frac{1}{6} \nu_{el} \, a^2 = \frac{1}{6} \left(\frac{\hbar}{ma^2}\right) a^2 = \frac{1}{6} \frac{\hbar}{m}$$

where ν_{el} is the electronic frequency ($\approx \hbar/ma^2$).
Therefore,

$$\mu_0 = \frac{1}{6} \frac{\hbar}{m} \left(\frac{e}{kT}\right)$$

$$\mu_0 = \frac{1}{6} \frac{e}{kT} a v \qquad (3)$$

The third effect that must be taken into account is that the drift mobility in an amorphous semiconductor is trap limited by band-tail states, so that [Street, 1984]

$$\tau_F = \mu\tau/\mu_0 \qquad (4)$$

Thus, combining eqs. (1) and (4) , we have

$$\frac{\mu_0}{\tau \mu} = \sigma v N_D \qquad (5)$$

From eqs. (3) and (5) we get

$$\mu \tau N_D \approx \frac{1}{6} \frac{e}{kT} \frac{a}{\sigma}$$

Table 1 **dE/dx of heavy particles in silicon**

TABLE 1

STOPPING POWER IN MEV.SQCM/GM FOR SILICON Z= 14 A= 28.086 I= 173.5

E(MEV)	P	D	T	HE 3	HE 4	LI 7	E(MEV)	P	D	T	HE 3	HE 4	LI 7
1.00	174.902	256.298	307.610	1183.209	1274.494	1870.058	7.00	45.385	75.662	100.662	402.595	488.091	1409.919
1.10	165.072	244.187	291.546	1156.467	1211.196	1893.188	7.20	44.431	74.142	98.715	394.809	478.985	1393.568
1.20	156.418	233.336	281.238	1118.590	1200.907	1913.675	7.40	43.521	72.689	96.853	387.360	470.250	1377.744
1.30	148.741	223.585	271.825	1083.337	1186.984	1942.589	7.60	42.652	71.299	95.068	380.223	461.878	1362.466
1.40	141.866	214.715	263.028	1052.493	1174.378	1964.550	7.80	41.821	69.968	93.357	373.379	453.832	1347.721
1.50	135.680	206.694	256.091	1023.798	1144.776	1963.405	8.00	41.026	68.697	91.714	366.806	446.100	1333.419
1.60	130.074	199.255	247.847	991.295	1116.573	1956.030	8.20	40.264	67.468	90.135	360.491	438.660	1319.588
1.70	124.969	192.440	240.251	960.909	1089.796	1946.316	8.40	39.533	66.292	88.616	354.418	431.494	1306.250
1.80	120.298	186.134	233.137	932.455	1065.739	1936.883	8.60	38.831	65.162	87.155	348.573	424.601	1293.289
1.90	116.006	180.289	226.535	906.050	1043.222	1933.778	8.80	38.156	64.075	85.747	342.942	417.949	1280.725
2.00	112.048	174.850	220.344	881.286	1021.891	1930.895	9.00	37.508	63.029	84.390	337.513	411.532	1265.955
2.10	108.382	169.776	214.526	858.015	996.904	1927.222	9.20	36.883	62.020	83.080	332.276	405.332	1250.702
2.20	104.982	165.021	209.077	836.219	973.550	1922.947	9.40	36.281	61.047	81.817	327.222	399.343	1235.909
2.30	101.816	160.560	203.934	815.648	951.332	1902.113	9.60	35.701	60.113	80.596	322.340	393.554	1221.570
2.40	98.859	156.369	199.073	796.207	930.182	1880.232	9.80	35.142	59.205	79.416	317.620	387.951	1207.624
2.50	96.091	152.420	194.472	777.803	910.254	1862.314	10.00	34.602	58.328	78.274	313.053	382.529	1194.099
2.60	93.494	148.694	190.108	760.350	891.262	1844.916	10.20	34.080	57.480	77.168	308.632	377.272	1180.970
2.70	91.051	145.164	185.959	743.755	873.132	1827.693	10.40	33.575	56.659	76.098	304.351	372.179	1168.184
2.80	88.748	141.821	182.015	727.977	855.850	1810.699	10.60	33.087	55.864	75.061	300.203	367.239	1155.745
2.90	86.573	138.650	178.263	712.971	839.407	1793.971	10.80	32.615	55.093	74.056	296.184	362.449	1143.552
3.00	84.515	135.636	174.682	698.650	823.665	1777.537	11.00	32.157	54.346	73.081	292.285	357.792	1131.528
3.10	82.566	132.768	171.265	684.984	808.583	1762.768	11.20	31.714	53.622	72.136	288.503	353.272	1119.816
3.20	80.717	130.031	167.992	671.889	794.126	1749.186	11.40	31.284	52.920	71.217	284.828	348.880	1108.417
3.30	78.959	127.422	164.859	659.362	780.251	1739.309	11.60	30.866	52.238	70.324	281.257	344.608	1097.302
3.40	77.285	124.928	161.858	647.356	766.923	1729.595	11.80	30.461	51.575	69.456	277.786	340.455	1086.464
3.50	75.690	122.543	158.974	635.822	754.098	1720.013	12.00	30.068	50.932	68.613	274.413	336.414	1075.902
3.60	74.168	120.258	156.214	624.781	741.752	1710.571	12.20	29.687	50.307	67.791	271.128	332.480	1065.587
3.70	72.715	118.068	153.557	614.156	729.866	1701.809	12.40	29.316	49.699	66.992	267.932	328.651	1055.515
3.80	71.325	115.967	151.002	603.936	718.429	1693.280	12.60	28.955	49.106	66.214	264.821	324.919	1045.689
3.90	69.993	113.949	148.543	594.103	707.383	1684.886	12.80	28.604	48.530	65.457	261.792	321.284	1036.002
4.00	68.717	112.010	146.170	584.608	696.726	1676.694	13.00	28.262	47.969	64.719	258.841	317.739	1026.226
4.20	66.316	108.346	141.675	566.631	676.479	1660.556	13.20	27.930	47.421	64.000	255.964	314.282	1016.685
4.40	64.098	104.946	137.487	549.883	657.508	1643.923	13.40	27.606	46.888	63.299	253.160	310.908	1007.356
4.60	62.042	101.781	133.568	534.208	639.704	1624.916	13.60	27.290	46.368	62.615	250.424	307.615	998.231
4.80	60.139	98.825	129.895	519.514	622.996	1604.689	13.80	26.982	45.862	61.947	247.753	304.401	989.313
5.00	58.349	96.058	126.444	505.712	607.239	1589.405	14.00	26.683	45.368	61.295	245.147	301.262	980.583
5.20	56.680	93.462	123.196	492.722	592.373	1572.889	14.20	26.390	44.885	60.664	242.624	298.198	972.037
5.40	55.114	91.019	120.130	480.458	578.295	1557.033	14.40	26.105	44.414	60.042	240.135	295.204	963.678
5.60	53.642	88.717	117.231	468.866	564.959	1541.818	14.60	25.826	43.954	59.436	237.704	292.279	955.489
5.80	52.257	86.542	114.489	457.897	552.320	1522.427	14.80	25.554	43.504	58.840	235.326	289.418	947.471
6.00	50.951	84.486	111.888	447.495	540.297	1501.768	15.00	25.289	43.065	58.259	233.003	286.620	939.630
6.20	49.717	82.537	109.417	437.612	528.862	1481.907	15.50	24.651	42.009	56.862	227.416	279.884	920.698
6.40	48.548	80.688	107.067	428.213	517.948	1462.831	16.00	24.048	41.010	55.538	222.122	273.497	902.680
6.60	47.439	78.931	104.831	419.270	507.543	1444.522	16.50	23.477	40.063	54.282	217.097	267.430	885.512
6.80	46.386	77.257	102.698	410.740	497.601	1426.896	17.00	22.936	39.163	53.089	212.324	261.663	869.140
7.00	45.385	75.662	100.662	402.595	488.091	1409.919	17.50	22.423	38.308	51.953	207.783	256.172	853.297

Stopping power S of p, d, t, ^{3}He, α and ^{7}Li ions in silicon

TABLE 1 (continued)

STOPPING POWER IN MEV.SQCM/GM FOR SILICON Z= 14 A= 28.086 I= 173.5

E(MEV)	P	D	T	HE 3	HE 4	LI 7	E(MEV)	P	D	T	HE 3	HE 4	LI 7
17.50	22.423	38.308	51.953	207.783	256.172	833.297	40.00	11.723	20.189	27.668	110.654	137.680	473.728
18.00	21.934	37.493	50.872	203.458	250.937	837.499	40.50	11.610	19.993	27.402	109.592	136.375	469.398
18.50	21.469	36.717	49.840	199.311	245.938	822.376	41.00	11.499	19.802	27.142	108.553	135.094	465.076
19.00	21.025	35.975	48.854	195.388	241.179	807.881	41.50	11.391	19.614	26.888	107.537	133.841	460.807
19.50	20.601	35.267	47.911	191.617	236.600	793.990	42.00	11.285	19.431	26.639	106.541	132.613	456.784
20.00	20.197	34.589	47.008	188.004	232.214	780.647	42.50	11.181	19.251	26.395	105.566	131.412	452.761
20.50	19.809	33.939	46.142	184.544	228.008	767.822	43.00	11.079	19.075	26.156	104.611	130.235	448.815
21.00	19.438	33.316	45.313	181.226	223.970	755.487	43.50	10.980	18.903	25.922	103.674	129.081	444.947
21.50	19.083	32.719	44.516	178.038	220.089	743.615	44.00	10.883	18.734	25.693	102.757	127.949	441.152
22.00	18.741	32.145	43.750	174.975	216.356	732.180	44.50	10.787	18.568	25.468	101.857	126.840	437.431
22.50	18.413	31.593	43.013	172.028	212.766	721.156	45.00	10.694	18.406	25.247	100.975	125.751	433.779
23.00	18.098	31.062	42.304	169.190	209.308	710.190	45.50	10.602	18.247	25.031	100.109	124.684	430.195
23.50	17.795	30.550	41.620	166.455	205.973	699.313	46.00	10.513	18.091	24.819	99.260	123.636	426.676
24.00	17.503	30.057	40.960	163.818	202.761	688.809	46.50	10.425	17.938	24.610	98.427	122.608	423.220
24.50	17.222	29.582	40.324	161.274	199.658	678.657	47.00	10.338	17.788	24.406	97.610	121.598	419.826
25.00	16.950	29.123	39.710	158.816	196.660	668.846	47.50	10.254	17.641	24.205	96.807	120.608	416.498
25.50	16.689	28.680	39.116	156.440	193.762	659.355	48.00	10.171	17.496	24.008	96.019	119.636	413.231
26.00	16.436	28.251	38.541	154.143	190.958	650.165	48.50	10.089	17.354	23.815	95.246	118.682	410.020
26.50	16.192	27.837	37.986	151.921	188.242	641.257	49.00	10.009	17.215	23.625	94.487	117.744	406.864
27.00	15.956	27.436	37.448	149.769	185.613	632.621	49.50	9.931	17.078	23.439	93.742	116.823	403.761
27.50	15.727	27.048	36.926	147.684	183.068	624.246	50.00	9.854	16.944	23.256	93.009	115.918	400.711
28.00	15.506	26.672	36.421	145.663	180.600	616.118	51.00	9.704	16.682	22.899	91.582	114.154	394.764
28.50	15.292	26.308	35.931	143.702	178.205	608.225	52.00	9.560	16.430	22.554	90.203	112.448	389.016
29.00	15.085	25.955	35.456	141.802	175.880	600.558	53.00	9.420	16.186	22.221	88.869	110.799	383.451
29.50	14.883	25.612	34.994	139.958	173.625	593.108	54.00	9.285	15.950	21.898	87.579	109.203	378.060
30.00	14.688	25.279	34.546	138.165	171.432	585.867	55.00	9.155	15.721	21.586	86.331	107.658	372.836
30.50	14.499	24.955	34.111	136.424	169.301	578.825	56.00	9.028	15.500	21.283	85.121	106.162	367.776
31.00	14.315	24.641	33.687	134.730	167.227	571.974	57.00	8.906	15.286	20.990	83.949	104.712	362.867
31.50	14.136	24.336	33.275	133.082	165.210	565.302	58.00	8.788	15.079	20.706	82.813	103.305	358.102
32.00	13.962	24.038	32.875	131.480	163.249	558.804	59.00	8.673	14.878	20.431	81.711	101.940	353.473
32.50	13.793	23.749	32.485	129.921	161.338	552.474	60.00	8.562	14.682	20.163	80.641	100.614	348.976
33.00	13.629	23.468	32.105	128.403	159.477	546.352	61.00	8.454	14.493	19.904	79.603	99.327	344.609
33.50	13.469	23.194	31.735	126.923	157.663	540.330	62.00	8.350	14.309	19.651	78.594	98.076	340.363
34.00	13.314	22.927	31.375	125.481	155.894	534.455	63.00	8.248	14.130	19.406	77.614	96.859	336.231
34.50	13.162	22.667	31.023	124.075	154.170	528.720	64.00	8.150	13.957	19.168	76.660	95.676	332.209
35.00	13.014	22.414	30.680	122.704	152.488	523.128	65.00	8.054	13.788	18.936	75.733	94.526	328.293
35.50	12.871	22.167	30.346	121.366	150.847	517.667	66.00	7.961	13.624	18.710	74.831	93.407	324.479
36.00	12.730	21.925	30.020	120.061	149.245	512.333	67.00	7.870	13.464	18.491	73.952	92.316	320.766
36.50	12.594	21.690	29.701	118.788	147.680	507.119	68.00	7.782	13.308	18.277	73.097	91.254	317.148
37.00	12.460	21.460	29.391	117.545	146.152	502.026	69.00	7.696	13.157	18.068	72.263	90.219	313.620
37.50	12.330	21.236	29.087	116.331	144.658	497.045	70.00	7.613	13.009	17.865	71.451	89.210	310.177
38.00	12.203	21.017	28.790	115.144	143.199	492.174	71.00	7.532	12.866	17.667	70.659	88.226	306.818
38.50	12.079	20.803	28.500	113.984	141.773	487.408	72.00	7.452	12.725	17.474	69.886	87.265	303.539
39.00	11.957	20.593	28.216	112.849	140.379	482.748	73.00	7.375	12.589	17.286	69.133	86.328	300.337
39.50	11.839	20.389	27.939	111.740	139.015	478.191	74.00	7.300	12.455	17.102	68.398	85.414	297.211
40.00	11.723	20.189	27.668	110.654	137.680	473.728	75.00	7.226	12.325	16.923	67.680	84.520	294.158

Stopping power S of p, d, t, ^{3}He, α and ^{7}Li ions in silicon

TABLE 1 (continued)

STOPPING POWER IN MEV.SQCM/GM FOR SILICON

E(MEV)	P	D	T	HE 3	HE 4	LI 7
75.00	7.226	12.325	16.923	67.680	84.520	294.158
76.00	7.155	12.198	16.747	66.980	83.648	291.174
77.00	7.085	12.074	16.576	66.295	82.795	288.257
78.00	7.016	11.953	16.409	65.627	81.962	285.405
79.00	6.950	11.834	16.246	64.973	81.148	282.614
80.00	6.885	11.718	16.086	64.334	80.352	279.884
81.00	6.821	11.605	15.930	63.709	79.573	277.212
82.00	6.759	11.495	15.777	63.098	78.811	274.596
83.00	6.698	11.386	15.627	62.500	78.065	272.034
84.00	6.638	11.280	15.481	61.914	77.335	269.529
85.00	6.580	11.177	15.338	61.341	76.620	267.076
86.00	6.523	11.075	15.197	60.780	75.920	264.671
87.00	6.467	10.976	15.060	60.230	75.234	262.315
88.00	6.413	10.879	14.925	59.692	74.561	260.004
89.00	6.359	10.783	14.793	59.164	73.903	257.739
90.00	6.307	10.690	14.664	58.647	73.257	255.517
91.00	6.256	10.598	14.537	58.141	72.624	253.337
92.00	6.206	10.509	14.413	57.644	72.003	251.199
93.00	6.157	10.421	14.291	57.156	71.394	249.101
94.00	6.108	10.334	14.172	56.678	70.796	247.041
95.00	6.061	10.250	14.054	56.209	70.210	245.019
96.00	6.015	10.167	13.939	55.749	69.635	243.035
97.00	5.969	10.085	13.826	55.297	69.070	241.088
98.00	5.925	10.005	13.715	54.854	68.516	239.175
99.00	5.881	9.927	13.607	54.419	67.971	237.296
100.00	5.838	9.850	13.500	53.991	67.437	235.449
101.00	5.796	9.774	13.395	53.572	66.912	233.634
102.00	5.754	9.701	13.292	53.159	66.396	231.851
103.00	5.714	9.628	13.190	52.754	65.889	230.097
104.00	5.674	9.556	13.091	52.356	65.390	228.373
105.00	5.635	9.486	12.993	51.965	64.901	226.677
106.00	5.596	9.416	12.897	51.580	64.419	225.010
107.00	5.558	9.348	12.802	51.202	63.945	223.369
108.00	5.521	9.282	12.709	50.830	63.480	221.755
109.00	5.485	9.216	12.618	50.465	63.022	220.167
110.00	5.449	9.151	12.528	50.105	62.571	218.604
111.00	5.413	9.087	12.440	49.751	62.128	217.066
112.00	5.379	9.025	12.353	49.403	61.691	215.553
113.00	5.344	8.963	12.267	49.061	61.262	214.064
114.00	5.311	8.903	12.183	48.724	60.839	212.597
115.00	5.278	8.843	12.100	48.392	60.423	211.153
116.00	5.245	8.785	12.018	48.065	60.014	209.731
117.00	5.213	8.727	11.938	47.744	59.610	208.330
118.00	5.182	8.670	11.858	47.427	59.213	206.950
119.00	5.151	8.614	11.781	47.115	58.822	205.590
120.00	5.120	8.559	11.704	46.808	58.436	204.250

Z= 14 A= 28.086 I= 173.5

E(MEV)	P	D	T	HE 3	HE 4	LI 7
120.00	5.120	8.559	11.704	46.808	58.436	204.250
122.00	5.061	8.451	11.554	46.208	57.683	201.628
124.00	5.003	8.347	11.408	45.625	56.951	199.081
126.00	4.947	8.245	11.266	45.058	56.240	196.604
128.00	4.893	8.147	11.129	44.508	55.548	194.196
130.00	4.840	8.051	10.995	43.974	54.877	191.853
132.00	4.789	7.958	10.865	43.454	54.223	189.572
134.00	4.739	7.867	10.738	42.948	53.587	187.351
136.00	4.690	7.779	10.615	42.455	52.968	185.189
138.00	4.643	7.694	10.496	41.976	52.366	183.082
140.00	4.597	7.610	10.379	41.509	51.778	181.029
142.00	4.552	7.529	10.265	41.054	51.206	179.027
144.00	4.509	7.450	10.154	40.611	50.648	177.073
146.00	4.467	7.372	10.046	40.178	50.104	175.167
148.00	4.425	7.297	9.941	39.757	49.573	173.307
150.00	4.385	7.224	9.838	39.345	49.055	171.491
152.00	4.346	7.152	9.738	38.946	48.549	169.717
154.00	4.308	7.082	9.640	38.554	48.055	167.984
156.00	4.270	7.014	9.544	38.171	47.573	166.290
158.00	4.234	6.947	9.451	37.797	47.101	164.634
160.00	4.198	6.882	9.359	37.432	46.641	163.016
162.00	4.164	6.818	9.270	37.075	46.190	161.432
164.00	4.130	6.756	9.183	36.726	45.750	159.883
166.00	4.097	6.695	9.097	36.384	45.319	158.368
168.00	4.064	6.636	9.014	36.050	44.897	156.884
170.00	4.033	6.578	8.932	35.723	44.485	155.432
172.00	4.002	6.521	8.852	35.403	44.081	154.010
174.00	3.971	6.465	8.774	35.090	43.686	152.618
176.00	3.942	6.411	8.697	34.783	43.299	151.254
178.00	3.913	6.357	8.622	34.483	42.919	149.917
180.00	3.884	6.305	8.548	34.189	42.548	148.607
182.00	3.857	6.254	8.476	33.901	42.183	147.322
184.00	3.829	6.203	8.406	33.618	41.826	146.062
186.00	3.803	6.154	8.337	33.341	41.476	144.827
188.00	3.777	6.106	8.269	33.070	41.133	143.615
190.00	3.751	6.059	8.202	32.804	40.797	142.425
192.00	3.726	6.012	8.137	32.542	40.466	141.258
194.00	3.701	5.967	8.073	32.286	40.142	140.113
196.00	3.677	5.922	8.010	32.035	39.824	138.988
198.00	3.654	5.879	7.948	31.788	39.512	137.884
200.00	3.631	5.836	7.888	31.546	39.206	136.799

Stopping power S of p, d, t, ^{3}He, α and ^{7}Li ions in silicon

Table 2 Range of heavy particles in silicon

TABLE 2

RANGES IN GM/SQCM FOR SILICON Z= 14 A= 28.086 I= 173.5

E(MEV)	P	D	T	HE 3	HE 4	LI 7	E(MEV)	P	D	T	HE 3	HE 4	LI 7
1.00	.003830	.002863	.002553	.001039	.000960	.000750	7.00	.089838	.055734	.043135	.011181	.009508	.004331
1.10	.004389	.003260	.002887	.001115	.001042	.000803	7.20	.094292	.058405	.045141	.011682	.009922	.004474
1.20	.005011	.003679	.003236	.001203	.001125	.000856	7.40	.098841	.061127	.047187	.012194	.010344	.004619
1.30	.005667	.004117	.003598	.001294	.001209	.000908	7.60	.103483	.063908	.049271	.012715	.010779	.004764
1.40	.006356	.004573	.003969	.001388	.001294	.000959	7.80	.108219	.066739	.051394	.013246	.011229	.004912
1.50	.007077	.005048	.004353	.001484	.001383	.001013	8.00	.113047	.069624	.053556	.013786	.011694	.005061
1.60	.007830	.005541	.004750	.001583	.001468	.001061	8.20	.117969	.072562	.055756	.014336	.012176	.005212
1.70	.008614	.006052	.005160	.001686	.001559	.001112	8.40	.122982	.075553	.057993	.014896	.012666	.005364
1.80	.009430	.006580	.005582	.001791	.001652	.001163	8.60	.128087	.078596	.060269	.015465	.013133	.005518
1.90	.010277	.007126	.006018	.001900	.001747	.001215	8.80	.133283	.081692	.062583	.016043	.013598	.005673
2.00	.011154	.007690	.006465	.002012	.001843	.001267	9.00	.138570	.084839	.064934	.016631	.013990	.005830
2.10	.012062	.008270	.006925	.002127	.001941	.001319	9.20	.143947	.088038	.067323	.017228	.014483	.005989
2.20	.012999	.008868	.007398	.002245	.002044	.001371	9.40	.149415	.091288	.069749	.017835	.014977	.006150
2.30	.013967	.009482	.007882	.002366	.002148	.001423	9.60	.154972	.094590	.072212	.018451	.015481	.006313
2.40	.014964	.010113	.008378	.002490	.002254	.001476	9.80	.160619	.097942	.074712	.019076	.015993	.006478
2.50	.015990	.010761	.008887	.002618	.002363	.001529	10.00	.166354	.101346	.077248	.019710	.016513	.006644
2.60	.017045	.011425	.009407	.002748	.002474	.001583	10.20	.172179	.104800	.079822	.020354	.017039	.006813
2.70	.018129	.012106	.009939	.002881	.002587	.001638	10.40	.178091	.108305	.082432	.021006	.017573	.006983
2.80	.019241	.012803	.010482	.003016	.002703	.001693	10.60	.184092	.111860	.085078	.021668	.018114	.007155
2.90	.020382	.013516	.011037	.003155	.002821	.001748	10.80	.190180	.115465	.087761	.022339	.018662	.007329
3.00	.021551	.014246	.011604	.003297	.002941	.001804	11.00	.196356	.119120	.090480	.023018	.019217	.007505
3.10	.022749	.014991	.012182	.003442	.003064	.001861	11.20	.202619	.122825	.093234	.023707	.019780	.007683
3.20	.023974	.015752	.012772	.003589	.003189	.001918	11.40	.208969	.126580	.096025	.024405	.020353	.007862
3.30	.025226	.016529	.013373	.003739	.003316	.001975	11.60	.215405	.130384	.098851	.025112	.020926	.008043
3.40	.026507	.017321	.013985	.003892	.003445	.002033	11.80	.221928	.134237	.101713	.025827	.021513	.008227
3.50	.027814	.018130	.014608	.004048	.003577	.002091	12.00	.228537	.138139	.104610	.026551	.022101	.008412
3.60	.029149	.018954	.015243	.004207	.003710	.002149	12.20	.235231	.142091	.107542	.027285	.022699	.008598
3.70	.030511	.019793	.015889	.004368	.003846	.002207	12.40	.242011	.146090	.110510	.028027	.023306	.008787
3.80	.031899	.020647	.016545	.004532	.003984	.002266	12.60	.248875	.150139	.113513	.028778	.023916	.008977
3.90	.033315	.021517	.017213	.004699	.004125	.002326	12.80	.255825	.154236	.116551	.029537	.024535	.009169
4.00	.034757	.022403	.017892	.004869	.004267	.002385	13.00	.262859	.158381	.119624	.030306	.025161	.009363
4.20	.037720	.024218	.019282	.005217	.004558	.002505	13.20	.269978	.162575	.122732	.031083	.025794	.009559
4.40	.040788	.026094	.020715	.005575	.004858	.002626	13.40	.277181	.166816	.125874	.031868	.026434	.009757
4.60	.043960	.028030	.022191	.005944	.005167	.002748	13.60	.284468	.171105	.129051	.032663	.027081	.009956
4.80	.047235	.030024	.023710	.006324	.005484	.002872	13.80	.291838	.175443	.132262	.033466	.027735	.010158
5.00	.050612	.032077	.025270	.006714	.005809	.002997	14.00	.299292	.179827	.135508	.034277	.028395	.010361
5.20	.054090	.034188	.026873	.007115	.006142	.003124	14.20	.306829	.184262	.138788	.035097	.029062	.010566
5.40	.057669	.036357	.028517	.007526	.006484	.003252	14.40	.314449	.188739	.142102	.035926	.029736	.010772
5.60	.061347	.038583	.030203	.007947	.006834	.003381	14.60	.322152	.193266	.145450	.036763	.030417	.010981
5.80	.065125	.040865	.031929	.008379	.007192	.003511	14.80	.329937	.197839	.148832	.037609	.031105	.011191
6.00	.069002	.043205	.033696	.008821	.007558	.003643	15.00	.337805	.202460	.152249	.038463	.031799	.011403
6.20	.072976	.045600	.035504	.009273	.007932	.003777	15.50	.357533	.214216	.160936	.040635	.033565	.011940
6.40	.077047	.048051	.037352	.009735	.008314	.003913	16.00	.378371	.226264	.169534	.042860	.035372	.012489
6.60	.081215	.050557	.039240	.010207	.008705	.004051	16.50	.399416	.238603	.178941	.045137	.037221	.013048
6.80	.085479	.053118	.041168	.010689	.009103	.004193	17.00	.420964	.251226	.188256	.047466	.039111	.013618
7.00	.089838	.055734	.043135	.011181	.009508	.004331	17.50	.443014	.264134	.197777	.049847	.041043	.014199

Ranges R in silicon

TABLE 2 (continued)

RANGES IN GM/SQCM FOR SILICON Z= 14 A= 28.086 I= 173.5

E(MEV)	P	D	T	HE 3	HE 4	LI 7
17.50	.443014	.264134	.197777	.049847	.041043	.014199
18.00	.465561	.277328	.207504	.052279	.043015	.014790
18.50	.488604	.290805	.217434	.054762	.045028	.015393
19.00	.512140	.304563	.227568	.057295	.047081	.016006
19.50	.536166	.318601	.237903	.059879	.049174	.016630
20.00	.560680	.332918	.248439	.062514	.051307	.017266
20.50	.585679	.347512	.259176	.065198	.053480	.017911
21.00	.611161	.362382	.270111	.067933	.055693	.018566
21.50	.637123	.377527	.281244	.070716	.057945	.019235
22.00	.663564	.392945	.292575	.073549	.060236	.019913
22.50	.690480	.408635	.304101	.076431	.062567	.020601
23.00	.717871	.424597	.315823	.079362	.064936	.021299
23.50	.745734	.440829	.327740	.082342	.067345	.022009
24.00	.774066	.457330	.339850	.085370	.069791	.022729
24.50	.802866	.474099	.352153	.088446	.072276	.023461
25.00	.832132	.491135	.364649	.091570	.074800	.024203
25.50	.861861	.508436	.377336	.094743	.077361	.024956
26.00	.892052	.526002	.390214	.097963	.079961	.025719
26.50	.922702	.543832	.403282	.101230	.082598	.026494
27.00	.953810	.561925	.416539	.104545	.085273	.027279
27.50	.985374	.580280	.429985	.107907	.087986	.028075
28.00	1.017393	.598896	.443620	.111316	.090735	.028881
28.50	1.049863	.617772	.457442	.114772	.093523	.029698
29.00	1.082785	.636907	.471451	.118275	.096347	.030525
29.50	1.116155	.656300	.485646	.121824	.099208	.031363
30.00	1.149973	.675951	.500027	.125420	.102106	.032211
30.50	1.184237	.695859	.514592	.129062	.105041	.033070
31.00	1.218944	.716022	.529343	.132750	.108013	.033939
31.50	1.254094	.736441	.544277	.136484	.111021	.034818
32.00	1.289685	.757114	.559395	.140264	.114066	.035708
32.50	1.325715	.778041	.574695	.144090	.117147	.036607
33.00	1.362183	.799220	.590178	.147961	.120264	.037518
33.50	1.399087	.820652	.605843	.151878	.123417	.038438
34.00	1.436426	.842334	.621688	.155840	.126607	.039368
34.50	1.474198	.864267	.637715	.159847	.129832	.040309
35.00	1.512401	.886450	.653922	.163899	.133093	.041260
35.50	1.551035	.908882	.670309	.167997	.136390	.042220
36.00	1.590097	.931563	.686875	.172139	.139722	.043191
36.50	1.629587	.954491	.703621	.176326	.143090	.044172
37.00	1.669502	.977666	.720544	.180557	.146495	.045163
37.50	1.709843	1.001088	.737645	.184833	.149932	.046164
38.00	1.750606	1.024756	.754923	.189155	.153406	.047175
38.50	1.791791	1.048669	.772379	.193518	.156916	.048196
39.00	1.833397	1.072827	.790011	.197926	.160460	.049227
39.50	1.875422	1.097229	.807819	.202379	.164039	.050267
40.00	1.917865	1.121874	.825803	.206876	.167653	.051318

E(MEV)	P	D	T	HE 3	HE 4	LI 7
40.00	1.917865	1.121874	.825803	.206876	.167653	.051318
40.50	1.960725	1.146761	.843962	.211416	.171302	.052378
41.00	2.004000	1.171891	.862296	.216000	.174986	.053449
41.50	2.047689	1.197262	.880805	.220628	.178705	.054529
42.00	2.091790	1.222875	.899488	.225299	.182459	.055618
42.50	2.136304	1.248727	.918344	.230014	.186245	.056718
43.00	2.181227	1.274823	.937373	.234772	.190067	.057827
43.50	2.226560	1.301151	.956575	.239573	.193924	.058946
44.00	2.272301	1.327722	.975949	.244418	.197814	.060074
44.50	2.318448	1.354530	.995496	.249305	.201739	.061213
45.00	2.365001	1.381570	1.015214	.254235	.205698	.062360
45.50	2.411959	1.408859	1.035104	.259209	.209691	.063518
46.00	2.459319	1.436379	1.055165	.264225	.213719	.064685
46.50	2.507082	1.464135	1.075396	.269283	.217780	.065862
47.00	2.555245	1.492126	1.095798	.274384	.221875	.067048
47.50	2.603808	1.520352	1.116370	.279528	.226003	.068244
48.00	2.652770	1.548813	1.137111	.284714	.230166	.069449
48.50	2.702130	1.577509	1.158022	.289942	.234362	.070664
49.00	2.751886	1.606436	1.179101	.295213	.238592	.071888
49.50	2.802037	1.635597	1.200349	.300526	.242855	.073121
50.00	2.852582	1.664990	1.221765	.305881	.247152	.074364
50.50	2.903519	1.724471	1.265100	.316716	.255845	.076879
51.00	2.954850	1.784876	1.309135	.327719	.264672	.079431
51.50	3.006575	1.845200	1.353376	.338888	.273631	.082020
52.00	3.058693	1.905441	1.397811	.350224	.282722	.084646
52.50	3.111203	1.966599	1.442437	.361725	.291945	.087310
53.00	3.164104	2.028670	1.487253	.373390	.301299	.090011
53.50	3.217395	2.091653	1.532258	.385220	.310784	.092748
54.00	3.271074	2.155547	1.577451	.397214	.320399	.095522
54.50	3.325140	2.220350	1.622830	.409371	.330144	.098333
55.00	3.379593	2.285063	1.668395	.421690	.340019	.101180
55.50	3.434433	2.349684	1.714144	.434172	.350022	.104064
56.00	3.489657	2.414212	1.760077	.446815	.360154	.106984
56.50	3.545265	2.478647	1.806193	.459619	.370414	.109943
57.00	3.601256	2.543987	1.852491	.472583	.380803	.112939
57.50	3.657628	2.609232	1.898970	.485708	.391318	.115960
58.00	3.714382	2.674380	1.945631	.498992	.401961	.119024
58.50	3.771516	2.739430	1.992473	.512435	.412730	.122124
59.00	3.829029	2.804381	2.039495	.526036	.423625	.125259
59.50	3.886921	2.869233	2.086697	.539796	.434646	.128430
60.00	3.945190	2.934984	2.134078	.553713	.445793	.131637
60.50	4.003836	3.000634	2.181637	.567787	.457065	.134878
61.00	4.062860	3.066181	2.229375	.582018	.468462	.138155
61.50	4.122260	3.131624	2.277290	.596405	.479984	.141467
62.00	4.182034	3.196962	2.325382	.610947	.491630	.144814
62.50	4.242181	3.262194	2.373650	.625645	.503399	.148196
63.00	4.302700	3.327319	2.422094	.640497	.515292	.151613
63.50	4.363590	3.392336	2.470713	.655503	.527308	.155065
64.00	4.424850	3.457245	2.519507	.670663	.539446	.158552
64.50	4.486479	3.522044	2.568475	.685977	.551707	.162074
65.00	4.548476	3.586733	2.617616	.701444	.564090	.165631
65.50	4.610839	3.651311	2.666929	.717064	.576594	.169223
66.00	4.673568	3.715777	2.716414	.732836	.589220	.172850
66.50	4.736663	3.780130	2.766071	.748759	.601967	.176511
67.00	4.798889	3.844369	2.815898	.764833	.614834	.180207
67.50	4.862589	3.908493	2.865895	.781057	.627821	.183938
68.00	4.926089	3.972501	2.916061	.797430	.640928	.187703
68.50	4.989584	4.036392	2.966396	.813952	.654154	.191503
69.00	5.055284	4.049622	2.157267	.539796	.434646	.128430
69.50	5.120980	4.062852	2.348138	.265639	.215138	.065357
70.00	5.185722	4.026359	2.212947	.553713	.445793	.131637
70.50	5.250464	3.989866	2.077756	.841787	.676448	.198916
71.00	5.317994	3.103356	2.269235	.567787	.457065	.134878
71.50	5.385525	3.216846	2.460714	.293788	.237682	.070839
72.00	5.451475	3.181511	2.324150	.582018	.468462	.138155
72.50	5.517425	3.146176	2.187586	.870248	.699242	.205471
73.00	5.586365	3.263521	2.383689	.596405	.479984	.141467
73.50	5.655305	3.380866	2.579792	.322121	.260726	.077463
74.00	5.722657	3.343383	2.447551	.610947	.491630	.144814
74.50	5.790009	3.305900	2.315310	.899773	.722534	.212164
75.00	5.863344	3.421075	2.506634	.625645	.503399	.148196

Ranges R in silicon

TABLE 2 (continued)

RANGES IN GM/SQCM FOR SILICON

Z= 14 A= 28.086 I= 173.0

E(MEV)	P	D	T	HE 3	HE 4	LI 7
75.00	5.860344	3.421995	2.500634	.625645	.533190	.146195
76.00	5.999422	3.532654	2.560336	.640495	.515292	.151613
77.00	6.139882	3.583056	2.620355	.655505	.527309	.155305
78.00	6.281720	3.668300	2.680690	.670666	.539445	.159051
79.00	6.424928	3.752383	2.741938	.685980	.551717	.162873
80.00	6.569502	3.837302	2.803799	.701448	.564096	.165629
81.00	6.715434	3.923054	2.866273	.717068	.576601	.169218
82.00	6.862719	4.009637	2.929351	.732840	.589229	.172843
83.00	7.011351	4.097049	2.993038	.748755	.601974	.176532
84.00	7.161323	4.185287	3.057332	.764840	.614849	.180175
85.00	7.312631	4.274348	3.122230	.781067	.627839	.183922
86.00	7.465268	4.364233	3.187730	.797445	.640951	.187683
87.00	7.619229	4.454931	3.253832	.813973	.654183	.191479
88.00	7.774509	4.546444	3.320534	.830650	.667535	.195308
89.00	7.931100	4.638778	3.387833	.847473	.681006	.199171
90.00	8.088998	4.731920	3.455730	.864454	.694597	.203067
91.00	8.248198	4.825871	3.524221	.881580	.708307	.206998
92.00	8.408693	4.920627	3.593306	.898854	.722135	.210962
93.00	8.570479	5.016171	3.662984	.916276	.736084	.214960
94.00	8.733550	5.112555	3.733252	.933845	.750150	.218991
95.00	8.897901	5.209719	3.804110	.951563	.764334	.223056
96.00	9.063526	5.307680	3.875556	.969427	.778636	.227154
97.00	9.230420	5.406417	3.947587	.987438	.793055	.231285
98.00	9.398578	5.505907	4.020207	1.005595	.807592	.235449
99.00	9.567995	5.606328	4.093409	1.023898	.822245	.239647
100.00	9.738665	5.707458	4.167193	1.042347	.837016	.243878
101.00	9.910584	5.809374	4.241559	1.060941	.851903	.248141
102.00	10.083746	5.912069	4.316504	1.079680	.866906	.252438
103.00	10.258147	6.015545	4.392027	1.098564	.882025	.256767
104.00	10.433781	6.119801	4.468128	1.117591	.897260	.261130
105.00	10.611646	6.224835	4.544804	1.136763	.912611	.265525
106.00	10.788730	6.330646	4.622055	1.156079	.928076	.269953
107.00	10.968035	6.437230	4.699879	1.175538	.943657	.274414
108.00	11.148554	6.544586	4.778275	1.195140	.959353	.278937
109.00	11.330282	6.652711	4.857242	1.214884	.975163	.283432
110.00	11.513214	6.761605	4.936779	1.234771	.991088	.287991
111.00	11.697346	6.871264	5.016883	1.254800	1.007127	.292581
112.00	11.882672	6.981687	5.097554	1.274971	1.023280	.297204
113.00	12.069189	7.092872	5.178792	1.295284	1.039546	.301860
114.00	12.256891	7.204817	5.260593	1.315737	1.055926	.306547
115.00	12.445774	7.317519	5.342959	1.336331	1.072420	.311267
116.00	12.635833	7.430977	5.425886	1.357066	1.089026	.316019
117.00	12.827064	7.545193	5.509375	1.377942	1.105745	.320803
118.00	13.019463	7.660154	5.593423	1.398957	1.122577	.325619
119.00	13.213024	7.775869	5.678030	1.420112	1.139522	.330467
120.00	13.407743	7.892332	5.763194	1.441406	1.156578	.335347

E(MEV)	P	D	T	HE 3	HE 4	LI 7
120.00	13.407743	7.892332	5.763194	1.441406	1.156578	.335347
122.00	13.803539	8.127495	5.935191	1.484411	1.191027	.345203
124.00	14.178116	8.355629	6.109424	1.527771	1.225923	.355196
126.00	14.629135	8.576715	6.285924	1.572083	1.261261	.365233
128.00	15.076671	8.850753	6.464443	1.616746	1.297047	.375311
130.00	15.417682	9.097739	6.645252	1.663953	1.333272	.385893
132.00	15.833139	9.347553	6.828242	1.707707	1.369937	.396350
134.00	16.253304	9.600351	7.013424	1.754304	1.407040	.406893
135.00	16.677249	9.856038	7.200731	1.800843	1.444581	.417732
138.00	17.105841	10.114535	7.390213	1.845223	1.482557	.428592
140.00	17.538747	10.375971	7.581843	1.875135	1.520967	.439578
142.00	17.975936	10.640152	7.775612	1.944584	1.559809	.450688
144.00	18.417377	10.907014	7.971513	1.973566	1.597312	.461921
146.00	18.863040	11.177095	8.169537	2.043080	1.638785	.473278
148.00	19.312899	11.449781	8.369676	2.093122	1.678916	.484757
150.00	19.766927	11.725259	8.571924	2.143691	1.719474	.496358
152.00	20.225352	12.003515	8.776269	2.194785	1.763457	.508081
154.00	20.687298	12.284544	8.982694	2.245399	1.801865	.519926
156.00	21.153617	12.568325	9.191205	2.298534	1.843695	.531893
158.00	21.623983	12.854849	9.401792	2.351189	1.885946	.543981
160.00	22.098357	13.144103	9.614453	2.404351	1.928618	.556189
162.00	22.576722	13.436075	9.829170	2.458048	1.971708	.568518
164.00	23.059045	13.730754	10.045945	2.512250	2.015216	.580967
166.00	23.545303	14.028128	10.264767	2.566964	2.059140	.593536
168.00	24.035460	14.329194	10.485631	2.622188	2.103479	.606225
170.00	24.529496	14.630912	10.708528	2.677920	2.148231	.619033
172.00	25.027383	14.936299	10.933452	2.734159	2.193397	.631959
174.00	25.529093	15.244334	11.160396	2.790903	2.238973	.645005
176.00	26.034601	15.555037	11.389353	2.848151	2.284959	.658169
178.00	26.543881	15.868335	11.620316	2.905900	2.331354	.671450
180.00	27.056906	16.184217	11.853278	2.964149	2.378157	.684850
182.00	27.573652	16.502733	12.088233	3.022896	2.425366	.698367
184.00	28.094094	16.823842	12.325174	3.082140	2.472981	.712001
186.00	28.618235	17.147532	12.564094	3.141878	2.520999	.725753
188.00	29.145952	17.473772	12.804987	3.202110	2.569420	.739620
190.00	29.677243	17.802613	13.047847	3.262836	2.618244	.753605
192.00	30.212315	18.133984	13.292668	3.324048	2.667469	.767705
194.00	30.753852	18.467894	13.539439	3.385753	2.717091	.781922
196.00	31.292959	18.804332	13.788152	3.447939	2.767113	.796254
198.00	31.838580	19.143298	14.038822	3.510613	2.817532	.810701
200.00	32.387724	19.484753	14.291418	3.573772	2.868347	.825263

Ranges R in silicon

Table 3 dE/dx and range of electrons in silicon

Table 4.–Continued

ELECTRONS IN SILICON

ENERGY	STOPPING POWER COLLISION	RADIATION	TOTAL	RANGE	RADIATION YIELD
MEV	MEV CM2/G	MEV CM2/G	MEV CM2/G	G/CM2	
0.010	1.692E 01	9.576E-03	1.693E 01	3.454E-04	3.274E-04
0.015	1.253E 01	9.459E-03	1.254E 01	6.933E-04	4.389E-04
0.020	1.011E 01	9.344E-03	1.012E 01	1.140E-03	5.392E-04
0.025	8.570E 00	9.286E-03	8.579E 00	1.679E-03	6.321E-04
0.030	7.491E 00	9.252E-03	7.501E 00	2.304E-03	7.198E-04
0.035	6.693E 00	9.223E-03	6.702E 00	3.011E-03	8.034E-04
0.040	6.077E 00	9.241E-03	6.086E 00	3.795E-03	8.839E-04
0.045	5.586E 00	9.280E-03	5.595E 00	4.653E-03	9.622E-04
0.050	5.185E 00	9.333E-03	5.194E 00	5.581E-03	1.039E-03
0.055	4.851E 00	9.396E-03	4.860E 00	6.577E-03	1.114E-03
0.060	4.568E 00	9.467E-03	4.578E 00	7.638E-03	1.188E-03
0.065	4.326E 00	9.544E-03	4.335E 00	8.761E-03	1.261E-03
0.070	4.116E 00	9.626E-03	4.125E 00	9.944E-03	1.333E-03
0.075	3.932E 00	9.713E-03	3.942E 00	1.118E-02	1.404E-03
0.080	3.769E 00	9.803E-03	3.779E 00	1.248E-02	1.474E-03
0.085	3.625E 00	9.906E-03	3.635E 00	1.383E-02	1.544E-03
0.090	3.495E 00	1.000E-02	3.505E 00	1.523E-02	1.613E-03
0.095	3.379E 00	1.010E-02	3.389E 00	1.668E-02	1.682E-03
0.100	3.273E 00	1.020E-02	3.284E 00	1.818E-02	1.750E-03
0.150	2.592E 00	1.125E-02	2.603E 00	3.550E-02	2.406E-03
0.200	2.246E 00	1.230E-02	2.258E 00	5.625E-02	3.027E-03
0.250	2.039E 00	1.348E-02	2.053E 00	7.955E-02	3.624E-03
0.300	1.904E 00	1.472E-02	1.919E 00	1.048E-01	4.207E-03
0.350	1.805E 00	1.602E-02	1.821E 00	1.316E-01	4.784E-03
0.400	1.739E 00	1.730E-02	1.756E 00	1.596E-01	5.352E-03
0.450	1.689E 00	1.860E-02	1.707E 00	1.885E-01	5.909E-03
0.500	1.651E 00	1.989E-02	1.671E 00	2.181E-01	6.459E-03
0.550	1.621E 00	2.117E-02	1.642E 00	2.483E-01	6.999E-03
0.600	1.598E 00	2.245E-02	1.620E 00	2.790E-01	7.530E-03
0.650	1.580E 00	2.372E-02	1.603E 00	3.100E-01	8.053E-03
0.700	1.565E 00	2.499E-02	1.590E 00	3.413E-01	8.567E-03
0.750	1.553E 00	2.626E-02	1.579E 00	3.729E-01	9.074E-03
0.800	1.544E 00	2.753E-02	1.571E 00	4.046E-01	9.574E-03
0.850	1.536E 00	2.887E-02	1.565E 00	4.365E-01	1.007E-02
0.900	1.530E 00	3.014E-02	1.560E 00	4.685E-01	1.056E-02
0.950	1.525E 00	3.140E-02	1.557E 00	5.006E-01	1.104E-02
1.000	1.522E 00	3.267E-02	1.554E 00	5.327E-01	1.152E-02
1.100	1.516E 00	3.519E-02	1.552E 00	5.971E-01	1.246E-02
1.200	1.514E 00	3.772E-02	1.551E 00	6.616E-01	1.338E-02
1.300	1.513E 00	4.024E-02	1.553E 00	7.260E-01	1.428E-02

Table 4.–Continued

ELECTRONS IN SILICON

ENERGY	STOPPING POWER COLLISION	RADIATION	TOTAL	RANGE	RADIATION YIELD
MEV	MEV CM2/G	MEV CM2/G	MEV CM2/G	G/CM2	
1.400	1.513E 00	4.275E-02	1.556E 00	7.904E-01	1.517E-02
1.500	1.514E 00	4.527E-02	1.560E 00	8.546E-01	1.604E-02
1.600	1.516E 00	4.778E-02	1.564E 00	9.186E-01	1.690E-02
1.700	1.519E 00	5.011E-02	1.569E 00	9.824E-01	1.774E-02
1.800	1.521E 00	5.264E-02	1.574E 00	1.046E 00	1.857E-02
1.900	1.525E 00	5.521E-02	1.580E 00	1.109E 00	1.939E-02
2.000	1.528E 00	5.779E-02	1.586E 00	1.173E 00	2.021E-02
2.200	1.534E 00	6.303E-02	1.598E 00	1.298E 00	2.182E-02
2.400	1.541E 00	6.835E-02	1.610E 00	1.423E 00	2.342E-02
2.600	1.548E 00	7.374E-02	1.622E 00	1.547E 00	2.500E-02
2.800	1.555E 00	7.891E-02	1.634E 00	1.670E 00	2.656E-02
3.000	1.562E 00	8.445E-02	1.647E 00	1.792E 00	2.811E-02
3.500	1.578E 00	9.874E-02	1.677E 00	2.092E 00	3.196E-02
4.000	1.593E 00	1.136E-01	1.706E 00	2.388E 00	3.581E-02
4.500	1.606E 00	1.292E-01	1.735E 00	2.679E 00	3.966E-02
5.000	1.618E 00	1.449E-01	1.763E 00	2.964E 00	4.353E-02
5.500	1.629E 00	1.610E-01	1.790E 00	3.246E 00	4.740E-02
6.000	1.639E 00	1.773E-01	1.817E 00	3.523E 00	5.126E-02
6.500	1.649E 00	1.939E-01	1.843E 00	3.796E 00	5.512E-02
7.000	1.657E 00	2.107E-01	1.868E 00	4.066E 00	5.897E-02
7.500	1.665E 00	2.277E-01	1.893E 00	4.332E 00	6.280E-02
8.000	1.673E 00	2.449E-01	1.918E 00	4.594E 00	6.663E-02
8.500	1.680E 00	2.623E-01	1.942E 00	4.853E 00	7.044E-02
9.000	1.686E 00	2.815E-01	1.968E 00	5.109E 00	7.425E-02
9.500	1.692E 00	2.993E-01	1.992E 00	5.362E 00	7.806E-02
10.000	1.698E 00	3.172E-01	2.016E 00	5.611E 00	8.184E-02
20.000	1.773E 00	6.976E-01	2.470E 00	1.008E 01	1.522E-01
30.000	1.812E 00	1.101E 00	2.913E 00	1.380E 01	2.122E-01
40.000	1.839E 00	1.515E 00	3.354E 00	1.700E 01	2.632E-01
50.000	1.859E 00	1.936E 00	3.795E 00	1.980E 01	3.070E-01
60.000	1.875E 00	2.362E 00	4.237E 00	2.229E 01	3.449E-01
80.000	1.899E 00	3.224E 00	5.123E 00	2.658E 01	4.076E-01
100.000	1.917E 00	4.093E 00	6.010E 00	3.018E 01	4.573E-01
200.000	1.972E 00	8.504E 00	1.048E 01	4.263E 01	6.076E-01
300.000	2.004E 00	1.296E 01	1.496E 01	5.057E 01	6.857E-01
400.000	2.026E 00	1.743E 01	1.946E 01	5.642E 01	7.349E-01
500.000	2.043E 00	2.192E 01	2.396E 01	6.104E 01	7.691E-01
600.000	2.057E 00	2.641E 01	2.846E 01	6.486E 01	7.945E-01
800.000	2.079E 00	3.540E 01	3.748E 01	7.097E 01	8.301E-01
1000.000	2.096E 00	4.439E 01	4.649E 01	7.575E 01	8.541E-01

References

Abeles, B. and Tiedje, T. [1983], Phys. Rev. Lett., 51, 2003.

Adler, D. [1978], Phys. Rev. Lett. 41,1755.

Adler, D., Schwartz, B. and Steele, M. [1985], Physical Properties of Amorphous Materials, Plenum Press, page 48.

Adler, D. [1984], Semiconductors and Semimetals, J. I. Pankove, Vol. 21, Part A, Chapter 14.

Adler, D. [1983], Solar Cells 9, 133.

Anderson, P. W. [1958], Phys. Rev. 109, 1492.

Cohen, M. H. [1970], J. Non-Cryst. Solids 4, 391.

Crandall, R. S. [1989], Proc. Mat. Res. Soc. Vol. 149, 589.

Dersch, H., Stuke, J. and Beichler, J. [1981], Phys. Stat. Solidi B105, 265.

Dersch, H., Stuke, J. and Beichler, J. [1981], Appl. Phys. Lett. 38, 456.

Enge, H. [1966], Introduction to Nuclear Physics, Addison Wesley Publishing Company.

Equer, B. and Karar, A. [1988], Nucl. Instr. and Meth. A271, 574.

Fujieda, I., Cho, G. , Kaplan, S. N., Perez-Mendez, V., Qureshi, S., Ward, W. and Street, R. A. [1988], Proc. Mater. Res. Soc. Vol. 118, 467.

Fujieda, I. [1990] , Ph.D thesis.

Goldwasser, E. L. , Mills, F. E. and Hanson, A. O. [1952], Phys. Rev. 88, 1137 .

Goulding, F. S. and Landis, D. A. [1982], IEEE Trans. Nucl. Sc., Vol. NS-29, No.3,1125.

Goulding, F. S., [1972], Nucl. Instr. and Meth., 100, 493.

Hanak, J. J., Chen, E. and Myatt, A. [1987], Ninteenth IEEE Photovoltaic Conf. , New Orleans.

Heitler, W. [1954], Quantum Theory of Radiation, Oxford University Press.

Hill, R. M. [1971], Phil. Mag. 23, 59.

Imagawa, O., Yasuda, K. and Yoshida, A. [1989], J. Appl. Phys. 66 (10) , 4719.

Jones, D. I. ,Gibson, R. A. , Le Comber, P. G. and Spear, W. E. [1980], Phil. Mag. B.

Kampas, F. J. [1982], J. Appl. Phys. 53, 6408.

Kampas, F. J. and Griffith, R. W. [1981], Appl. Phys. Lett. 39, 407.

Kaplan, S. N. , Morrel, J., Mulera, T. A., Perez-Mendez, V., Schnurmacher, C. and Street, R. A. [1986], IEEE Trans. Nucl. Sc. NS-33, 351.

Klein, C. A. [1968], J. Appl. Phys. 39, 2029.

Knoll, G. F. [1979], Radiation Detection and Measurement, John Wiley and Sons.
Leal Ferriera, G. F. [1977], Phys. Rev. B, Vol. 16, No.10, 4719.
LeComber, P. G. and Spear, W. E. [1970] , Phys. Rev. Lett. 25, 509.
Lindhard, J. , Nielsen, V. , Scharff, M. , Thomsen, P. V. [1963], Mat. Fys. Medd. , Dan. Vid. , Selsk. 33, No. 10.
Lucovsky, G. , Nemanich, R. J. and Knight, J. C. [1979], Phys. Rev. B19, 2064.
Madan, A. [1973], Ph.D. Thesis, University of Dundee.
Madan, A., LeComber, P. G. and Spear, W. E. [1976], J. Non-Cryst. Solids 20, 239.
Madan, A. and Shaw, M. P. [1988], Physics and Applications of Amorphous Silicon, Academic Press.
Marmier, P. and Sheldon E. [1969], Physics of Nuclei and Particles, Academic Press.
Matsuura, H. [1988], J. Appl. Phys. 64(4), 1964.
Mott, N. F. [1967], Adv. Phys. 16, 49.
Mott, N. F. [1985], Phil. Mag. B, Vol. 51, No. 1, 19.
Mott, N. F. [1968], J. Non. Cryst. Solids 1, 1.
Perez-Mendez, V. , Kaplan, S. N. , Ward, W. , Qureshi, S. and Street, R. A. [1987] Nucl. Instr. and Meth. A260,195.
Perez-Mendez, V. , Kaplan, S. N. , Cho, G. , Fujieda, I. , Qureshi, S. Ward,. W. and Street, R. A. [1988], Nucl. Instr. and Meth. A273, 127.
Perez-Mendez, V. , Cho, G. , Drewery, J. , Fujieda, I. , Kaplan, S. N. , Qureshi, S. , Street, R. A. , [1990] , LBL report-28339.
Pfister, G. and Scher, H. [1978], Adv. Phys. , Vol. 27, No. 5, 747.
Pochet, T., Dubeau, J. , Hamel, L. A. , Equer, B. and Karar, A. [1989], Proc. Mat. Res. Soc. Vol. 149, 661.
Polk, D. E. [1971], J. Non-Cryst. Solids 5, 365.
Qureshi, S. , Perez-Mendez, V. , Kaplan, S. N. , Fujieda, I , Cho, G. and Street, R. A. [1988], IEEE Trans. Nucl. Sc. , Vol. 36, No. 1, 194.
Qureshi, S. , Perez-Mendez, V. , Kaplan, S. N., Fujieda, I. , Cho, G. and Street, R. A. , [1989], Proc. Mat. Res. Soc. Vol. 149, 649.
Sandia report, SAND85-0776, [1985], Basic Radiation Effects in Nuclear Power Electronics Technology, J. E. Gover and J. R. Srour.
Segre, E. [1977], Nuclei and Particles, Benjamin / Cummings publishing Company.
Scher, H. and Montroll, E. W. [1975], Phys. Rev. B12, 2455.
Silver, M. , Cohen, L. and Adler, D. [1982], Appl. Phys. Lett., 40, 261.

Spear, W. E. [1973], Proc. 5th Int. Conf. on Amorphous and Liquid semiconductors, Taylor and Francis.
Spear, W. E. , Loveland, R. J. and Al-Shabaty, A. [1974], J. Non-Cryst. Solids 15, 410.
Spear,w. E. [1969], J. Non-Cryst. Solids 1, 197
Staebler, D. L. and Wronski, C. R. [1977], Appl. Phys. Lett. 31, 292.
Street, R. A. [1983], Phys. Rev. B, Vol. 27, No. 8, 4924.
Street, R. A. [1982], Appl. Phys. Lett. 41(11), 1060.
Street, R. A. [1984], Phil. Mag. B, Vol. 49, No. 1, L15.
Street, R. A. [1979], Phil. Mag. B 40, No. 6, 451.
Street, R. A., Nelson, S. , Antonuk, L. and Perez-Mendez, V. [1990], Mat. Res. Soc. Sym. Proc. , Vol. 192 , 441.
Tiedje, T. and Rose, A. [1980], Solid Stata Communications, Vol. 37, 49.
Tiedje, T., Cebulka, J. M., Morel, D. L. and Abeles, B. [1981], Phys. Rev. Lett. 46, 1425.
Tiedje, T. [1984], Physics of Hydrogenated Amorphous Silicon II, Springer Verlag.
Waite, T. R. [1957], Phys. Rev. , 107, 463.

LAWRENCE BERKELEY LABORATORY
UNIVERSITY OF CALIFORNIA
INFORMATION RESOURCES DEPARTMENT
BERKELEY, CALIFORNIA 94720